POLITECNICO DI MILANO

SCUOLA DI INGEGNERIA INDUSTRIALE E DELL' INFORMAZIONE

DIPARTIMENTO DI CHIMICA, MATERIALI E INGEGNERIA CHIMICA "G.NATTA"

TESI DI LAUREA MAGISTRALE

Combustion of monocyclic aromatic hydrocarbons. Theoretical investigation of the potential energy surface of phenyl radical + O2 and impact on bio-oils combustion and molecular growth kinetics

Relatore:
Prof. Matteo PELUCCHI

Correlatore:
Prof. Marco VANNI

Tesi di Laurea di:
Elena LOPES
922111

Anno Accademico 2020 / 2021

“Don’t lose sight of Ithaca,
for that’s your destination.”

A tutti coloro che
credono in me.

Sommario

L'adozione di risorse energetiche alternative rappresenta, oggigiorno, una priorità per contrastare l'imminente minaccia del cambiamento climatico. Se per la produzione di energia elettrica, numerose soluzioni sono state trovate, quali l'energia nucleare, idroelettrica, solare, eolica, soluzioni altrettanto valide per il trasporto non sono state ancora definite. L'insostituibilità dei combustibili fossili deriva dalla loro elevata densità energetica, e ad oggi, l'unica possibile e realistica alternativa è rappresentata dai biocombustibili. La potenzialità dei biocombustibili risiede non solo in una densità energetica elevata ma, soprattutto, nel bilancio netto di emissioni di CO2 che è pari a zero. Infatti, i biocombustibili derivano da biomasse vegetali il cui ciclo di vita prevede l'assorbimento della CO2 per compiere il processo di fotosintesi.

L'adozione di un nuovo combustibile, derivante anche dalla miscelazione di combustibili di origine organica e fossile, richiede una valutazione della compatibilità con tecnologie motori già esistenti, delle performance di combustione e delle emissioni derivanti. Tale valutazione rappresenta un problema a carattere cinetico. Una descrizione accurata del processo reattivo di combustione delle nuove miscele consentirebbe di prevedere le concentrazioni dei prodotti di combustione e di individuare quali componenti sono maggiormente responsabili della produzione di sostanze inquinanti quali NO_X, gas serra e particolato.

Negli ultimi decenni, gli sforzi della ricerca sono stati concentrati principalmente sulla modellazione della combustione degli alcani; oggi l'attenzione è spostata sulla combustione degli aromatici, per giungere, in un futuro prossimo, ad una descrizione accurata anche della componente ossigenata dei biocombustibili.

L'obiettivo di questa tesi è quello di contribuire al miglioramento del modello cinetico di combustione del gruppo di ricerca CRECK (Politecnico di Milano), mediante investigazioni sulle dinamiche di ossidazione di un radicale chiave per lo sviluppo del meccanismo cinetico: il radical fenile (C_6H_5).

La rilevanza dello studio non è data solo dal ruolo che il radicale fenile assume nella combustione di aromatici presenti nei surrogati delle benzine commerciali (e.g. Toluene). Infatti, la stima accurata dei parametri cinetici può essere estesa per analogia alla modellazione cinetica di aromatici ossigenati come catecolo, guaiacolo e anisolo, presenti nei biocarburanti.

Lo studio è iniziato con l'identificazione dei canali reattivi più rilevanti per il sistema in esame, poi implementati nella superficie di energia potenziale (PES). Il lavoro è proseguito con la determinazione dei contenuti energetici e delle frequenze sia per le specie coinvolte che per gli stati di transizione, attraverso metodi "ab-initio". A seguire, le costanti di velocità sono state calcolate mediante la risoluzione della "Multi-well Master Equation". La realizzazione di questa parte del progetto di tesi è stata possibile grazie all'utilizzo del software EstokTP, sviluppato dal Politecnico di Milano.

Infine, le nuove costanti sono state implementate nel meccanismo cinetico già esistente per valutarne gli effetti sulle performance predittive. Questa fase, anche detta di validazione, consiste nel simulare la combustione di surrogati dei nuovi combustibili in reattori ideali, utilizzando il software OpenSMOKE ++, sviluppato dal gruppo di ricerca CRECK del Politecnico di Milano.

Questa attività di ricerca pone una solida base per sforzi futuri nell'indagine della reattività di altre specie chimiche rilevanti, per le quali mancano ancora stime teoriche accurate.

Abstract

The adoption of alternative energy sources is now a priority to address the imminent threat of climate change. Despite the numerous solutions currently available for electricity generation (nuclear, hydroelectric, solar and wind power), valid alternatives for transportation have not been defined yet. Due to their high energy density, fossil fuels are hardly replaceable, and at present, biofuels represent the only possible and realistic alternative.

In addition to the significant energy density, the potential of biofuels lies in the net-zero CO2 balance. In fact, biofuels are produced from vegetable biomass, whose life cycle involves the absorption of CO2 to complete the photosynthesis process.

The adoption of a new fuel, that may result from the blending of organic and fossil fuels, requires a strict evaluation of compatibility with existing engine technologies, combustion performances and resulting emissions. Such assessment consists in a kinetic investigation. An accurate description of the new fuel reaction mechanism would allow to predict the combustion products concentration and which species are most responsible for pollutants production (NOX, greenhouse gases, soot).

In recent decades, the combustion kinetic model has been widely developed for alkanes. However, today the focus has shifted to the combustion of aromatics, and, in the near future, more attention will be paid to build an accurate mechanism for oxygenated components of biofuels.

The aim of this thesis is to contribute to the improvement of the detailed kinetic combustion model of the CRECK research group of the Politecnico di Milano, investigating the oxidation of the phenyl radical (C6H5), which is a key player in the combustion mechanism of aromatics.

From a fuel and engines design perspective such system is of relevance not only due to the intrinsic connections between benzene and aromatics chemistry (e.g. toluene) of interest for surrogate fuels formulations of commercial gasoline, but also provides an accurate estimation of model parameters that can be extended through analogy to the

kinetic modelling of oxygenated aromatics biofuels components such as catechol, guaiacol, anisole etc.

The investigation started with the identification of the most important reaction channels, then implemented in the potential energy surface (PES). The work continued with the determination of energy contents and frequencies for the involved species and transition states, through "ab-initio" methods. Then, the kinetic rate constants were computed with the resolution of the multi-well "Master Equation". This part of the thesis project was accomplished by using the EstokTP software, developed by the Politecnico di Milano. Finally, the new kinetic constants were implemented in the already existing kinetic mechanism to evaluate their effects on predictive performances. This step, named model validation, consists in simulating the combustion of fuel surrogates into ideal reactors by using the OpenSMOKE++ solver, developed by the CRECK research group of the Politecnico di Milano.

This paper lays the foundation for future efforts in the investigation of other relevant species reactivity, for which accurate theoretical estimates are still lacking.

Table of Contents

List of figures

List of tables

Chapter1
Introduction

1.1 The Study Aim

1.1.1 Current Issues

In recent decades, the use of fossil fuels as a primary energy source has resulted in critical societal issues, namely climate change and security of supply.

Fossil fuels are currently used for energy production and transportation. Internal combustion engines produce, among others, CO_2, that is a major greenhouse gas contributing to the global warming effect. The main issue is not precisely its production, since most fuels combustion is responsible of CO2 emissions, but rather the fact that the amount released by fossil fuels cannot be reconverted to the original fuel, hampering a possible circular system.

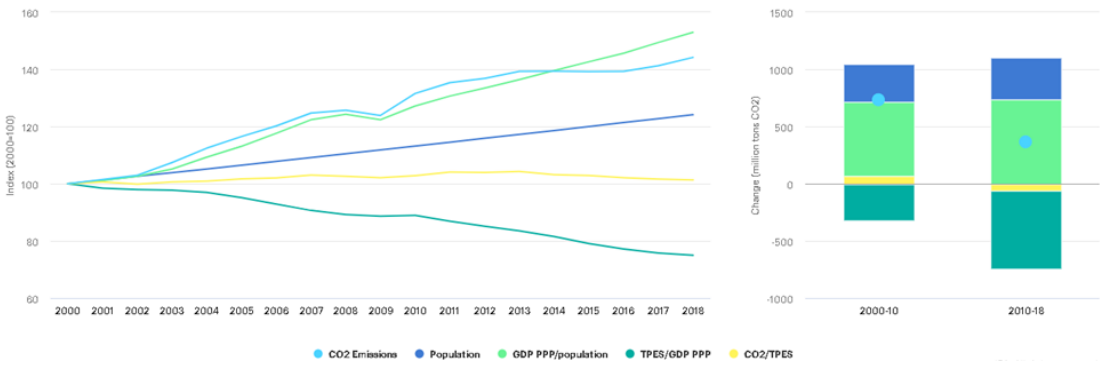

Figure 1 Historical data collection proving the correlation between economic-demographical growth and CO2 emissions.[1]

Man-caused CO2 emissions have an immeasurable impact on climate change, causing harm to ecosystems worldwide, and they are almost entirely ascribed to the use of fossil fuels to meet the society energy demand.

The above charts show the close correlation between demographic and economic growth and CO2 emissions. This data becomes more interesting when expanding economies are taken into account. For these fast-growing economies, it has been registered an exponential increase of CO2 emissions that goes hand in hand with the GDP growth. The main cause lies in the increasing level of industrialization and in the expansion of the middle class. These two factors combined translate into higher living standards thus, higher demand for energy and goods.

If the climate change is not already a serious threat to humanity, the increased energy consumption is also coupled with a limited availability of oil reserves. This has enhanced the energy dependence of many countries around the world since oil production is over 55% localized in the Middle East. As a result, countries with high energy dependence suffer from "energy insecurity" and this impacts also on the commodity prices.

Although it is challenging to forecast the end of fossil reservoirs, recent studies proposed that, by keeping the current rate of products utilization, reservoirs will last for no more than one hundred years[2].

1.1.2 The Possible Solutions

In view of analysed issues, alternative fuels have been sought after. Wind, solar and nuclear energy are promising options with respect to electricity production and heat generation. However, they carry drawbacks that should be considered. Taking as an example nuclear energy, the one surely capable of responding to the high demand, accidents such as the one of Fukushima nuclear power plant, have raised many concerns related to the hazards of nuclear power plants, yielded somewhat to scepticism.

If, on the one hand, alternatives for energy production proved to have some limitations, on the other hand there are no valid alternatives for covering transportation needs, since their energy density is not comparable to the one of liquid fuels (gasoline, diesel, kerosene), except for biofuels.

Biofuels have received increasing attention in the past years as a renewable option. With the term "biofuel" it is intended any fuel produced from biomass. Its main advantage is

that the CO_2 emitted from its combustion takes part to the photosynthetic process of plants, which use sunlight and CO_2 to build their cells, reproducing the biofuel by natural processes. Thus, biofuels have the potential to be CO_2 neutral.

The most spread biofuel is bioethanol, largely produced in Brazil and USA. The European Union ranks third in terms of bioethanol production, while leading the production of biodiesels (fatty acid methyl esters from esterification of vegetal and animal fats). Bioethanol and biodiesel are already blended in commercial gasolines such as E5 gasoline (5 vol% bio-ethanol) and B7 (7 vol% bio-diesel) diesel.

However, biofuels have some drawbacks. Their usage raised ethical concerns about the raw materials employed: being produced also from sugar and vegetable oils, biofuels may affect land use, altering food supplies and prices.

A possibly better alternative is to start the production from not-edible biomass, these biofuels are categorized as "second generation". As an example, the lignocellulosic biomass, from which "second-generation" biofuels are produced through thermochemical or biochemical processes. Lignin can be converted into bio-oils through fast pyrolysis, getting a mixture mainly made of oxygenated aromatic hydrocarbons (OAHs) such as anisole, phenol, guaiacol and catechol. Bio-oils can be used as an energy source for house and industrial heating applications. In addition, their oxygenated aromatic fraction, is potentially a good gasoline additive due to its impressively high knock resistance. Finally, cultivation of algae as a feedstock to bio-refineries is also attracting a strong interest to produce the so-called "third generation" biofuels.

As recently reviewed by Sadeghinezhad et al.[3], even though the use of biofuels generally reduces particulate matter (PM), carbon monoxide (CO), unburned hydrocarbons (HC) and aromatic compounds emissions, the carbonyl compounds (aldehydes and ketones) emissions increase. Some controversial findings are reported also with respect to NOx emissions. To better predict the pollutants formation, it is necessary to develop a well-validated detailed kinetic model for the combustion of blended mixtures, or biofuels. Kinetic modelling is a way to gain this knowledge through the examination of the oxidation characteristics of fuels and can greatly increase the efficiency of studying a variety of combustion systems.

The tough part of real fuels kinetic modelling lies in their complex and fairly heterogeneous composition. If dealing with blended mixture, the biofuel portion might be a pure compound (butanol, ethanol etc.), but the fossil fuel portion is a mixture of 10^2-10^3 different components. On the other hand, also the chemical composition of bio-oils is varied. To tackle this issue, a common practice is to use surrogate mixtures made of a limited number of reference components that match the characteristics of the real fuel with a much lower computational requirement. To reproduce the chemistry and reactivity of these surrogate mixtures, the chemistry of combustion of every component must be well-described.

1.1.3 The Thesis Objective

The goal of this thesis is to investigate the oxidation mechanism of a key player for the combustion of aromatics, the phenyl radical. Its reactivity is of interest for the combustion of mono-aromatic hydrocarbons (MAHs), present in fossil fuel fractions, of OAHs, present in bio-oils from biomass fast pyrolysis, but it also interests the growth of poly-aromatic hydrocarbons (PAHs), that leads to soot formation.

Despite the relevant role in combustion systems, the current knowledge of the kinetic parameters and the reaction channels of phenyl oxidation is incomplete. This work aims at filling this lack by reassessing the oxidation mechanism of phenyl, calculating the kinetic parameters characterizing the identified reaction channel and by validating the updated kinetic model through the comparison of model predictions with experimental data.

1.2 The Fuel Characterization

The reactivity assessment of a new formulation of gasoline is largely a chemical kinetic problem, whose solution, as already mentioned in the previous paragraph, allows to predict combustion performances and emissions potential. Once this knowledge is gained, two different approaches can be adopted: to customize the new fuel blend to

already existing technologies or to tune an engine to the given fuel. Nowadays, the first solution is the chosen one. The fuel market penetration depends on its adherence to performance standards, measured according to specific test procedure.

Based on the type of ignition, internal combustion engines can be classified into spark ignition (SI) and compression ignition (CI) engines.

To the latter belong diesel and HCCI engines, whose auto-ignition is allowed by the pressure value reached through compression in the combustion chamber. The feed of air and the feed of fuel are placed in different parts of the combustion chamber and are inserted in different instants of time: air enters inside the engine, later on the fuel is sprayed shortly before the pressure peak, allowing fuel instant ignition. HCCI type engines, as diesel ones, still rely on auto-ignition, thanks to the temperature and pressures reached inside the combustion chamber, but the engine takes in both air and fuel.

In spark-ignition engines, the fuel is generally gasoline; the engine takes in a mixture of air and fuel, which is compressed such as in CI engines, but reaching a pressure value not high enough to allow auto-ignition. Indeed, the reaction is activated by a spark that occurs when the engine piston achieves almost the top of the combustion chamber thus, while the fuel is still being compressed. Along the cylinder of the engine an increase in pressure and temperature is registered. Due to temperature inhomogeneity, there might be some hotspots inside the combustion chamber where auto-ignition may start. An independent flame front spreads, causing a sharp rise in the heat release rate, which translates into pressure waves propagation producing a characteristic metallic sound. This phenomenon is known as "knocking" or "detonation" and it might permanently damage the engine. According to Kalghatgi et al.[4] a current trend to improve engine efficiency is to increase compression ratios and implement turbocharging. This makes knocking, or "*super-knocking*", more likely to occur and the accurate assessment of fuel ignition propensity becomes more and more necessary.

In order to evaluate the autoignition property (or anti-knocking) of fuels, some experimental parameters have been introduced: the Research Octane Number (RON) and Motor Octane Number (MON) for gasoline spark ignited engines (SI)[5], and the Cetane

Number (CN) for diesel compression ignition (CI) engines. The RON test is performed in a cylinder research engine running at 600 rpm at 52°C. The MON test, instead, is run at 900 rpm and 149°C.

The antiknock quality of a gasoline is defined by the Octane Index:

$$\mathrm{OI} = \mathrm{RON} - \mathrm{KS}$$

Where K is an empirical parameter (depending on temperature and pressure of the system) and S the Octane Sensitivity ($S = RON - MON$) which measures the difference of autoignition propensity between the given fuel and a reference fuel. Indeed, RON and MON are defined by referring to the two components of the main gasoline surrogate: n-heptane (RON=MON=0, low antiknock capacity) and iso-octane (RON=MON=100, good antiknock capacity).

Autoignition, laminar flame speed, NOx and soot formation, are fundamental combustion properties that influence engine performance and emissions.

Dealing with biofuels, while at high temperatures oxygenated and synthetic-hydrocarbon biofuels (BTL) behave similarly to conventional hydrocarbon fuels, at low-temperature, their chemistry differs significantly, because of the different reactivity of the functional group neighbourhood. The main goal of kinetic modelling of combustion is to characterize and quantify the impact of these different molecular features. This work theoretically investigates the C6H5+O2 potential energy surface, and application of transition state theory and master equation provides rate constants for direct implementation in existing kinetic models. From a fuel and engines design perspective such system is of relevance not only due to the intrinsic connections between benzene and aromatics chemistry (e.g. toluene) of interest for surrogate fuels formulations of commercial gasoline, but also provides an accurate estimation of model parameters that can be extended through analogy to the kinetic modelling of oxygenated aromatics biofuels components such as catechol, guaiacol, anisole etc.

1.3 Basis of Kinetic Modelling

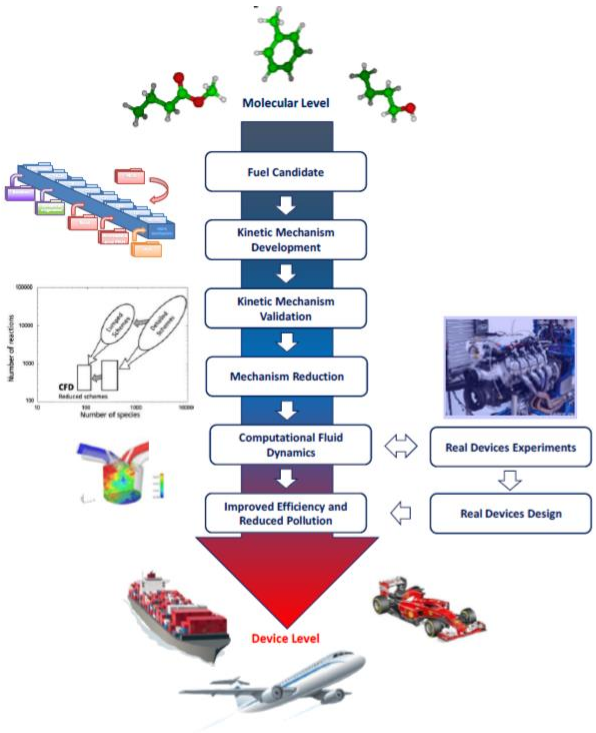

Figure 2 Flow chart of the research protocol to implement a new fuel or fuel mixture into existing technologies. [6]

In paragraph 1.1 and 1.2, issues related to the complexity of developing a reliable kinetic mechanism for fuel mixtures were presented, but these are not the only ones to tackle.

The first challenge in which researchers stumble into is the number of species to introduce in the mechanism. Unfortunately, the number of intermediates increases exponentially with the increase of the fuel molecular weight. A high number of species means an incredible computational effort, whose costs scale by the second/third power of the number of species. Similar considerations can be made for the number of reactions. The Chemical Reaction Engineering and Chemical Kinetics (CRECK) group at Politecnico di Milano (POLIMI), to deal with this drawback, adopted, since Ranzi et al.[7], the chemical lumping procedure: starting from a detailed mechanism, more molecules (isomers) are grouped in one single pseudo species, reducing not only the overall number of species, but also the number of reaction steps[8]. Another solution was to use

a skeletal reduction approach: species and reactions with a negligible relevance in the operating conditions of interest are not included.

Another issue to tackle is how to structure the mechanism. The POLIMI mechanism was developed with a hierarchical and modular approach in the last 40 years[9], Figure 3.

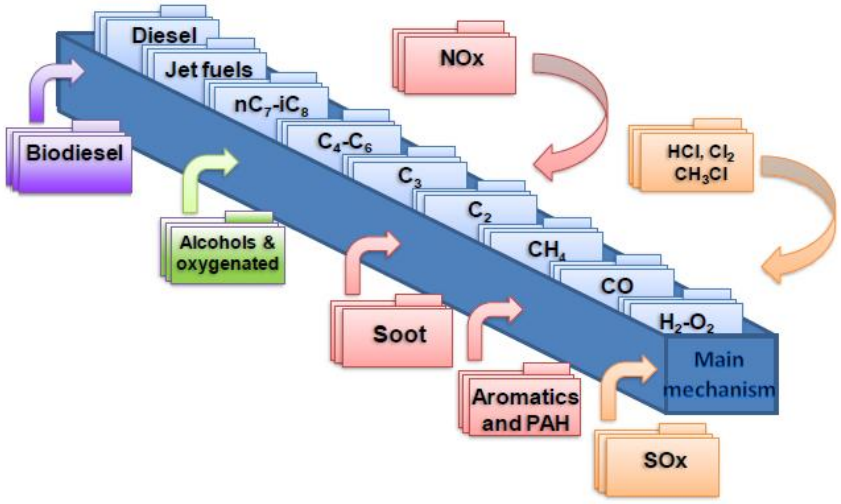

Figure 3 Schematic representation of the hierarchical modularity of the POLIMI kinetic mechanism.[6]

Any kinetic mechanism starts with a core mechanism made of the simplest species, common to all species combustion. In the core mechanism are introduced H_2/O_2 and their radical species, which dominate the reactivity of any fuel, follow the C_1 (CH4, $CH3$, CH2O, CO and CO2) and C_2 modules (C2H6, C2H4, C2H2), that are implemented together since, for example, ethane can be formed by the recombination of two methyl radicals. In a similar fashion C_3 hydrocarbons are inserted. For all the successive modules, only the primary reactions have to be included, as smaller species reactions will be already defined in previous modules. Another great advantage of modularity is that when compiling the mechanism, it is possible to exclude modules that are not of interest for our analysis.

When defining a reaction, clearly, kinetic parameters must be provided. Historically, these were experimentally measured but, beside an unavoidable intrinsic uncertainty, experimental facilities limitations did not allow to measure them covering all the operating conditions of interest. Thanks to the progresses have been made by researchers, since the beginning of the XX century, nowadays it is possible to compute

the rate constants using ab-initio methods, which provide a higher accuracy to the measured parameters and overcome experimental limitations. For such reasons, theoretical chemistry is a necessary and a powerful tool for advances in kinetic modelling and therefore in combustion science and engineering.

Since the formalization of the bond increment theory of Benson and Buss [49], it is possible to determine kinetic parameters for reaction belonging to the same class according to analogy rules. Analogy rules exploit the obeying of species, in elementary reactions, to additivity rules of bond properties and to experimental evidence, which can be generalized by means of rate ruling. Benson's work is based on the core concept that only a small portion of the molecule influences rate parameters, as the dominant forces among atoms are short range.

Once the kinetic mechanism is fully implemented, together with thermodynamic and transport properties for every species, it can be processed by the opensource solver OpenSMOKE++ [66]. OpenSMOKE++ runs the kinetic simulations whose results are compared with experimental measurements in ideal reactors, to check the model predictive performances. This part of the procedure is commonly called "*validation*".
If the model poorly predicts the experimental data under some specific operating conditions, OPENSMOKE++ offers kinetic analysis tools to figure out the lacks and improvement margins of the mechanism. One of these tools is the sensitivity analysis, which identifies the rate constants that strongly affect a key output. Another important tool is the rate-of-production analysis (ROPA), which lists the contribution of the reactions with the highest rates for the net production or consumption of a species. If the sensitivity analysis and the ROPA do not help in pointing out the reactions that affect the model prediction performance, a right track may be to identify missing reaction pathways.

1.4 Thesis Overview

This work aims to revise and update the kinetic model of the research group CRECK, by calculating and implementing the rate constants of the most meaningful reaction channels for the phenyl radical oxidation. At the end of the work, the updated model was validated by comparing its prediction performances with the ones of the previous mechanism and with a large database of experimental values.

Chapter 2

The basic principles of chemical kinetic modelling are explained, providing insight to the approach to kinetic modelling adopted at POLIMI.

Chapter 3

An in-depth analysis on the opensource solver OPENSMOKE++ used for the model validation is provided.

Chapter 4

It introduces ab-initio theoretical methods and the EStokTP software used to derive the kinetic parameters of the investigated reaction channels.

Chapter 5

The "state of the art" of the current CRECK mechanism is discussed, focusing on its performances at defined operating conditions and pointing out the central role of the phenyl radical in the combustion mechanism. It is also given a highlight about the state of the art, in the literature, of the kinetic parameters estimation for the phenyl radical oxidation.

Chapter 6

In this chapter the construction and results of the potential energy surface investigation for the reactive system C6H5 + O2 are presented and discussed.

Chapter 7

The results of the model validation with the new rate constants implementation are shown.

Chapter 8

The conclusions, providing suggestions for further developments, are drawn.

Chapter2
Chemical Kinetic Modelling

The aim of this chapter is to introduce concepts essential to deal with chemical kinetic modelling. Theoretical principles are briefly discussed to allow a deeper understanding of the upcoming chapters.

2.1 Radical Chain Reactions

A combustion reaction can be easily synthesized through the global oxidation reaction of a fuel:

$$C_xH_yO_z + \left(x + \frac{y}{4} - \frac{z}{2}\ O_2\right) => x\ CO_2 + \frac{y}{2}\ H_2O + \ Energy$$

Clearly, a combustion mechanism cannot be represented through such a general formulation, since it includes a huge number of reaction steps and intermediates.

The first step of combustion reactions is the *chain initiation* reaction, so called because a stable molecule is turned into a radical, enhancing its reactivity.

Radical species are reactive and unstable intermediates generated from the decomposition reactions of stable molecules. They can be produced via homolytic scission of covalent bonds, or via H-abstraction reactions, in both cases they will provide an unpaired electron responsible of their instability.

To *chain initiation* reactions follow *chain propagation* ones: these convert radical species into other radical species, or, through a bimolecular process, into radical and stable species. Net, the number of radicals keeps constant.

Products of the fuel decomposition can be involved into branching reaction. Chain branching reactions are responsible of the radical species number increase and then the system reactivity goes up.

The reaction chain mechanism ends with termination reactions which lower the reactivity of the system by turning radicals into species with paired electrons.

Follow some examples of radical chain reactions from the combustion kinetic scheme of molecular hydrogen to better explain what introduced above.

$$Global\ reaction: \quad H_2 + 0.5\ O_2 => H_2$$

$$Chain\ Initiation\ reactions: \quad H_2 => H\cdot + H\cdot$$

$$O_2 => O\cdot + O\cdot$$

$$H_2 + O_2 => HO_2\cdot + H\cdot$$

$$Chain\ Propagation\ reactions: \quad HO_2\cdot => H\cdot + H_2O_2$$

$$H_2 + HO_2 => H\cdot + H_2O_2$$

$$Chain\ Branching\ reactions: \quad H\cdot + O_2 => \ddot{O} + OH\cdot$$

$$\ddot{O} + H_2 => OH\cdot + H\cdot$$

$$Chain\ Termination\ Reactions: \quad HO_2\cdot + HO_2\cdot => O_2 + H_2O_2$$

When developing a kinetic model, the first stage is the identification of this steps of reaction to build up the kinetic scheme of combustion process. The following challenge is to find or compute kinetic rate constants to characterize the reactivity of the species involved.

2.2 Reaction Rates Constants

The reaction rate measures the velocity of reduction or increase of a molecule concentration in an instant of time.

$$r_i = \frac{d[c_i]}{dt} = \frac{mol}{m^3 \cdot s}$$

In other words, it can be defined as the derivative of the concentration of species with respect to time. This definition well expresses what the reaction rate measures, but it does not give any further information about which variables affect its value.

Considering the following elementary reaction:

$$aA \rightarrow bB$$

It is possible to state that the rate of consumption of A is proportional to the a power law of its real time concentration, where the proportionality constant is a function of the operating conditions temperature and pressure.

$$r_A = k(T, P)[A]^a$$

k represents the reaction rate constant.

The fact that the power law equals to the stochiometric coefficient of the examined reaction is a feature of elementary reaction, but in case of non-elementary reaction, these coefficients must be quantified experimentally.

Consider a bimolecular reaction:

$$aA + bB => products$$

$$r = k(T, P)[A]^a[B]^b$$

The term reaction order refers to the sum of the power laws of concentrations, that in this case, is equal to $a + b$.

Considering that the unit of measure of reaction rates is obviously fixed, the kinetic rate constant dimensions depend on the reaction order.

In the next paragraphs a deep dive about the dependence of the kinetic rate constant is provided.

2.3 The Reaction Rate Constant Temperature Dependence

The reaction rate constant temperature dependence was studied by Van't Hoff[10] and Arrhenius during the late XIX century, and it was formulized in the following way:

$$k = A\, e^{(-\frac{Ea}{RT})}$$

A is the frequency factor and E_a is the activation energy, or better, the energy barrier that must be overcome by molecules to make the reaction occur. R is the molar gas constant equal to 1.987 cal/mol/K.

The exponential factor exp $(-E_A/RT)$ is also known as the Boltzmann factor, a distribution function describing the fractional population of reactive species with sufficient energy to overcome the reaction barrier at a given temperature.

It is possible to linearize the Arrhenius dependence by applying the logarithmic function:

$$\ln(k) = \ln(A) - \frac{Ea}{RT}$$

This form reveals to be very useful when E_a and A must be defined starting from a set of experimental data, because a linear regression can be applied to quantify their values. Moreover, the logarithmic form is very handy when rate constants must be plotted.

However, it is possible to come across some rate constants that do not present a linear dependence between ln(k) and $\frac{1}{T}$, in this case it is applied a modified form of Arrhenius law:

$$k = A\, T^n\, e^{(-\frac{Ea}{RT})}$$

The Arrhenius parameters A, n, E_A, beside representing a rate constant over a wide temperature range, are the key inputs of kinetic models.

2.4 Pressure Dependent Reaction Rate Constants

The reaction rate contains only an implicit dependence on pressure in the expression of reactants concentration according to which:

$$c_i = \frac{p_i}{RT}$$

However, it is not unlikely to come across some reactions for which the kinetic rate constant presents a dependence on pressure.

According to the Boltzmann-Arrhenius collision theory, a reaction occurs when particles take part in what called a "successful collision", a collision through which molecules acquire sufficient energy to overcome the activation energy, breaking the pre-existing molecules bonds and forming new ones.

The same evolution must apply for unimolecular reaction: a given molecule A must collide with another molecule, without reacting with the latter, to gain the energy necessary to the reaction fruition.

The implicit inconsistency was solved by Lindemann[6] , who introduced the concept of "third-body collision", justifying the unexplained pressure dependence of the rate constant. Given the reaction:

$$A \rightarrow B + C$$

According to Lindemann, the reaction complete expression is:

$$M + A \leftrightarrow A^* + M \rightarrow B + C$$

M is a gas molecule, also named *third body,* able to absorb energy excess of unstable products. A^* is the activated complex, a very reactive intermediate.

Being the activated complex very reactive, it is possible to apply the pseudo-steady state assumption:

$$\frac{dA^*}{dt} = k_E AM - k_D A^* M - k_R A^* = 0$$

$$A^* = \frac{k_e AM}{k_d M + k_R}$$

Being M a gas molecule:

$$M = \frac{p_M}{RT}$$

The rate of production becomes:

$$r = k_R A^* = k_R \frac{k_e A M}{k_d M + k_R} = kA$$

M can be included or not in the expression of the reaction rate since it is not a real reactant.

The high-pressure and low-pressure limits allow to get simplified expressions of the rate equation.

$$\lim_{p\to\infty} r = \frac{k_R k_e A}{k_d}$$

$$\lim_{p\to 0} r = k_e M A$$

At high pressure, the reaction rate is independent of M (high-pressure limit), at low pressure its contribution cannot be neglected thus, the reaction rate depends on the pressure.

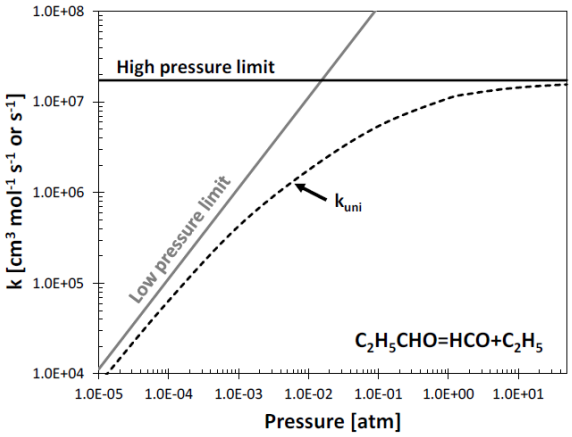

Figure 4 Rate constant for the unimolecular reaction C2H5CHO=HCO+C2H5 as a function of pressure at the fixed temperature of 1600K

Regarding Figure 4, the reaction rate is given by the combination of the two asymptotes. It can be observed, that at intermediate pressures, the approximation is no more accurate. This is the main limit of Lindemann theory, the impossibility to apply the same approach to what is known as *fall-off* regime. In addition, Lindemann supposed the

existence of just one molecular conformation for the activated complex. Further development will be computed, such as the Rice-Ramsperger-Kassel-Marcus (RRKM) theory, explained in the next chapters (Chapter 4).

2.5 Chemical Thermodynamics

Chemical thermodynamics is the branch of chemical engineering that deals with systems in equilibrium. When studying a reacting system, it is not possible to decouple the thermodynamic and kinetic aspects, which are both essential to build a reliable kinetic model.

Thermodynamic properties that are necessary to write energy balances are the enthalpy (H), the entropy (S) and the heat capacity (Cp and Cv).

The enthalpy for a closed ideal gaseous system is defined as a function of the internal energy U as:

$$H = U + pV = U + nRT$$

With p and V respectively the system pressure and volume.

The internal energy is a measure of the kinetic and potential energy stored in all the components of the system. The second term stands for the energy to be supplied to bring n moles of gas of volume V, pressure p and temperature T to its present state from the reference state.

Thus, the enthalpy of formation ΔHf of any chemical species is the energy required to form one mole of that species starting from its elements in the reference state.

Formation enthalpies are also used to compute the enthalpy of reaction:

$$\Delta H_r = \sum v_i \Delta H_{f,i}$$

Where the summation is defined with respect to the number of products and reactants and v are the stoichiometric coefficients. When the enthalpy variation is negative, the reaction is exothermic, since the products are more stable than the reactants, conversely, an energy supply is required, and the reaction is endothermic.

Another thermodynamic property is entropy, which represents the measure of the disorder of a system. In a spontaneous process the system tends to reach a more chaotic status thus, the entropy increases. Therefore, a positive entropy variation states a spontaneous reaction. As the reaction enthalpy, the entropy variation correlated to a reaction is calculated as:

$$\Delta S_r = \sum v_i \Delta S_{f,i}$$

The Gibbs free energy, G, is a function of enthalpy and entropy. By definition:

$$\Delta G = \Delta H - T\Delta S$$

The Gibbs free energy is a measure of the energy available in the system to do work (ΔHf) minus the energy stored in random motions in the molecules ($T\Delta Sf$).

Again, Gibbs free energy variation can be defined, exploiting reactants and products properties, as:

$$\Delta G_r = \sum v_i \Delta G_{f,i}$$

Now, consider a general reversible chemical reaction in a closed system:

$$aA + bB \leftrightarrow cC + dD$$

It is possible to define the reaction rate constants of the backword and forward reaction. When equilibrium inside the closed system is reached, the backword and forward reaction rates are equal. As a consequence, the net concentration of the species involved in the reaction keeps constant. If kinetic deals with time dependent variables, in this case the concentration does not change with the passing of time and can be computed as a function of thermodynamic variables such as the equilibrium constant K_{eq}.

$$K_{eq} = \prod_{i=1}^{Nc} a_i^{vi}$$

Where a_i is the activity of the species. The activity is defined as the ratio between a species *fugacity* values calculated at the system temperature and pressure and at a reference state, with the same system temperature and a reference pressure p_r. For an ideal gas system, the fugacity is the partial pressure of the species, thus:

$$K_{eq} = \prod_{i=1}^{Nc} (x_i p_i)^{vi} = p^{\Delta n} \frac{x_c^c x_d^d}{x_a^a x_b^b}$$

Δn is the mole variation in the reaction: $\Delta n = c + d - a - b$.

The equilibrium constant can be related to the Gibbs free energy:

$$\Delta G(T) = -RTlnK_{eq}$$

$$K_{eq} = \exp\left(-\frac{\Delta G(T)}{RT}\right) = p^{\Delta n} \frac{x_c^c x_d^d}{x_a^a x_b^b}$$

This equation, coupled with the energy balance, allows to evaluate the temperature and the equilibrium composition of the reacting system at the equilibrium.

Moreover, knowing the rate for either the forward or reverse direction, from the thermodynamic properties it is possible to compute the rate constant for the opposite process, according to the principle of *microscopic reversibility:*

$$K_{eq} = \frac{kf}{k_b}$$

The last thermodynamic property to be considered for the development of a kinetic mechanism is the heat capacity c. The heat capacity measures the amount of heat required to change the temperature of one mole of a substance by a fixed amount (e.g. 1K). Since the heat capacity is not a state function, it depends on the type of transformation. Therefore, it is possible to define two heat capacities: one computed at constant pressure and the other one at constant volume.

$$c_p = \left(\frac{\partial H}{\partial T}\right)_p \qquad c_V = \left(\frac{\partial U}{\partial T}\right)_V$$

The relationship correlating the two measure is the following:

$$R = c_p - c_v$$

Heat capacities are used into enthalpy balances to compute enthalpy in a state different from the reference one:

$$\Delta H_f(T) = \Delta H_{f,ref}\left(T_{ref}\right) \int_T^{T_{ref}} c_p(T)\, dT$$

And also, to compute the entropy:

$$\Delta S(T) = \Delta S_{ref}\left(T_{ref}\right) \int_T^{T_{ref}} c_p(T)\, dT$$

2.6 Transport Properties

Plug flow reactors, shock tubes, rapid compression machines and batch reactors are used to investigate the kinetics of combustion reaction. However, it may happen that mass and heat transfer phenomena occur at the same timescale of kinetic processes and cannot be neglected anymore. When such phenomena are accounted for in the mass, energy and momentum equations some other properties such as diffusion coefficients, viscosities, thermal conductivities and thermal diffusion need to be estimated for any species in the mechanism.

Chapter 3
OpenSMOKE++

All the kinetic simulations for the model validation were carried out using the OpenSMOKE++ Solver by Cuoci et al.[11] OpenSMOKE++ is an open-source framework written in C++ and conceived to compute numerical simulations of reacting systems with detailed kinetic mechanisms. The framework handles simulations of all types of ideal chemical reactors (plug-flow, batch, and jet stirred reactors), shock-tubes, rapid compression machines. As an input, the solver requires the mechanism with the kinetic parameters in the modified Arrhenius form A, n, E_a (Chapter 2.3), the thermodynamic data in the NASA[12] polynomial format and the transport properties of each species computed according to the standard kinetic theory[13]. In this Chapter further information about the structure and the functioning of the OpenSMOKE++ solver is given.

3.1 The OpenSMOKE++ structure

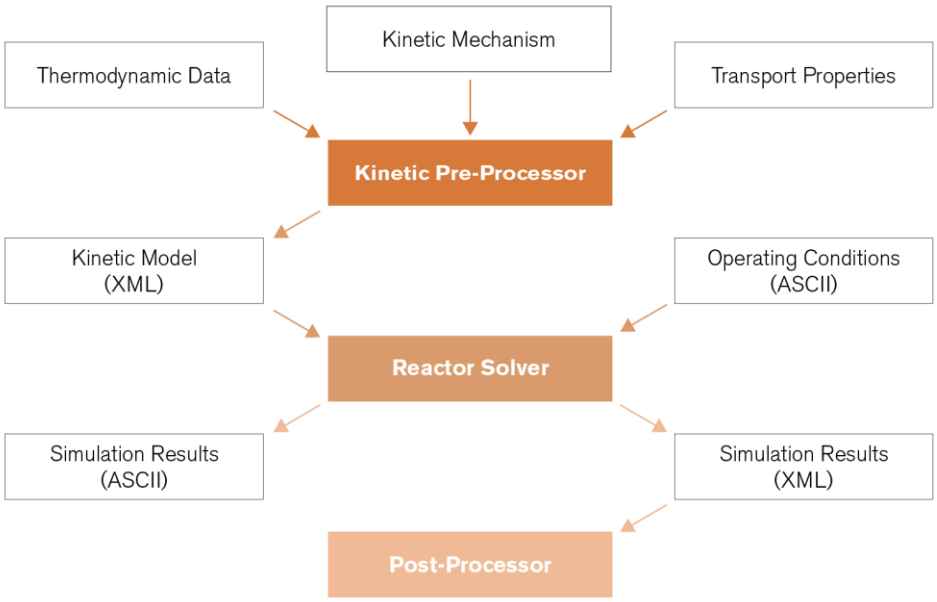

Figure 5 OpenSMOKE++ Suite structure

In Figure 5., it is represented the structure of the software. The first step of the numerical simulation consists in the kinetic pre-processor use. To the kinetic pre-processor three different input files are given: the kinetic mechanism, the transport properties, and the thermodynamic data; as an output, it gives back the kinetic mechanism written in an XML format. This file, combined with the input file in which information about the operating conditions is given, is processed by the reactor solver. When writing the input file, it must be provided not only the temperature and pressure values, but also the type of reactor, the inlet mixture composition and conditions, the output options etc. The simulation outcome is provided in two different formats: XML and ASCII. The XML output can be read by the Post-Processor that runs the sensitivity analysis or the rate of production analysis.

3.2 Kinetic Pre-Processor input files

3.2.1 The Thermodynamic Data File

According to Gordon and Mc. Bride, the thermodynamic properties are expressed through a set of coefficients as follows:

$$\frac{c_{p,i}}{R} = a_{i,1} + a_{i,2}T + a_{i,3}T^2 + a_{i,4}T^3 + a_{i,5}T^4$$

$$\frac{\widetilde{H_i}}{RT} = a_{i,1} + \frac{a_{i,2}}{2}T + \frac{a_{i,3}}{3}T^2 + \frac{a_{i,4}}{4}T^3 + \frac{a_{i,5}}{5}T^4 + \frac{a_{i,6}}{T}$$

$$\frac{\widetilde{S_i}}{R} = a_{i,1}\,ln\,T + a_{i,2}T + \frac{a_{i,3}}{2}T^2 + \frac{a_{i,4}}{3}T^3 + \frac{a_{i,5}}{4}T^4 + a_{i,7}$$

For each species, to determine the variables values in two temperature intervals, two sets of seven parameters are provided.

```
C6H6                    C   6H   6          G    300.00   4000.00 1000.00      1
 1.10809576E+01 2.07176746E-02-7.52145991E-06 1.22320984E-09-7.36091279E-14    2
 4.30641035E+03-4.00413310E+01 5.04818632E-01 1.85020642E-02 7.38345881E-05    3
-1.18135741E-07 5.07210429E-11 8.55247913E+03 2.16412893E+01 9.96811598E+03    4
```

Figure 6 The two sets of thermodynamic parameters written in the thermodynamic input file for the kinetic pre-processor.

Other features include the computation of the kinetic parameters for the reverse rate constants together with explicit ΔGr, ΔHr, ΔSr and the equilibrium constant for every reversible reaction in the mechanism.

3.2.1 The Kinetic Mechanism

For what concerns the kinetic mechanism, in the input file are listed:

1. The chemical elements present in the molecules
2. The involved species
3. The chemical reactions with the kinetic parameters

An example is given:

```
ELEMENTS
C
H
O
N
HE
AR
END
```

Figure 7 Elements present in the CRECK kinetic mechanism

```
SPECIES
AR                  N2                  HE
H2                  H                   O2
O                   H2O                 OH
H2O2                HO2                 CO
CO2                 HOCO                CH4
...
END
```

Figure 8 An example of species in the CRECK kinetic mechanism

```
O+C2H4=CH3+HCO                          7.4530e+06    1.880       183.00

O+C2H4=H+CH2CHO                         6.0980e+06    1.880       183.00

CH4+CH=H+C2H4                           6.0000e+13    0.000         0.00
```

Figure 9 Some of the reactions present in the CRECK kinetic mechanism

As explained in Chapter 2.4, there are reactions whose kinetic constant is pressure dependent. To describe this dependence both TROE formalism and the logarithmic interpolation (PLOG) may be used.

```
C3H8(+M)=CH3+C2H5(+M)             1.2900e+37   -5.840     97380.00
LOW/                              5.64e+74    -15.740      98714.0/
TROE/          0.3100   50.00   3000.   9000./
H2/ 2.00/  H2O/ 6.00/  AR/ 0.70/  CO/ 1.50/  CO2/ 2.00/  CH4/ 2.00/  C2H6/ 3.00/  HE/ 0.70/
```

Figure 10 An example of TROE formalism for pressure dependent rate parameters

In the third line of TROE formalism the third body coefficients for different species are provided.

In the PLOG form parameters computed at different pressures are reported, the calculation of the parameters at intermediate pressure are carried out through interpolation. This is the format in which rate constants calculated in this study will be provided.

```
C2H5OH=H2O+C2H4          3.4100e+59      -14.200         83672.60
 PLOG /  1.000000e-03    3.410000e+59    -1.420000e+01   8.367260e+04     /
 PLOG /  1.000000e-02    2.620000e+57    -1.330000e+01   8.526220e+04     /
 PLOG /  1.000000e-01    1.650000e+52    -1.150000e+01   8.474560e+04     /
 PLOG /  1.000000e+00    5.230000e+43    -8.900000e+00   8.150670e+04     /
 PLOG /  1.000000e+01    4.590000e+32    -5.600000e+00   7.606240e+04     /
 PLOG /  1.000000e+02    3.840000e+20    -2.060000e+00   6.946550e+04     /
```

Figure 11 An example of PLOG formalism for pressure dependent kinetic rate parameters

3.3.3 The Transport Properties Data File

Transport properties data file contains a list of parameters to estimate diffusion and convection properties.

Species	Geometry Index	ε/kB (K)	σ (Å)	μ (D)	α (Å^3)	Zrot
C6H5	2	412.3	5.349	0	0	1
C6H6	2	468.5	5.23	0	10.3	1
C6H5O	2	450	5.5	0	0	1
C6H5OH	2	450	5.5	0	0	1

Table 1 An example of transport properties written in the transport input file.

The geometry index is 0 for atomic species, 1 for linear molecules and 2 for non-linear molecules. The second column parameter (ε /k_B) is Lennard-Jones well-depth, used to measure the strength of attraction forces between interacting molecules. σ is the collision diameter. Long range interactions are accounted for with the dipole moment μ , α is the polarizability and Zrot is the collision number.

3.3 The Input for the Reactor Solver

```
Dictionary PerfectlyStirredReactor
{
@KineticsFolder        ..\..\..\..\POLIMI_21_03;
@Type                  Isothermal-ConstantPressure;
@InletStatus           inlet-mixture;
@ResidenceTime         0.07 s;
@Volume                1 cm3;
@OdeParameters         ODE-Tolerance;
@Options               Output;
@ParametricAnalysis    parametric-analysis;}
Dictionary inlet-mixture
{
@Temperature       950.   K ;
@Pressure          1   atm;
@MoleFractions C6H6  0.001
               O2    0.025
               N2    0.974; }
Dictionary parametric-analysis
{
@Type              temperature;
@NumberOfPoints     20;
@MinimumValue       950 K;
@MaximumValue       1375 K;
@NumberOfThreads   3;}
Dictionary ODE-Tolerance
{
@RelativeTolerance     1e-12;
@AbsoluteTolerance     1e-14;
@MinimumStep       1e-9;
@MaximumStep       1e5;
@MaximumNumberOfSteps 100000;}
Dictionary Output
{
@OutputFolder      POLI2103;
@OutputSpecies     O2  CO  C6H6    CH2O    CO2 H2  C6H5OH  CH4 C2H6    C2H2    C3H6    C5H6    C2H4    C2H3CHO
C4H6   C4H4    C3H4-A  C3H4-P  C7H8;}
```

Figure 12 Example of an input file for the Reactor Solver in OpenSMOKE++

In the input file there are several dictionaries to characterize the simulation and the desired output. The first dictionary gives information about the reactor, the second one about the inlet mixture composition and conditions. The third dictionary allows to run a parametric analysis at different temperatures, the ODE-tolerance dictionary provides parameters to solve the ode-system. In the dictionary output are inserted the species that will be printed in the output file. If added, the sensitivity-analysis dictionary defines the species on which it has to be run.

3.4 The Post-Processor Tools

The post-processor provides several useful tools to perform sensitivity analysis, rate of production analysis and graphical representation of the reaction flow.

Sensitivity analysis is very important for kinetic studies, since it allows to figure out how the numerical solution of the governing equations depends on the various parameters contained in the model itself. Only the first-order sensitivity coefficients with respect to the reaction rate coefficients (pre-exponential factors, activation energy or kinetic constant) can be calculated. Since it is very time consuming, the user has to request explicitly the sensitivity analysis before running the simulation thus, the sensitivity dictionary must be added. The sensitivity analysis results are represented by means of bar charts using the post-processor.

Another useful tool is the ROPA, the result gives information about the reactions responsible of the net production and destruction of species and these too can be visualized by means of bar charts.

The post-processor can also graph the reaction flow of the simulation: starting from a species the post processor lists not only the obtained products, but also the percentage amount of the reactant that has led to the production of the accounted product.

Chapter 4
Theoretical Investigation of Rate Constants

Historically, when developing a kinetic mechanism, the estimation of kinetic parameters was largely based on experimental measurements and approximations from similar reactions involving the same functional groups. The impossibility to directly employ computational chemistry for these estimations was due to both computational limitations and the lack of appropriate theoretical approaches, that have been largely overcome in the last decades. In this chapter, a brief explanation of the methods used in this work for the theoretical estimation of rate constants is provided.

4.1 Rate Constants Determination: Ab-Initio Methodologies

In this thesis work, for the estimation of rate constants, ab-initio transition state theory based master equation calculations (AITSTME) were performed. According to the transition state theory, to determine the rate constants, the knowledge of the vibrational frequencies and energies of reactants, products, and transition state structures is necessary. Such variables were determined by means of ab-initio calculations. Ab initio quantum chemical calculations allow the frequencies and energies computation by solving the electronic Schrödinger equation from first principles, namely with only physical constants as an input. The rate constants determination is the outcome of multi-well RRKM-ME calculations, which allow to define the rate constants considering the competition between all the products and intermediates belonging to the potential energy surface (PES), whose definition is given in Chapter 4.5.

The main limitation of ab initio-based methods is that the computational effort required increases more than exponentially with the level of accuracy to be achieved and with the size of the molecules under investigation. Therefore, for high molecular weight species,

rate rules become a powerful solution, generally allowing to extend the results obtained from lighter species to heavier molecules with a reasonable accuracy. It is also highlighted that integrating quantum chemistry calculations into an already developed and validated model might disrupt error-compensation of inaccuracies within existing mechanism, not necessarily leading to an improvement of the model predictions.

4.2 The Time Independent Schrödinger Equation

The rate constants calculation largely depends on the energy barriers of the reactions; therefore, the computation of the energies is crucial.

The energies are given by the solution of the time independent Schrödinger equation:

$$H\big(\Psi(x,\sigma)\big) = E\Psi(x,\sigma)$$

Where H is the Hamiltonian operator, Ψ is the wavefunction and E is the total energy associated to the system.

The Hamiltonian is a mathematical operator that, applied to a state function, in this case the wavefunction, gives back the associated scalar, that is the energy.

According to the first postulate of quantum mechanics, the wavefunction completely describes the state of the system and, in the time independent form of the Schrödinger equation, it is a function of electron coordinates and spin numbers $\Psi(x,\sigma)$. Moreover, as stated in the fourth postulate of quantum mechanics, the wavefunction squared value $\Psi^2 d\tau$ represents the probability of a particle to be found in the portion $d\tau$ of the phase space where the wavefunction is defined.

The Hamiltonian operator is the sum of the kinetic energy operator T and the potential energy operator V.

These energetic terms refer to all particles belonging to the system: electrons and nuclei. According to the adiabatic and Born-Oppenheimer approximations it is possible to treat nuclei and electrons motions independently. Nuclei and electrons respective masses differ at least of four orders of magnitude thus, electrons speed reaches much higher

values than that of the nuclei. Follows that, because of the fast response of electrons to any change in nuclei configuration, electrons are considered in equilibrium positions. Hence, the motions of the electrons and nuclei may be decoupled and the equation becomes:

$$\frac{-\hbar^2}{2m}\sum_{i=1}^{Nel}\left(\frac{\partial^2\psi}{\partial x_i^2}+\frac{\partial^2\psi}{\partial y_i^2}+\frac{\partial^2\psi}{\partial z_i^2}\right)-\sum_{i=1}^{Nel}\sum_{I=1}^{Nnucl}\frac{z_I e^2}{4\pi\varepsilon_0 r_{iI}}\Psi+\frac{1}{2}\sum_{i=1}^{Nel}\sum_{j=1}^{Nnucl}\frac{e^2}{4\pi\varepsilon_0 r_{ij}}\Psi=E\Psi$$

Where N_{el} is the total number of electrons in the molecule and N_{nucl} is the number of atomic nuclei.

The approximate solution of the multi-electron stationary Schrodinger Equation provides the energy of the electrons. It is necessary to add to this value the repulsive energies belonging to the nuclei, previously neglected because of the Born-Oppenheimer approximation.

The theories used for the solution of this equation are presented in the followings.

4.3 Methods to solve the Stationary Schrödinger Equation

In the last decades, many theories have been developed to solve the electronic Schrödinger equation, among them the Hartree-Fock method (HF) must be mentioned.

Nowadays, it is no more the most common method of solution, indeed, it is useful not only to understand other methods developed afterwards, but also because it is often used in codes to obtain an initial guess for the wavefunction of the system.

The HF method introduces a model known as the "independent-particle model", where once the position of the nuclei has been defined, the Schrödinger equation is solved only for the electrons, considered independent from one another. Their interaction potential

is recovered through the mean-field approximation, where it is assumed that one electron is subject to an average potential (the mean field) generated from all the other electrons. In this way, the electrons may be treated independently. The final aim is to obtain an equation for a single electron, easier to solve. The system to solve is a non-linear system; the iterative computational procedure for the solution is called "self-consistent field" (SCF): in fact, the solution of the equation provides the potential generated by the electrons, which should correspond to the mean-field potential used in the first place. Convergence is reached when the energy and the spin-orbitals undergo no change from one iteration to the following one.

In accordance with the HF method, the wavefunction is expressed as the product between the single wave functions of the single electrons, that can be written as a product of spin-orbitals $X_i(x_i)$. The main limitation of the HF method lies right in the "independent-particle model", that leads to missing repulsion effects. As a consequence, in Hartree-Fock equations, the probability of two electrons with anti-parallel spins to occupy the same position in space is paradoxically not null. The error in the total energy is about 1%, which is however essential for the description of chemical phenomena and bond formation. This difference, that takes into account the missing electrons interactions, is known as correlation energy. The roughness of the results was overcome with the introduction of the Slater Determinant (SD), a new form to express the wavefunction. The SD estimates the interactions between electrons, obeying to the Pauli's exclusions principle. The Slater determinant is computed starting from the matrix of the electrons wavefunctions, where the rows correspond to the N electrons and the columns to the N spin-orbitals.

$$\psi_{el} = \frac{1}{\sqrt{N!}} \begin{bmatrix} X_1(x_1) & \cdots & X_N(x_1) \\ \vdots & \ddots & \vdots \\ X_1(x_N) & \cdots & X_N(x_N) \end{bmatrix}$$

Post-Hartree-Fock approaches are also present in the literature, like single-reference and multi-reference methods, which however may require a very high computational effort. In the single reference methods, a single Slater determinant is enough to describe the system. In the multireference methods, it is a set of determinants to constitute the model space, due to the mixing of different electronic states with small energy gaps.

A lot of effort was put in the development of electron correlation methods to include the missing correlation energy. Among these, the Coupled Cluster (CC) is probably the most used. It introduces a new way to obtain an excited Slater Determinant (SD): to the reference wavefunction it is added an operator exp(T) which generates the excitations.

The coupled-cluster singles, doubles and triples excitations (CCSDT) with subsequent extrapolation of the energies to the basis-set limit is the desirable standard. As this is hardly achievable, more common methods include the CCSD(T) methods, with perturbative inclusion of triple excitations. The application of such methods to systems with up to ~10 "heavy" atoms requires the adoption of a computationally suitable basis sets. Basis sets are used to represent the electronic wave turning the partial differential equations of the model into algebraic equations. The accuracy of the theoretical methods employed competes with the chosen basis-set: it is not possible to maximize both, otherwise the computational cost becomes not sustainable.

An alternative approach to Hartree-Fock is Density Functional Theory (DFT). DFT methods are based on Hohenberg and Kohn theorem, according to which the electronic energy may be completely determined from the electron density. The main advantage is that the electron density is only function of three spatial coordinates, thus significantly reducing the computational cost. Hence, the number of degrees of freedom is reduced from 3Nel to 3. Furthermore, the result is in principle exact, and this is why a lot of research is still focused on the development of such functionals. Then, the main challenge of DFT methodologies is to define a functional creating the one-to-one connection between electron density and electron energy. The main limitation of DFT methods lies in neglecting dispersion interactions that might be relevant for large systems. New DFT functionals have been recently proposed to overcome this problem: for example, the M05- and M06-2X of Zhao and Truhlar[14–16] and the B2PLYP-D3 of Grimme and coworkers[17].

Post-Hartree-Fock and DFT methods have been implemented in commercial computational software like Gaussian[18] and Molpro[19], used also in this work.

4.4 Statistical Mechanics

Statistical mechanics describes the macroscopic variables of a system as a function of microscopic parameters whose exact value is not cognizable, and it is assumed equal to the average value around which they fluctuate. According to Heisenberg uncertainty principle, it is impossible to completely describe the state of a system therefore, it must necessarily be treated with a statistical approach.

If ordinary mechanics takes into account the behaviour of a single state, statistical mechanics introduces the essential concept of statistical ensemble, which includes all the possible physical states of the system.

The number of states accessible to a system is accounted for by partition functions. The main advantage of partition functions is that they are directly related to macroscopic thermodynamic variables such as internal energy, entropy, Helmholtz free energy, and Gibbs free energy. Finally, transition state theory exploits the physical meaning of partition functions in order to derive rate constants of reactions with a well-defined saddle point, as discussed in *section 4.6.*

In the next paragraph, a discussion of statistical thermodynamics notions will be provided.

4.4.1 Statistical Thermodynamics

Given a system of N particles, the probability that a particle is in a given Ni state of energy 'e_i' is provided by the Boltzmann distribution, i.e. the most probable distribution for N particles at thermal equilibrium:

$$\frac{Ni}{N} = \frac{\exp\left(-\frac{e_i}{k_B T}\right)}{Q}$$

Where k_B is the Boltzmann constant (~1,381 × 10^{-23} $\frac{m^2 Kg}{s^2 K}$). Q is the normalization factor of the given distribution and is therefore defined as:

$$Q = \sum_i g_i \exp\left(-\frac{e_i}{k_B T}\right)$$

Where g_i is the grade of degeneracy: the number of states which have the same energy level. Hence, in this case the sum runs over the energy levels of the system rather than the states.

Considering a microcanonical ensemble of N molecules, the corresponding partition function Q accounts for the number of states that are accessible to a molecule at a given temperature T. It includes all the energy states associated to vibrational, translational, rotational and electronic "motions" of the molecule.

Assuming independent degrees of freedom (i.e. translational, rotational, vibrational, electronic) where the energy can be stored, Q may be derived as the product of individual partition functions representative of these degrees of freedom. In the space each non-linear molecule with N atoms has $3N$ degrees of freedom, namely 3 translational motions, 3 external rotations of the molecules (2 for linear molecules) , and the remaining $(3N-6/5)$ are vibrational modes. In a quantum system, the energy levels of each type of motion are derived by solving the time-independent Schrodinger equation with the appropriate potential energy and boundary conditions. The partition function is then derived as above.

Starting from the translational motion, the solution is obtained by modelling a particle of mass m, moving inside a volume V, at a defined temperature T. The solution is computed by setting a 1D problem, decoupling the three motions along the three different axis x,y,z. The translational partition function Q_T is

$$Q^t = Q_{T,x}\, Q_{T,y}\, Q_{T,z} = \left(\frac{2\pi m k_B T}{h^2}\right)^{\frac{2}{3}} V$$

Where h is the Planck constant ($\sim 6.626 \cdot 10^{-34}\, \frac{m^2 kg}{s}$).

The partition function QR represents the external rotational motion, which for a non-linear molecule is expressed as a function of its three rotational constants $I_{x,x}$, $I_{y,y}$, $I_{z,z}$ that

are the inertia momentums calculated with respect to the three principal axes of the molecule.

$$Q^r = \frac{8\pi^2(2\pi m k_B T)^{\frac{3}{2}}}{\sigma h^3} \sqrt{\mathrm{I}_{x,x}\ \mathrm{I}_{\mathrm{y,y}}\ \mathrm{I}_{\mathrm{z,z}}}$$

Where σ represents the external symmetry number.

Finally, the vibrational partition function is estimated by adopting the rigid rotor harmonic oscillator model (RRHO), according to which the atoms of a molecule oscillate around their equilibrium positions and the bonds are modelled as strings. Coherently with this last assumption, Hook's law describes the displacements of the atoms with respect to the equilibrium positions, and the corresponding restoring force is:

$$F = -kx$$

The proportionality constant is the elastic constant, directly related to vibrational frequencies: $\nu = \sqrt{\frac{k}{m}}$.

The vibrational energy of an oscillator is never null, not even at 0 K. Its minimum energy, calculated at 0 K, is known as zero point energy (ZPE) whose value is:

$$ZPE = \frac{1}{2}h\nu$$

The vibrational partition function assumes the following form:

$$Q^{vib} = e^{-\frac{ZPE}{k_B T}} \prod_{i=1}^{3N-6} \frac{1}{1 - e^{-\frac{h\nu_i}{k_B}T}}$$

The ν_i frequencies must be found experimentally or by means of ab initio methods.

The RRHO approximation fails for "anharmonic" internal motions generally characterized by low vibrational frequencies (i.e. low energies). In many cases, these motions

correspond to internal torsions of the molecule. The corresponding partition function may computed with the 1-dimensional hindered rotor model.

In the end, the last partition function characterizing the energy content of the molecule is the electronic one:

$$Q^{el} = \sum_i g_{el} e^{-\frac{E_{el}}{k_B T}}$$

Because commonly the separation between the ground state and excited electronic states is high, only the electronic ground state of the molecule is considered (Eel=0), with the exception of molecules with quasi-degenerate low-lying electronic energy levels such as OH and O_2. Hence, in most cases, the expression of the electronic partition function is simply the electronic degeneracy of the ground state.

4.4.2 Estimation of the equilibrium constant from the partition function

The above-described molecular partition functions can be used to calculate the equilibrium constant of a chemical reaction. To prove this correlation, it is necessary to introduce Z:

$$Z = \sum_{i=1}^{N_{particles}} \frac{(\sum Q_i^N)}{N!}$$

Z is the partition function related to the system and it is used to express thermodynamic variables:

$$F = -k_B T \, lnZ \; = -k_B T ln\left(\frac{Q^N}{N!}\right) = -k_B T(NlnQ - lnN!) \cong -k_B T(NlnQ - NlnN + N)$$

Remembering that N is the total number of particles, which can be expressed as the product between the number of moles n and the Avogadro number N_{Av}, and:

$$\tilde{G} = \tilde{F} + P\tilde{V} = \frac{F}{n} + P\tilde{V}$$

The following expression for $\tilde{G}$ is obtained:

$$\tilde{G} = -RTln(\frac{Q}{N})$$

For the thermodynamical definition of the equilibrium constant:

$$k_{eq} = \exp\left(-\sum_{i=1}^{N_{components}} \frac{v_i G_i^0(T, p_{ref})}{RT}\right) = \exp\left(\sum_{i=1}^{N_{components}} v_i ln Q_i/N_{ref}\right) = \prod_{i=1}^{N_{comp}} \left(\frac{Q_i}{N_{ref}}\right)^{v_i}$$

$$k_{eq} = \prod_{i=1}^{N_{comp}} \left(\frac{Q_i}{N_{ref}}\right)^{v_i} = \prod_{i=1}^{N_{comp}} C_i^{v_i}$$

4.5 Theoretical Framework of Transition State Theory

Before introducing transition state theory, the concepts of potential energy surface (PES) and minimum energy path (MEP) are clarified.

The configuration assumed by each molecule at a specific stable state minimizes the total energy content of the system. From a mathematical point of view, the function that relates the energy content to the atoms positioning is the potential energy surface (PES). A chemical reaction changes the molecule configuration thus, it is possible to figure a chemical reaction like a movement along the PES from one local minimum to another. The possible feasible trajectory to follow are multiple but the most favoured one minimizes the energy as it connects the reactants and products, and is therefore known as minimum energy path. According to this, the "reaction coordinate" describing the evolution of a molecular configuration from reactants to products can be defined as the curvilinear coordinate that defines the MEP.

A reaction path may present or not an energy maximum, known as reaction barrier. According to this characterization, reaction profiles are divided into barrier and barrierless types. The former is characterized by a well-defined saddle point along the MEP known as transition state (TS) or activated complex. In order to make a reaction occur, the reactants must overcome the transition state barrier, which is the bottleneck

for the reactive flux. In fact, its proper physical definition is as the dividing surface separating reactants from products that minimizes the reactive flux crossing it. With reactive flux it is intended the number of molecules that turn into the activated complex. For systems with well-defined barriers, the TS passes through the saddle point on the PES and it is orthogonal to the reaction coordinate. The quantification of this flux into a rate constant is explained in the next section.

4.6 The Transition State Theory

As already mentioned in the Chapter 4.4.1, it is possible to compute the rate constant as a product of partition functions. This relation has been postulated in the transition state theory (TST).

Transition state theory relies on five main assumptions, divided into two fundamental hypotheses and three restrictive hypotheses.

1. According to the Born-Oppenheimer approximation, the motion of nuclei and electrons can be treated independently, thus, during the translational movements of nuclei, electrons are considered in the equilibrium positions.

2. The velocity distribution of the molecules is described by the Maxwell-Boltzmann distribution.

The restrictive hypotheses of the transition state theory are:

1. Non-recrossing assumption: once the reactants have reached the transition state (TS,≠) configuration, it is no more possible for them to go back to the configuration of the reactants, they can only proceed to the formation of products. The non-recrossing assumption represents the most restrictive among the hypotheses of the TST.

2. At the transition state, the motion along the reaction coordinate is separated from the rest of the internal motions of the nolecule, and it can be treated as a translation. This assumption lies on the observation that, along the reaction coordinate, it is possible to identify an interval in which the potential energy surface is flat thus, being the potential constant, the motion is treated as a translation.

3. Between the reactants and the transition state molecules an equilibrium is established.

The transition state theory introduces the concept of reaction rate as a measure of the probability that a molecule passes through transition state barrier. Therefore, it is possible to define the rate of reaction as the flux of molecules that crosses the transition state configuration per unit of time and volume. In mathematical terms,

$$r = v\, C_{\neq}$$

Where v is the crossing frequency of the transition state and $C_{\neq}$is the molecules concentration at the transition state.

In the following paragraph the mathematical steps to find out an expression for the rate constant are presented.

4.6.1 Mathematical derivation of the rate constant

Starting from the last hypothesis, it is possible to consider the reactants in equilibrium with the activated complex that, because of the first restrictive hypothesis, goes directly to the products.

$R \rightleftarrows X^{\neq} \rightarrow P$

The molecular concentration of species at the TS can be computed from the partition functions as follows:

$$\mathrm{C}_{\neq} = \frac{\mathrm{Q}_{\neq}}{Q_R} C_R$$

For what concerns the estimation of the frequency factor, by exploiting the first fundamental hypothesis, it is possible to imagine the passage through the TS as a translational motion characterized by a velocity v_{δ}. As all the molecules are not able to reach the products configuration and considering a covered distance equal to δ, the final expression of the frequency factor becomes:

$$v = \frac{\mathrm{v}\delta}{2\delta}$$

By substitution:

$$r = \frac{\mathrm{v}\delta}{2\delta}\frac{\mathrm{Q}_{\neq}}{Q_R}C_R = k_c C_R$$

The final expression for the rate constant is derived as follows: v is expressed as the average velocity of Maxwell-Boltzmann distribution and, the partition functions, are expressed as the product of their independent contributions Qtr, Qvib, Qrot, Qel.

Focusing on the vibrational partition function, it is important to highlight that the vibrational frequency corresponding to the motion along the TS is imaginary. Actually, at the TS, for any displacement there is a reduction of the energy content; according to the RRHO approximation, the potential is expressed as an elastic one thus, being the displacement positive, to get a negative energy gradient, the elastic constant k must be negative, hence resulting in an imaginary frequency. This allows to easily identify the TS in the electronic structure calculations.

At the TS, the vibrational partition function is subjected to some changes: it is no more associated to 3N-6 internal molecular motions of vibration, but to 3N-7, because one of the internal motion degenerates into a translational motion.

The final expression for the kinetic constants becomes:

$$k_c = \frac{\mathrm{v}_\delta}{2\delta}\frac{\mathrm{Q}_{\neq}}{Q_R} = \frac{\sqrt{\frac{2k_bT}{\pi m}}}{2\delta}\frac{Q_{\neq}^{t\,/1D}\,Q_{\neq}^{vib\;3N-7}Q_{\neq}^{t}Q_{\neq}^{r}Q_{\neq}^{el}}{Q_R^{t}\,Q_R^{vib}Q_R^{r}Q_R^{el}} = \frac{k_bT}{h}\frac{Q_{\neq}^{vib\;3N-7}Q_{\neq}^{t}Q_{\neq}^{r}Q_{\neq}^{el}}{Q_R^{t}\,Q_R^{vib}Q_R^{r}Q_R^{el}}$$

By making explicit the electronic partition function and the term of the vibrational partition function containing the zero point energy, it is possible to define the Ea, or activation energy, that appears in the most generic form of the rate constant formula.

$$k_c = \frac{k_bT}{h}\frac{Q_{\neq}^{vib\;3N-7}Q_{\neq}^{t}Q_{\neq}^{r}Q_{\neq}^{el}}{Q_R^{t}\,Q_R^{vib}Q_R^{r}Q_R^{el}} = \frac{k_bT}{h}\frac{Q_{\neq}^{vib\;3N-7}Q_{\neq}^{t}Q_{\neq}^{r}e^{-\frac{ZPE_{X\neq}}{k_BT}}g_{\neq}^{el}e^{-\frac{E_{\neq}^{el}}{k_BT}}}{Q_R^{t}\,Q_R^{vib}Q_R^{r}g_R^{el}e^{-\frac{ZPE_R}{k_BT}}e^{-\frac{E_R^{el}}{k_BT}}}$$

$$k_c = \frac{k_bT}{h}\frac{Q_{x\neq}^{vib\;3N-7}Q_{x\neq}^{t}Q_{x\neq}^{r}}{Q_R^{t}\,Q_R^{vib}Q_R^{r}Q_R^{el}}g_{x\neq}^{el}e^{-\frac{Ea}{k_BT}}$$

Thus, the activation energy is equal to:

$$Ea = (E_{el} + ZPE)_{X\neq} - (E_{el} + ZPE)_R$$

Concisely, the most general form of the expression of the kinetic constant predicted by transition state theory becomes:

$$k_c = \frac{k_b T}{h} \frac{\mathrm{Q}_{\mathrm{X}\neq}}{Q_R}$$

4.6.2 The thermodynamic formulation of the TST

Remembering that, up to some multiplicative constants related to the reference concentrations, the ratio of the partition functions is equal to the equilibrium constant of a chemical reaction, and that this is equal to the variation of the standard free energy of the reaction divided by RT:

$$k_c = \frac{k_b T}{h} \frac{\mathrm{Q}_{\neq}}{Q_R} = C e^{\frac{\Delta S^{\circ}_{X\neq}}{R}} e^{\frac{-\Delta H^{\circ}_{X\neq}}{RT}}$$

This formulation is known as thermodynamic formulation of the transition state theory. This awards a physical meaning to the kinetic parameters: the Arrhenius pre-exponential factor is proportional to the exponential of the entropy variation established between the reactants and the transition state configurations, whereas, the activation energy portrays the energy jump that occurs by passing from the first to the second.

4.7 The Variational Transition State Theory

The transition state theory above presented, also defined as classical TST, has a limit: it is not able to characterize neither barrierless reactions (i.e. without a well-defined saddle point), such as many dissociation reactions of interest for radicals chemistry, nor reactions with a very loose transition state, where the minimum flux is not reached at the TS but at a different -variable- location along the MEP. The TST that deals with this problem is known as variational transition state theory (VTST). A full explanation of VTST can be provided as long as the definition of barrierless reactions and the difference between a tight and a loose transition state is highlighted.

A TS is defined “tight” when its configuration is geometrically similar to that of the reactants, hence the ratio between their rotational and vibrational partition functions is close to one. This is in general typical of reactions whose energy barrier is high and narrow.

A loose TS is characterized by a very different configuration with respect to the reactants. In this case, as the TS vibrational and rotational partition functions increase, the rate constant becomes higher. This behaviour is typical of reactions with a low and wide energy barrier. A barrierless reaction can be defined as an extreme example of loose transition state: being the products at the maximum energy, for the classical transition state theory, the TS configuration would coincide with the products one, the energy increases indefinitely up to a constant value. This means that for a barrierless reaction the non-recrossing hypothesis does not hold.

VTST identifies the rate constant as that corresponding to the minimum reactive flux along the MEP. This assumption is based on the concept that, being the rate constant a measure of the flux of molecules passing through a specific portion of the potential energy surface, likely, its minimum value is registered at the transition state. The VTST sets the rate constant calculated accordingly to the classical transition state theory as its upper limit value. In the past years, more accurate theories for the calculation of rate constants for barrierless reactions were provided, such as VRC-TST.

4.8 RRKM-ME Theory

TST is unable to account for any pressure dependence of rate coefficients. A possible way to account for pressure dependence is the use of Master Equation calculations which include RRKM theory for the calculation of the microcanonical rate constant k(E).

The concept central to pressure dependent kinetics is that molecules in the gas-phase can increase their internal energy through excitation induced by a collision with other molecules in the bath gas; hence, a large number of collisions (high pressure) changes the energy distribution in the molecules and therefore their probability to react.

According to what already explained in Chapter 2.4, Lindemann theory was not able to describe the pressure dependence of unimolecular reactions due to the hypothesis that the activated state can be described by only one molecular conformation. Actually, the activated state structure is a function of the vibrational energy amount reached after intermolecular collisions. Thus, a reactant molecule does not exist just in its fundamental vibrational energy state, but in N energy states, where N varies from 1 to ∞, whose existence is justified by the infinite dynamics of intermolecular collision through which a vibration stores energy in quanta $h\nu$ till an equilibrium value at high pressure.

RRKM theory provides a description of the rate constant in its microcanonical form, i.e. as a function of the energy of the system. In RRKM theory, it is considered that the total energy of the system E is redistributed among the harmonic vibrational motions of the molecule and the translational motion associated to the TST reaction coordinate. The reaction can only occur when the energy content overcomes the energy barrier. Naming P(E*) the probability that the system reaches the energy $E^*>E_a$, and supposing that the molecules velocity is equal to $\frac{v(E)}{2\delta}$, the kinetic constants can be defined as:

$$k(E^*) = \int_{Ea}^{E^*} \frac{v(E)}{2\delta} P(E)\, dE$$

Where P(E) is the probability that the total energy E* is split such that E goes into the internal translation and E*-E goes into the other vibrational DOFs.

mathematically, P(E) can be expressed in terms of density of translational and vibrational energy states:

$$P(E) = \frac{\rho^{vib}(E^* - E)\rho^{tr}(E)}{\rho^{vib}(E^*)}$$

Where ρ is the density of states. With some mathematical manipulation, the microcanonical rate constant is expressed as

$$k(E^*) = \int_{Ea}^{E^*} \frac{\rho^{vib}(E^* - E)}{h\,\rho^{vib}(E^*)} dE$$

With the RRKM theory, k(E*) is computed. Still keeps unknown the population n(E*) of the E* energy level. This is defined by the resolution of the Master Equation. The Master Equation is able to describe the evolution of this population as:

$$\frac{dn(E^*)}{dt} = Z \sum_{E^I=0}^{E_{max}} \left(P(E^*, E^I)n(E^I) - P(E^I, E^*)n(E^*)\right) - k(E^*)n(E^*)$$

Where Z is the number of collisions per unit time and volume, in which is contained the pressure dependence being a function of the concentration of the third body. $P(E^*,E^I)$ is the probability that a molecule with energy E^I moves to energy E* after a collision.

These probabilities may be determined according to the collisional exponential-down model:

$$P(E^*, E^I) = \frac{1}{C(E^I)} \exp(-\frac{E^I - E*}{\Delta E_{down}})$$

Where $C(E^I)$ is the normalization constant and ΔE_{down} represents the average energy lost upon a collision. ΔE_{down} is generally expressed as a function of temperature. In this work, the following expression was adopted:

$$\Delta \mathrm{E_{down}} = 260 \cdot \left(\frac{\mathrm{T(K)}}{298}\right)^{0.875}$$

The resulting problem is a complex integral-differential equation.[20] The final rate constant at the considered T and P will be obtained as:

$$k_{T,P} = \sum_{Ea}^{Emax} n(E^*)k(E^*)$$

Chapter 5
EStokTP

The determination of rate constants for each channel of the designed PES was performed using EStokTP[20], a modular computational environment designed to perform calculations to get a-priori predictions of temperature and pressure dependent rate constants k(T,P). As already highlighted, the software allows to compute rate constants starting from a first guess of the geometry of the molecules involved in the form of a z-matrix. Automatized protocols implemented for different reaction types (e.g. beta-scission reactions, H-atom abstraction reactions, isomerization tractions) allow to search for a specific transition state starting from the geometries of the reactants or of the products. In order to run the different modules for rate constants extrapolation and geometries optimization, EStokTP[19] relies on commercial software such as Gaussian and Molpro for electronic structure calculations, and MESS for Master Equation simulations.[20] The modules characterizing the EStokTP[20] algorithm are described as follows.

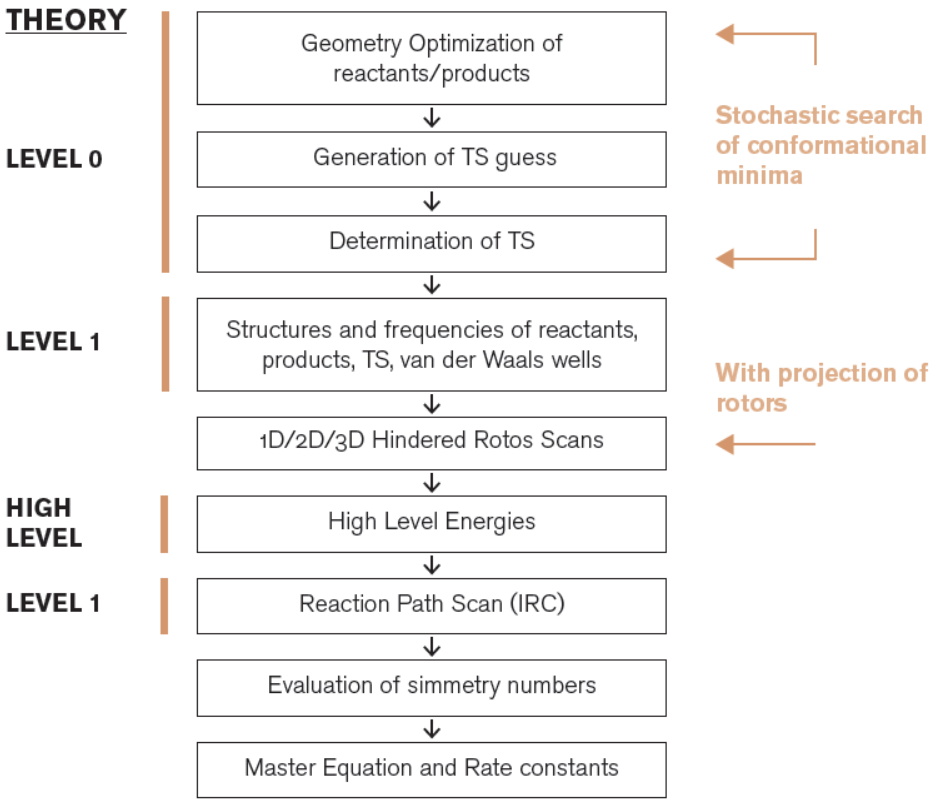

Figure 13 EStokTP modular structure.

5.1 Determination of Level 0 Geometries

The first step aims at a first geometry optimization performed at DFT level, (in this work wb97xd/6-31+g(d,p)), giving in input just the z-matrix guess. From the latter, EStokTP[19] generates a user specified number of starting structures with randomly chosen dihedral angles if necessary. The determined minimum energy structure is then used for successive calculations. No frequencies are computed in this step.

If dealing with the determination of a TS configuration, the z-matrix guess in input is not required. In this thesis work, mainly beta-scission and isomerization reactions were investigated and, being unimolecular, the TS z-matrix was built starting from the one of the single reactant. The user should provide the reaction type and the reaction coordinate, along which a constrained scan provides a first guess of the TS, identified as the configuration with the highest energy among the sampled points. In defining the reaction coordinate, the two atoms involved in the bond-breaking (beta-scission) or formation (isomerization) process are specified, giving also the upper and lower limit for the distance to be scanned. The TS geometry optimization is then performed with the level of theory chosen.

5.2 Determination of Level 1 Geometries and Vibrational Frequencies

At level1 further geometry optimization and frequency calculation is performed, generally using a bigger basis set (in this work, wb97xd/6-311+g(d,p)). The algorithm used in the code uses as a starting point the geometry obtained at level 0. The frequencies are then computed on the geometries optimized at this level.

5.3 Hindered Rotors Scan

EStokTP is able to include anharmonic torsions treating them as hindered rotors. To do so, the potential of the hindered rotation must be calculated. Hence, hindered rotors may be scanned at a user-specified interval. This step reveals to be crucial: the HR PES may provide negative energies indicating that the initial configuration does not correspond to the absolute energy minimum, making necessary to restart a part of the calculations. Once the scan is completed, the frequencies list is updated by automatically removing the vibrations corresponding to the torsional motions investigated. The hindered rotor PES and the new projected frequency list are saved for successive calculations.

In the code, it is also possible to include coupled (2D or 3D) hindered rotors.

5.4 High-Level Energies

An accurate energy estimation is performed at the High Level (HL) step. In this work, MOLPRO was used. The HL calculations are the most time consuming because requiring the largest computational effort. Coupled cluster calculations were performed at level CCSD(T)/aug-cc-pVTZ. The energy was then corrected using MP2/aug-cc-pVTZ and MP2/aug-cc-pVQZ to converge to the basis set limit, also including core corrections using cc-PVTZ basis set. The final energy was therefore obtained as

$$E = E_{CCSD(T)/aug-cc-pVTZ} + \left(E_{MP2/aug-cc-pVQZ} - E_{MP2/aug-cc-pVTZ}\right) + (E_{CCSD(T)/cc-pcVTZ} - E_{CCSD(T)/cc-pVTZ})$$

5.5 Reaction Path Scan

Before estimating the rate constant, it is possible to run a check on the evolution of the molecular configuration along the reaction path. This is possible by means of an optional intrinsic reaction coordinate (IRC) scan that helps to confirm that the specified TS connects the desired reactants and products. Additionally, in case variational calculations are needed, the IRC rebuilds the MEP at level1, computing the Hessian at every step, and

allowing the implementation of VTST, getting variational corrections to the conventional TST rate predictions. In order to be consistent with the set of vibrational frequencies computed at theory level 1, IRC calculations must be performed at the same theory level1.

5.6 Master Equation and Rate Constants Computation

At this step, the MESS code[19] is launched. All the required input data are automatically generated, and the output provides the pressure and temperature dependent kinetic rate constants for single reaction channels in the selected range of temperature and pressure.

5.7 The Multichannel RRKM Calculations

The same procedure cannot be applied for multi-well reactions, i.e. PES with multiple interconnected wells. When dealing with a full PES, different scenarios can occur:

1. Well-skipping, when the energy is high enough to jump from a configuration to another without the thermal stabilization of one or more intermediate wells.
2. The formation of thermally stable intermediates, for instance when a molecule at the configuration of the well collides and stabilizes transferring its energy to another complex.

For this reason, it is used an alternative formulation of the master equation for complex-forming chemical reactions with multiple wells and bimolecular products[21], always solved employing MESS. This reformulation, incorporated in the employed code, yields compact expressions for the phenomenological rate coefficients describing all chemical processes, i.e., internal isomerization reactions, bimolecular-to-bimolecular reactions, isomer-to-bimolecular reactions, and bimolecular-to-isomer reactions.

Chapter 6
CRECK Starting Model and Previous Studies on C6H5+O2.

The aim of this work is to refine the already existing kinetic detailed mechanism of the CRECK research group by estimating new rate constants using ab-initio methods for the phenyl radical oxidation ($C_6H_5+O_2$). Phenyl radical precursor is benzene, the first aromatic compound, which is also a key player for soot formation, therefore, its combustion reaction steps are pivotal to build a well-predictive kinetic mechanism. The following paragraph provides an insight into the CRECK kinetic detailed mechanism, which is the starting mechanism on which the calculated rate constants have been implemented. The model validation takes place by means of a large database of experimental data which is presented in this chapter. Follows a highlighting of the key simulations that have revealed the importance of the investigated reactions.

6.1 The Experimental Database

The model validation occurs by means of a set of simulations, performed by the OpenSmoke++ code, shaping the experimental database. Experimental data are categorized by the type of reactor and the operating conditions. In this chapter, only the most remarkable results to grasp the mechanism room of improvement are shown, but in the following table there is a summary of the whole experimental database used in this work. In Table 3 and in Table 4 are shown experimental database related to catechol and guaiacol oxidation and pyrolysis. These species are of interest for this study because phenyl is a precursor for their formation. This correlation will be highlighted in the next paragraphs.

In the reported plots, the mechanism CRECK_20_03, was named as STATE OF THE ART, just to point out that these are the performances of the current CRECK mechanism.

Benzene Database

Experimental data	Reactor type	Temperature (K)	Pressure (atm)	Equivalence ratio (ϕ)
CHAI	JSR (jet stirred)	900	0.46	0.19/1.02
DaCosta	JSR	923	1	1.9/3.6
Machal	JSR	950	10	0.5/1
Ristori	JSR	950	1	0.3/0.5/1/1.5
Brezinsky	PFR (plug flow)	1102	1	0.76/1/1.36
Venkat	PFR	1120	1	0.2
Burcat	ST (shock tube)	1200-1750	2.44	1/2/0.5
Burcat	ST	1200-1750	6.2	1
DaCosta	ST	1750 -2000	7.5	1.5/3
Da Costa	ST	1750 -2000	8.5	0.5/1
Da Costa	ST	1750 -2000	9	1
Comandini	ST	1226-1774	20	∞

Table 2 Benzene experimental database.

Catechol Database

Experimental data	Reactor type	Temperature (K)	Pressure (atm)	Equivalence ratio (ϕ)
Thomas	PFR	950-1275	1	0.22/0.58/0.92
Thomas	PFR	950-1275	1	∞
Wornat	PFR	950-1275	1	∞
Wornat (C2H2 mix)	PFR	950-1275	1	∞

Table 3 Catechol experimental database.

Guaiacol Database

Experimental data	Reactor type	Temperature (K)	Pressure (atm)	Equivalence ratio (ϕ)
Nowakoska	JS	650-950	1.06	1

Table 4 Guaiacol experimental database.

Benzene Premixed Flames

Experimental data	Temperature (K)	Pressure (atm)	Equivalence ratio (ϕ)
Bakali	450-1500	0.05	1
Bittner	400-1600	0.03	1.8
Tregrossi	500-1800	1	1.8

Table 5 Benzene premixed flames experimental database.

6.2 Benzene Oxidation in JSRs

6.2.1 Ristori et al.[21]

The first results (Figure14 and Figure15) come from the simulation for benzene oxidation in a jet-stirred reactor at atmospheric pressure. The considered temperature range was T=950-1350 K and the system is evaluated at different equivalence ratio: 0.3, 0.5, 1 and 1.5 in accordance with data reported by Ristori et al.[22]

At lean conditions (ϕ=0.3), comparing the model prediction with the experimental data, a general overrating of benzene reactivity is grasped. At high temperature, oxygen is subject to a steep reduction, almost the same applies for benzene. At phi=0.5 this trend is still present, but less evident. On the other hand, CO is underestimated, and CO2 is produced at lower temperatures compared to experimental data. Overall, in lean conditions the CO and CO2 trends are quite well described, whereas, in stochiometric and rich conditions there is a delay in their production. At ϕ=1/1.5, the system reactivity decreases, consuming both oxygen and benzene slowly.

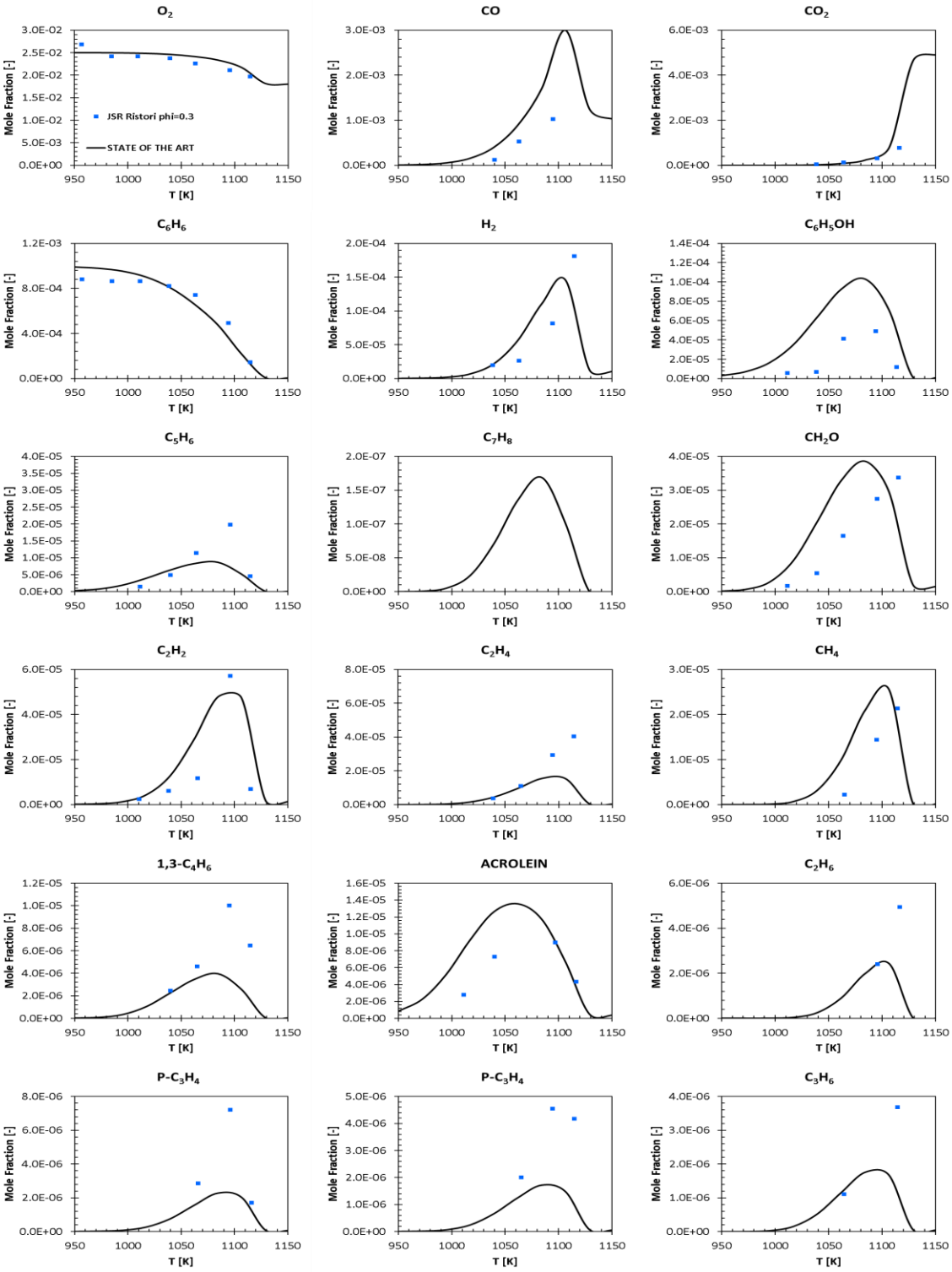

Figure 14 Ristori et al. experimental data (squares) for a jet stirred reactor with an equivalence ratio φ=0.3 at 1 atm. The model prediction is represented by the solid lines.

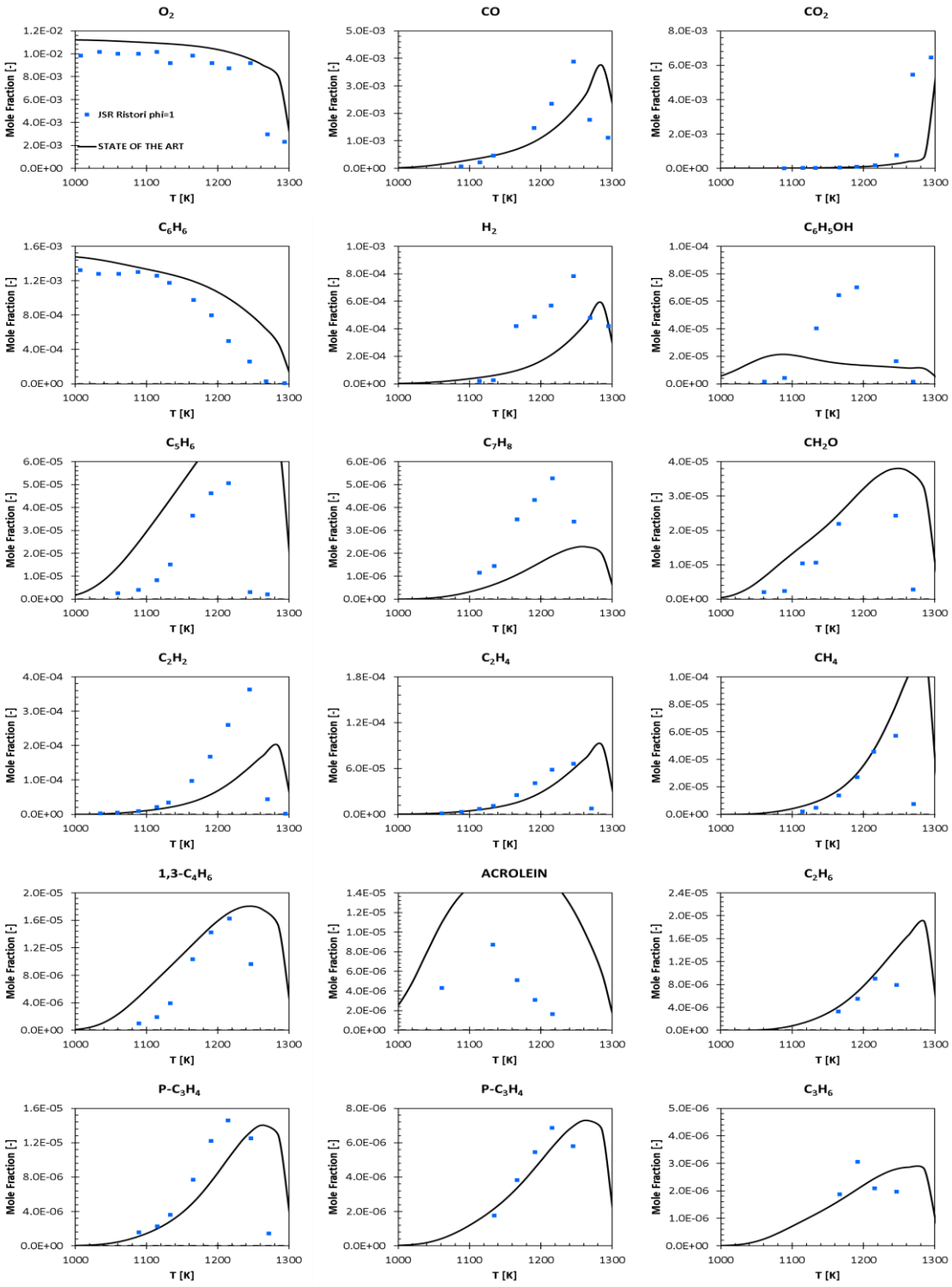

Figure 15 Ristori et al. experimental data (squares) for a jet stirred reactor with an equivalence ratio φ=1 at 1 atm. The model prediction is represented by the solid lines.

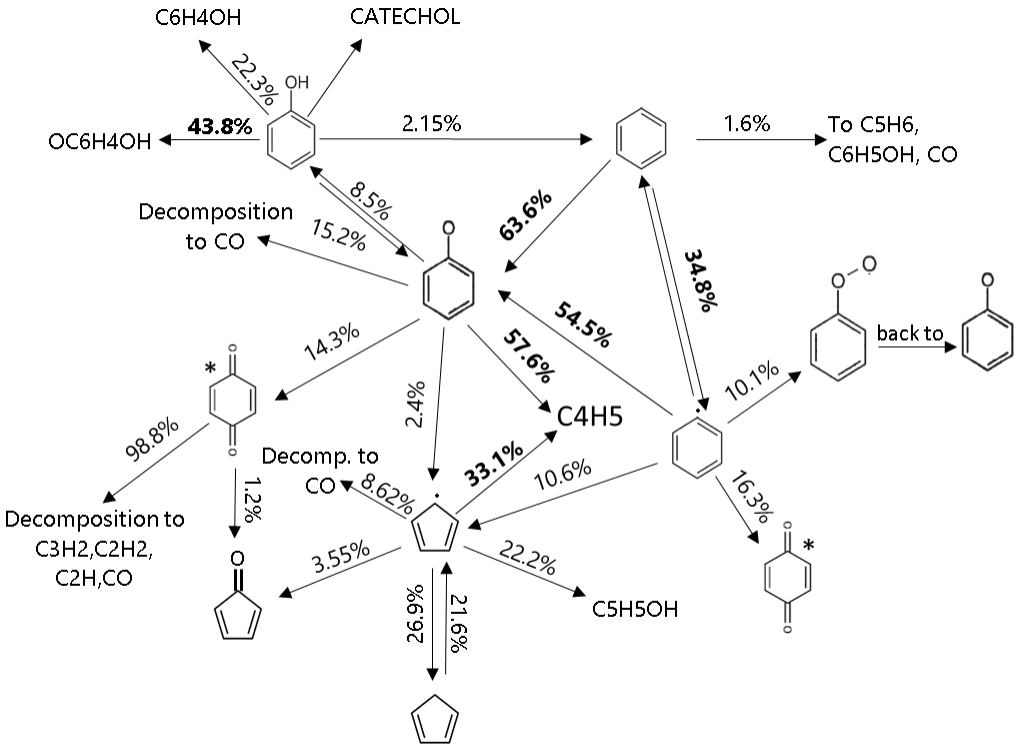

Figure 17 Reaction path analysis for benzene oxidation in a JSR at atmospheric pressure and φ=0.3.

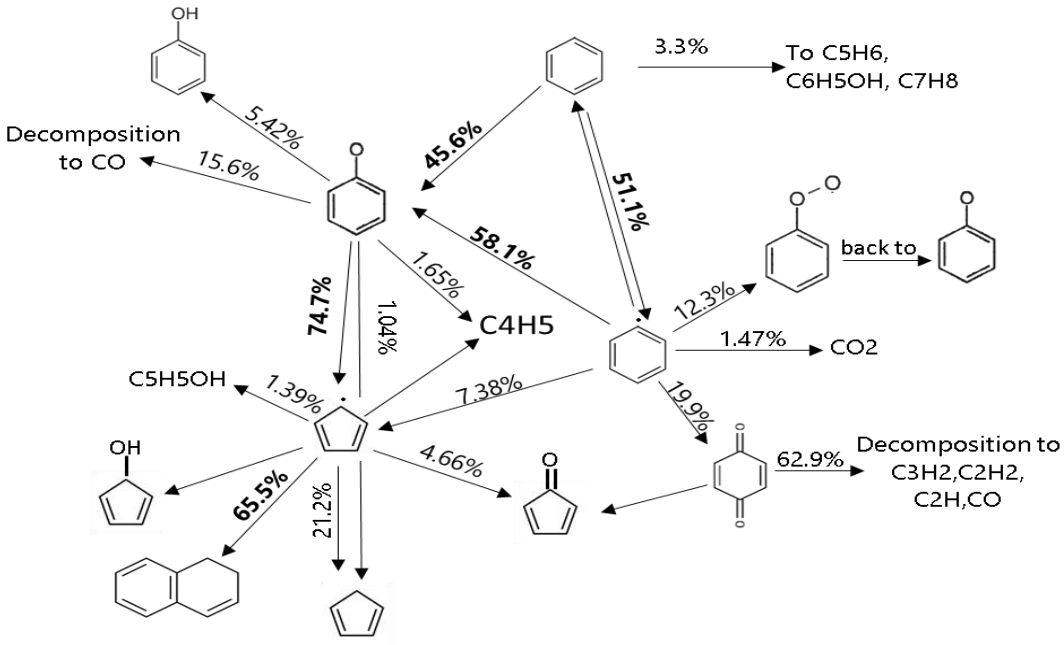

Figure 16 Reaction path analysis for benzene oxidation in a JSR at atmospheric pressure and φ=1.

To figure out the reasons behind this trend, a sensitivity analysis has been performed on benzene at ϕ=0.3 and ϕ=1.

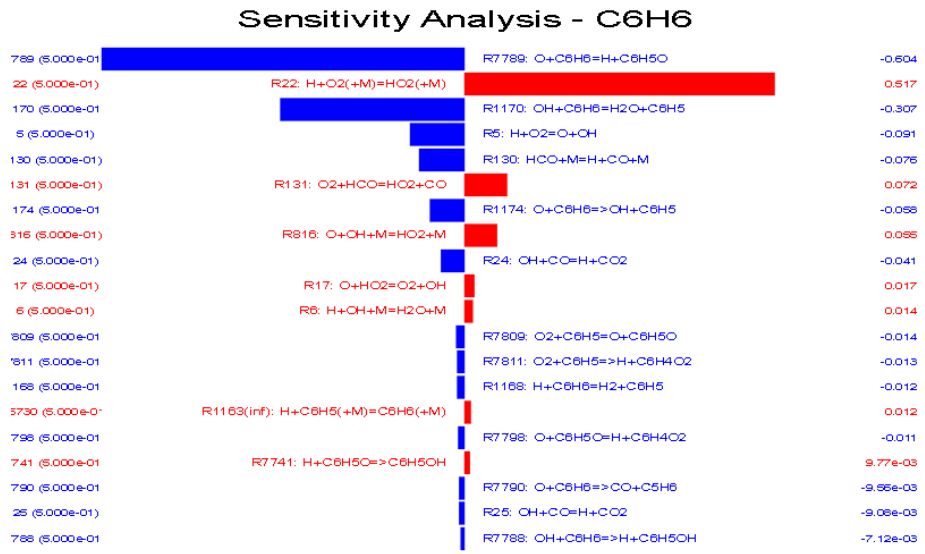

Figure 18 Sensitivity analysis of benzene oxidation at atmospheric pressure in a JSR at φ=0.3.

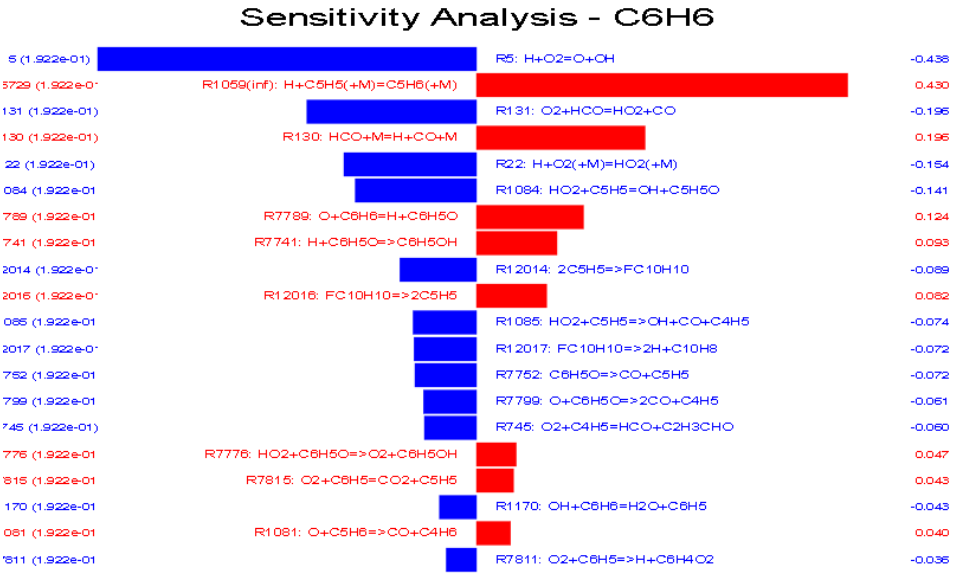

Figure 19 Sensitivity analysis of benzene oxidation at atmospheric pressure in a JSR at φ=1.

Under lean conditions (Figure 18), the formation of the phenoxy radical (R7789), due to the oxygen substitution reaction on the aromatic ring, strongly influences the enhanced consumption of benzene, together with the formation of the phenyl radical (R1170) as a result of the H abstraction by the OH radical. This does not hold true if we analyse the sensitivity analysis at ϕ = 1, where benzene is produced by cyclopentadienyl (R1059) and by phenoxy (R7789).

The reaction path analysis suggests that benzene can undergo two different type of reaction: it can form the phenyl radical by H abstraction, or it can produce the phenoxy radical by oxygen addition. Generally, the second path is favoured, probably because the energy required to the system to abstract a hydrogen from an aromatic ring is very high. Clearly, in lean conditions, the ratio between the percentage of the two possible reaction paths is higher than in stochiometric conditions.

The H-abstraction reactions have been already investigated by Pratali Maffei et al.[23] thus, this work represents a step further for the development of aromatics combustion kinetic.

Once phenyl radical is produced, it can add to molecular oxygen addition, to form C_6H_5OO that then turns into phenoxy, because unstable. Instead of forming phenoxy radical, another possibility, following the oxygen addition, is the formation of benzoquinone. Benzoquinone may decompose into lower weighted species or into C_5H_4O. The above mentioned are the main reaction channels for the phenyl radical, but, from the reaction paths analysis, it can be observed that these are not the only ones.

For what concerns the phenoxy radical, in stochiometric conditions, it is mainly responsible of the formation of C_5H_5, that then, preferentially, turns into dialin ($C_{10}H_{10}$) or cyclopentadienyl (C_5H_6). In lean conditions, the phenoxy mainly decomposes to C_4H_5 or it forms benzoquinone, a very low percentage leads to the formation of C_5H_5.

6.2.2 Chai et al.[24]

The kinetic mechanism was also tested on the basis of the experimental dataset obtained by Chai et al.[25] using a micro-jet reactor, at a pressure of 0.46 atm. The results reported in Figure23 are obtained at an equivalence ratio Φ = 1.02.

As in the case of Ristori lean conditions, there is an overestimation of benzene reactivity. The sensitivity analysis suggests that the reactions that mainly influence the benzene consumption are the oxygen addition of cyclopentadienyl radical with the formation of C_5H_5O and the phenoxy radical decomposition into cyclopentadienyl and carbon monoxide. In Ristori, the benzene reactivity overprediction at Φ = 1 was always influenced by C_5H_5, but with the three-body reaction of H addition to form C_5H_6, whose kinetic parameters where calculated through "ab-initio" methods. As a conclusion, CPD (cyclopentadienyl) and its radical play a key role in benzene production and consumption.

The cyclopentadienyl concentration is still overpredicted. The phenoxy radical decomposition into C_5H_5 and CO plays a major role in its production thus, a further improvement of the mechanism would include the estimation of kinetic parameters that involve the CPD formation.

The phenol fit is still not satisfactory, but as a contrary, if for Ristori the reached values were low and the shape was flatter, in this case it is strongly too high.

In Chai simulation, data about benzoquinone were also collected; focusing on them, there is a clear overprediction of $C_6H_4O_2$ concentration. In this case, the overprediction is mainly affected by the phenyl radical, that produces $C_6H_4O_2$ by adding molecular oxygen on the aromatic ring. For benzoquinone production too, the phenoxy radical is a key player. In the flow path just the para isomer of benzoquinone is present, but the formation of two different isomers, ortho and para, is widely supported by ab the initio study of Lin and Mebel[26] and by Tokmakov et al.[27]. In the CRECK mechanism, the two isomers are lumped.

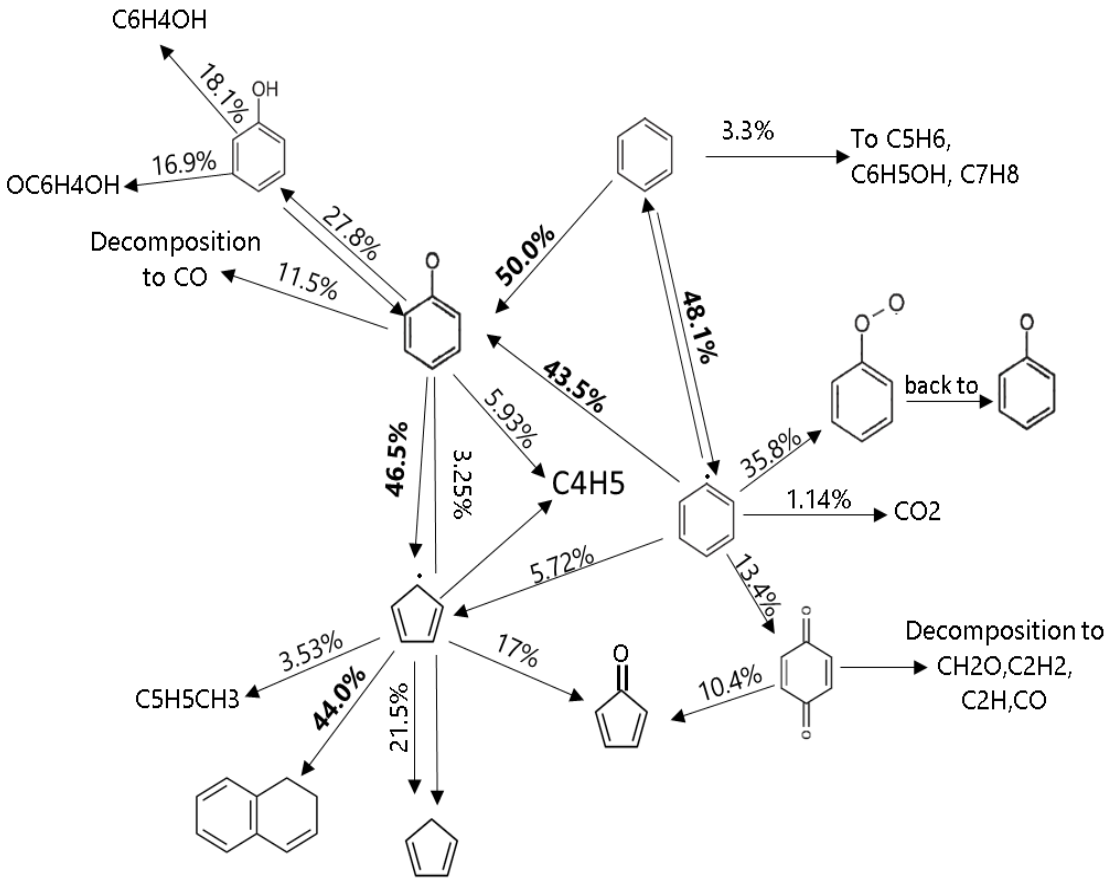

Figure 20 Reaction path analysis for benzene oxidation in a micro-JSR at 0.46 atm and φ = 1.02.

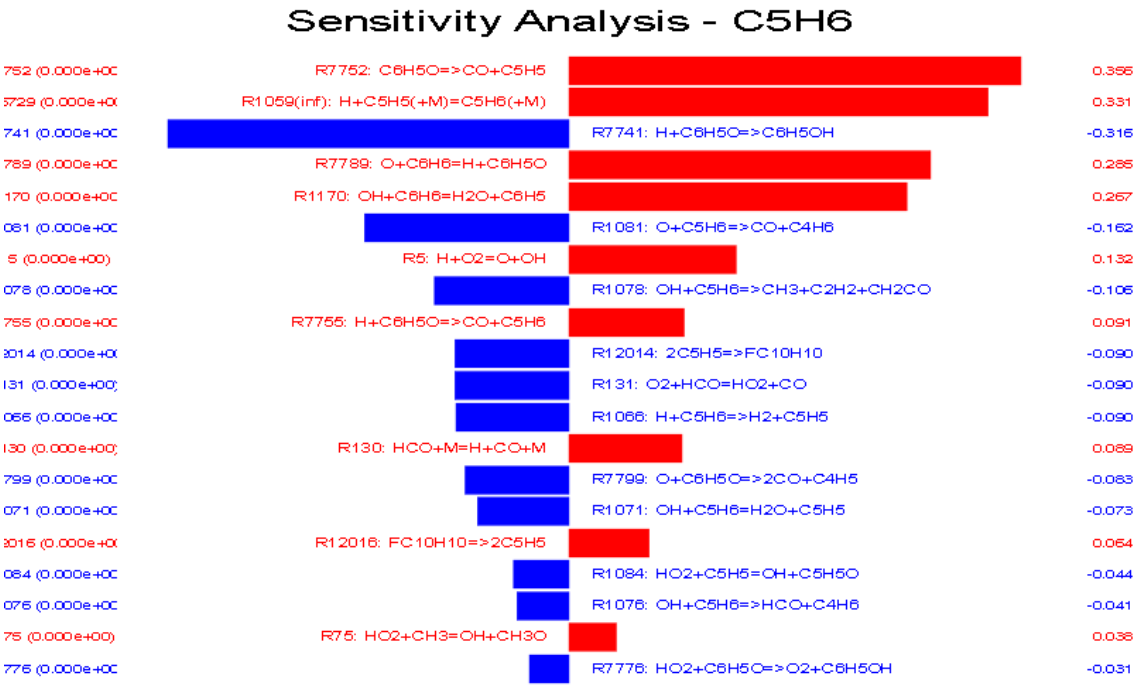

Figure 21 Sensitivity analysis of cyclopentadienyl production at 1075K and φ = 1.02.

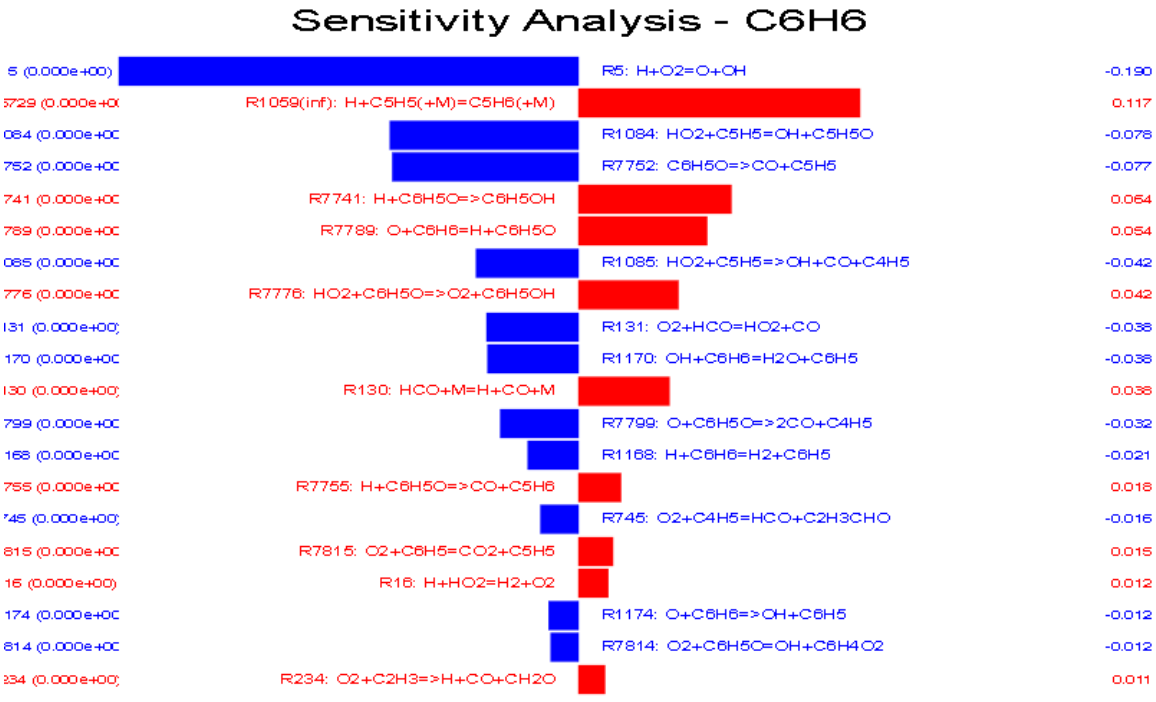

Figure 22 Sensitivity analysis of benzene oxidation at 1075K and φ = 1.02.

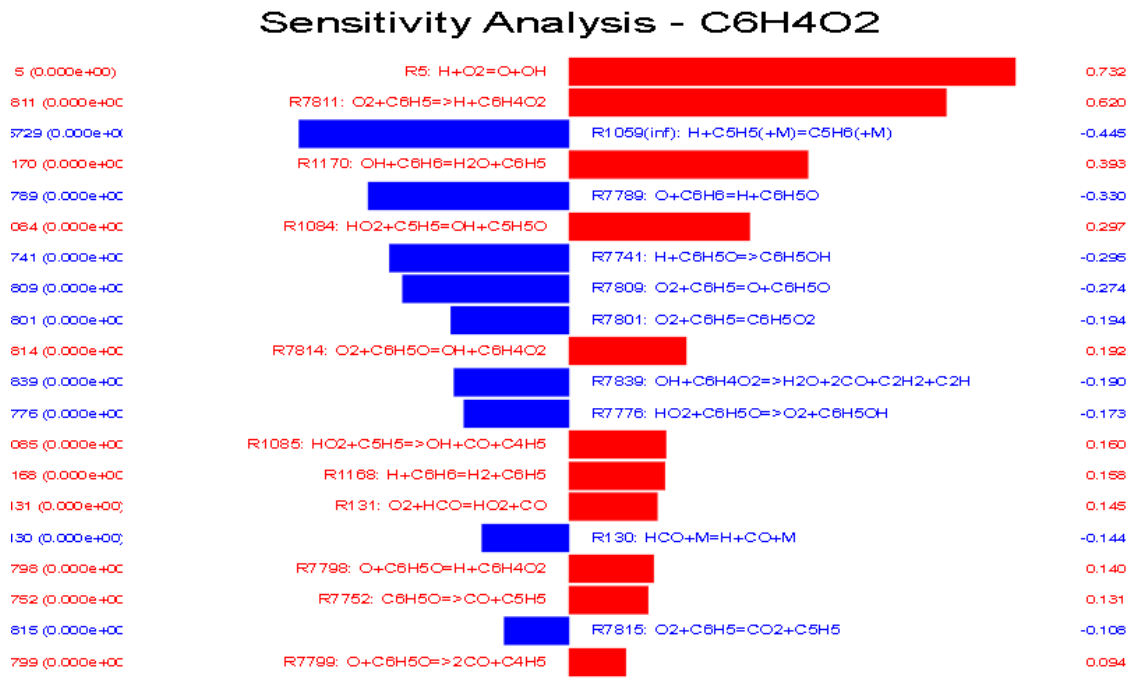

Figure 22 Sensitivity analysis of benzoquinone production at 1075K and φ=1.02.

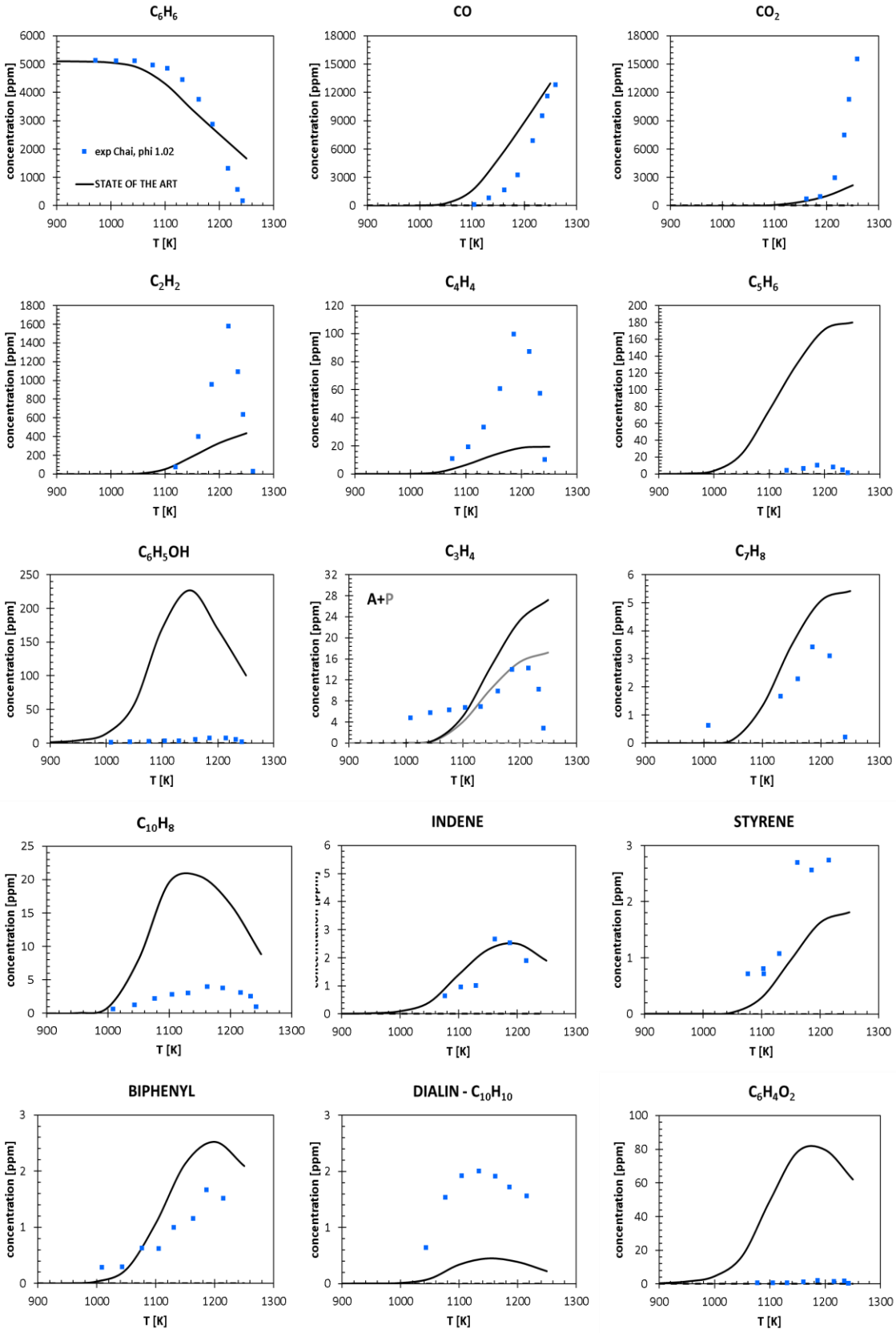

Figure 23 Chai et al. experimental data (squares) for a micro-jet stirred reactor with an equivalence ratio φ = 1 at 0.46 atm. The model prediction is represented by the solid lines.

6.3 Benzene Pyrolysis in Shock Tubes

In this second paragraph, the simulation results of a benzene pyrolysis in a shock tube are presented. The experiments were performed in the temperature range 1300–2100 K by Laskin and Lifshitz[28] at a pressure of 5 atm.

Globally, the model well predicts the trends but, it is shown an overestimation of benzene reactivity once again. Moreover, the model undervalues the amount of C_2H_2 and C_4H_2 and, alongside, it overpredicts C_6H_2 production.

At the range temperature of 1300-1700K, aromatics concentration is higher than linear molecules one, probably because the activation energy of beta-scission reactions it too high.

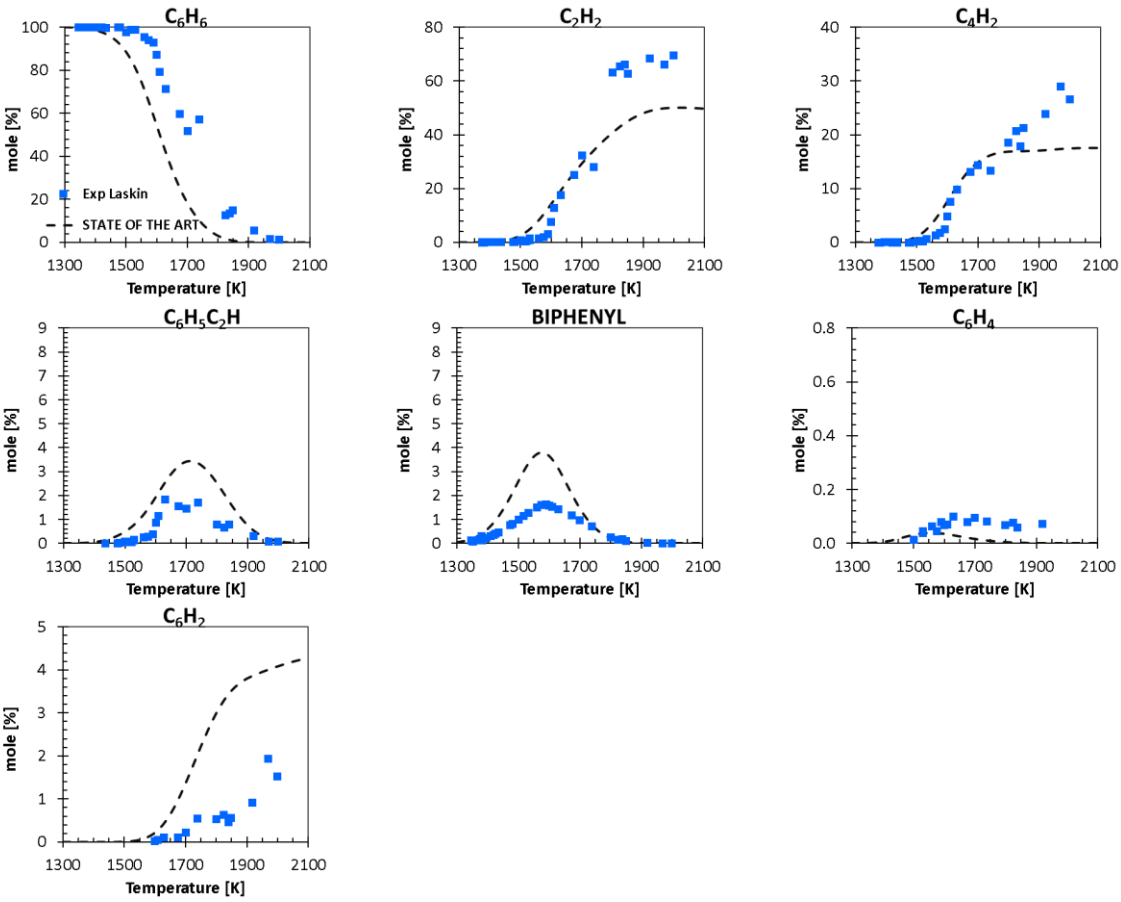

Figure 24 Model prediction for the benzene pyrolysis into a shock tube at 5 atm pressure and in a T range of 1300-2100K.

6.4 Benzene Oxidation in PFRs

The model prediction for a plug flow reactor is well represented by the simulation of the experimental dataset reviewed by Brezinsky[29]. This case study takes in exam an atmospheric plug flow reactor, at a constant temperature of 1102 K with a residence time of 0.2 s. The inlet mixture is made of air and benzene, nitrogen works as a thermal diluent. The database evaluates the model performances at different ϕ (0.76, 1, 1.36) but being the results coherent with all equivalence ratio values, just the ones computed at ϕ=1 are reported.

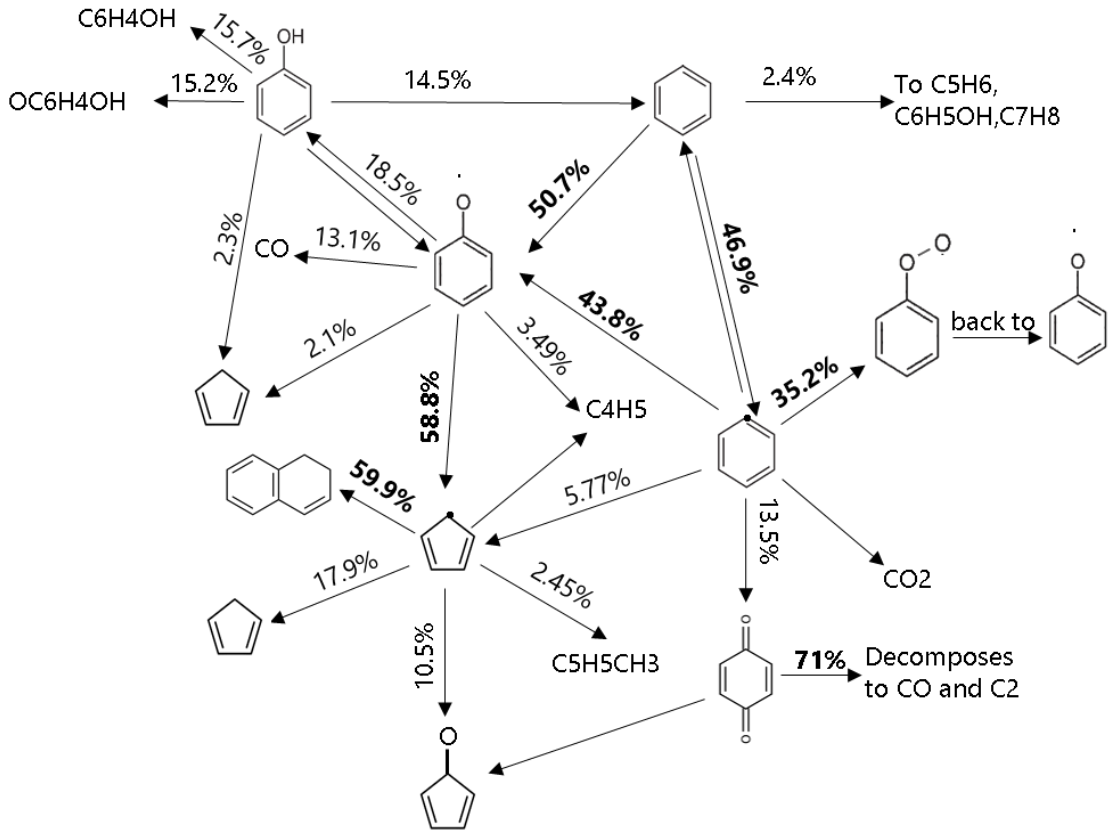

Figure 25 Reaction path analysis for benzene oxidation in a PFR at atmospheric pressure and φ=1.

The flow path shows that benzene mainly undergoes both H abstraction forming the phenyl radical and O addition producing the phenoxy radical. The O addition is not the only way to produce phenoxy radical: the phenyl radical can also react with molecular oxygen forming at a first instance C_6H_5OO, and then, phenoxy. The reaction of the phenyl

radical with molecular oxygen is a significant source of phenoxy radicals. The phenoxy radical is largely responsible of dialin ($C_{10}H_{10}$) and cyclopentadienyl formation.

Another important reaction product is benzoquinone, that is produced through the molecular O_2 addition onto the phenyl radical ring.

In the next figure the model prediction results are provided. In this case, the benzene reactivity is underestimated and there is a clear mismatch for phenol, C2 and C4 species. The CO species trend is well-described, even if with lower values of mole fraction, especially with the temperature rising.

It is worth to notice that cyclopentadienyl reaches too high values and from the sensitivity analysis (Fig. n.) it is possible to figure out that its formation truly affects the C6H6 production and C_6H_5OH consumption.

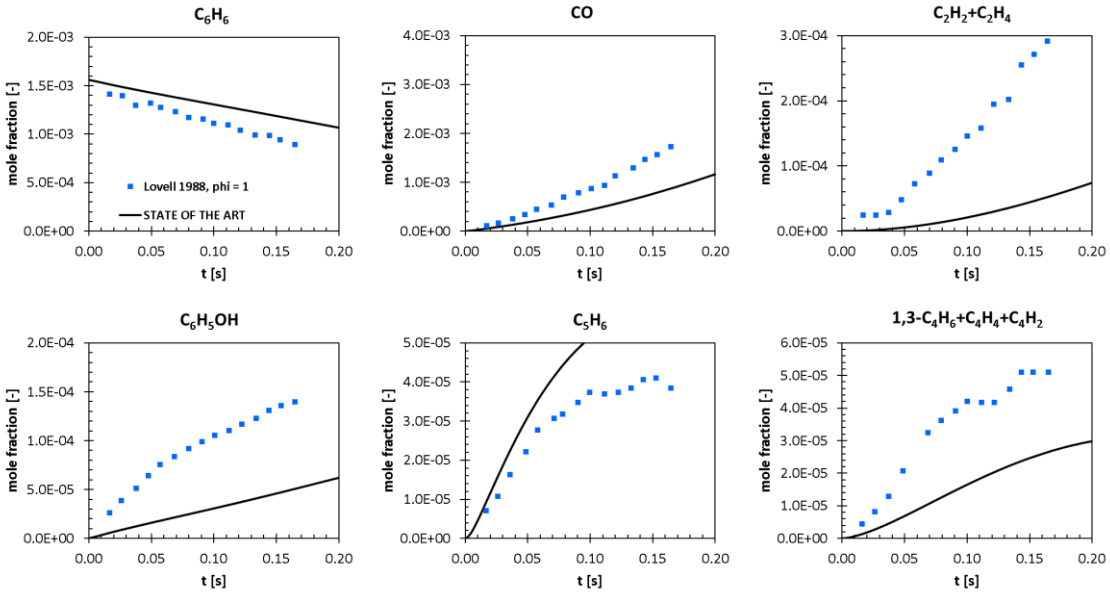

Figure 26 Benzene oxidation model prediction compared with experimental data.

To give a complete overview of benzene oxidation in PFRs the sensitivity analysis is reported.

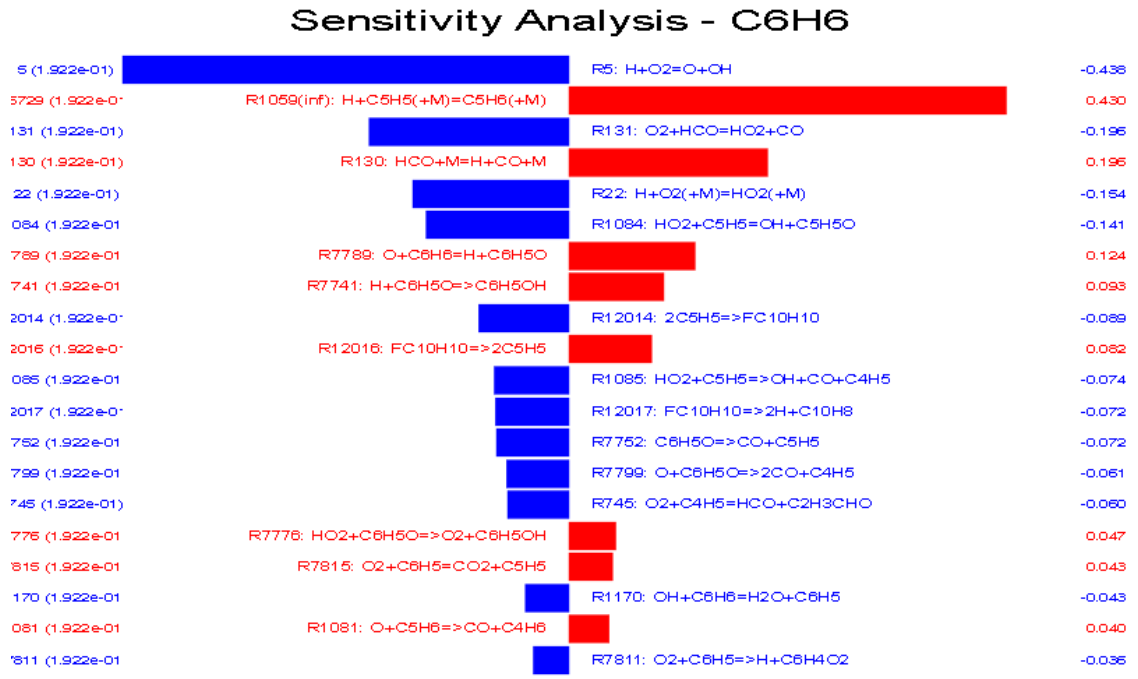

Figure 27 Benzene sensitivity analysis at 0.14 s and φ = 1.

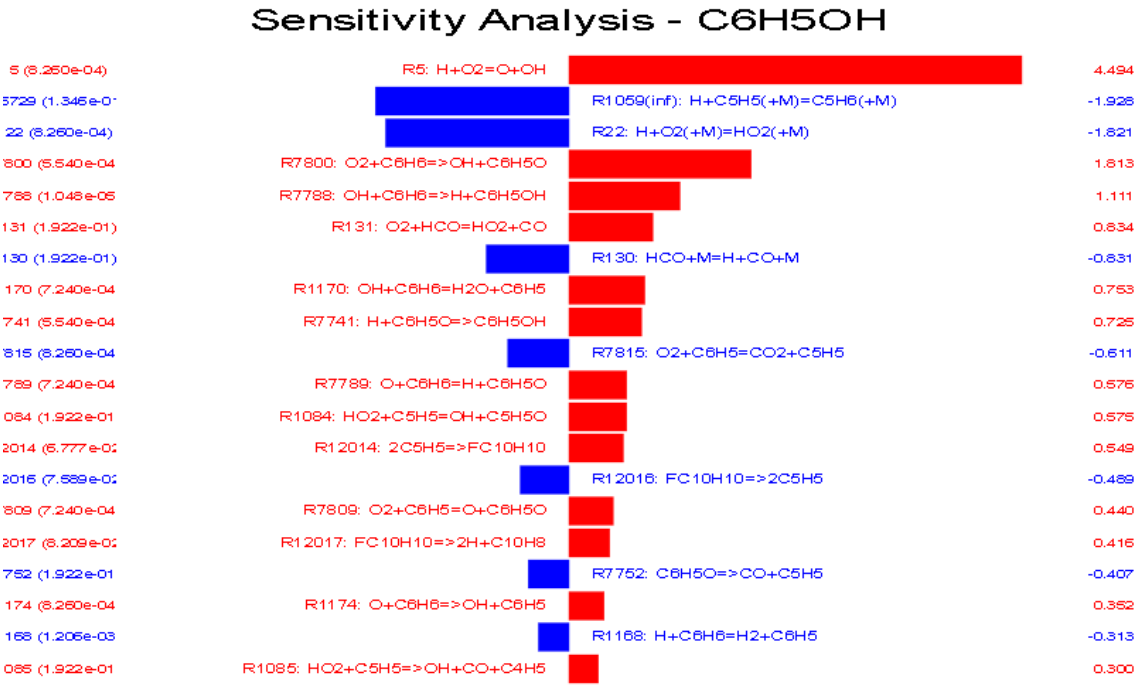

Figure 28 Phenol sensitivity analysis at 0.14 s and φ = 1.

6.5 Premixed Laminar Flames

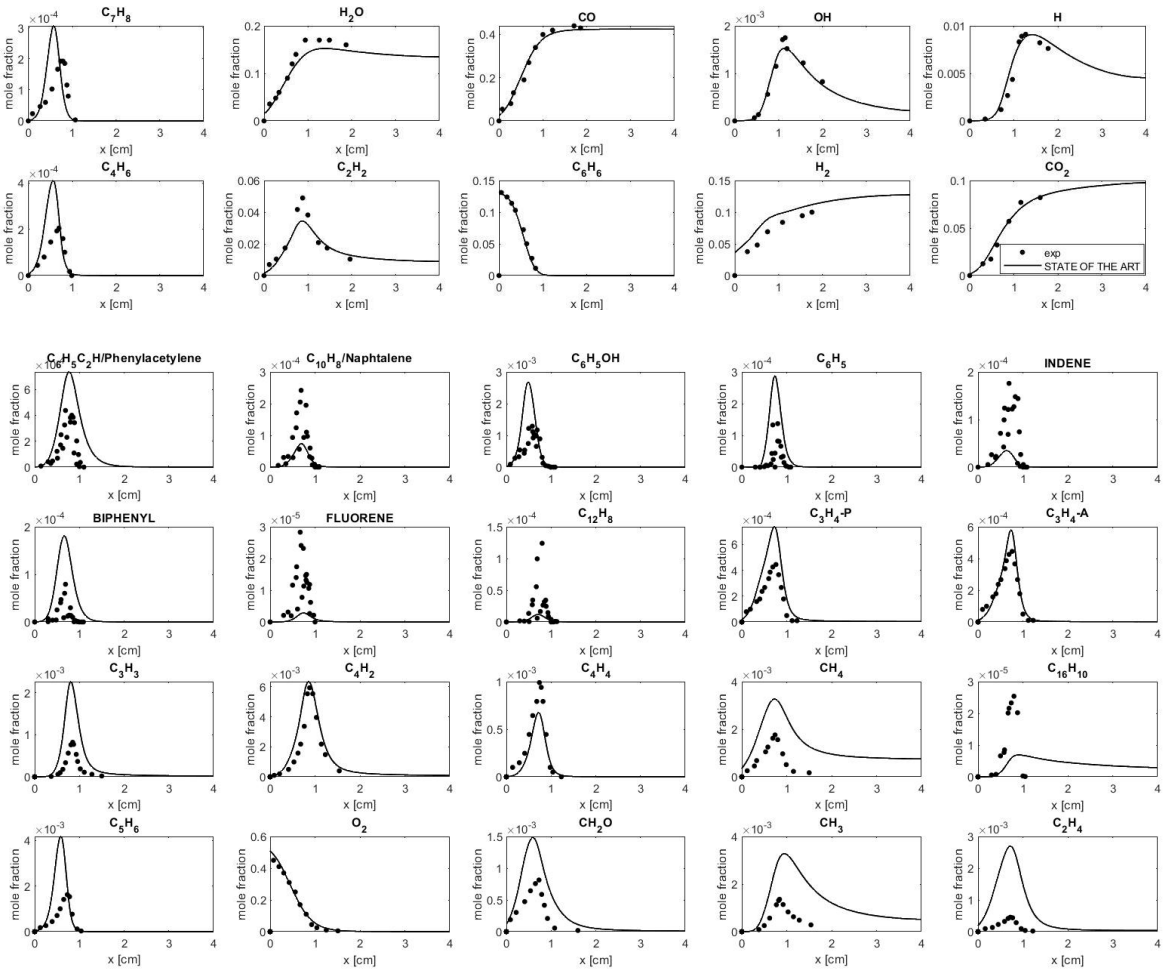

Figure 29 Premixed laminar flames. Model predictions for the experimental data collected by Tregrossi et al.[48]

The benzene oxidation was also predicted for high temperature ranges typical of flames. Thanks to the work of Bittner and Howard[26], the starting mechanism has been simulated for a database characterized by a large number of species, detected using molecular beam mass spectrometry. The system is in vacuum conditions, at a pressure of 0.03 atm and an equivalence ratio of 1.8 is used. The results show a good agreement between model prediction and experimental data trends, however, many species production is overestimated.

6.6 Overall View of the Starting Kinetic Mechanism

The abovementioned results provide a description of the starting benzene oxidation mechanism. The combustion starts with a competition between the H-abstraction and the O addition on the aromatic ring, which is generally favoured because the lower energy content required with respect to the break of the bond between hydrogen and the aromatic ring. As a result, the reactions of the phenoxy radical play a fundamental role inside the overall mechanism, being a key player in the production of many species, among them the cyclopentadienyl. However, not negligible amount of the phenoxy radical is produced starting from the reaction between the phenyl radical and molecular oxygen (O_2). This reaction is of great importance because, if phenyl radical does not undergo O_2 addition, it can participate as a building block to soot formation or can be subjected, at high temperature, to thermal decomposition in smaller fragments. The competition of these processes deeply affects the combustion products distribution. Despite the importance, current kinetic parameters still fail to accurately predict the experimental formation and concentrations of products at various temperatures from the combustion of benzene with oxygen.

6.7 Previous Theoretical Studies on $C_6H_5 + O_2$

The potential energy surface of the reactive system $C_6H_5+O_2$ has been already investigated in literature. Tokmakov et al.[25]made ab initio G2M calculations, finding out that phenoxy and C_5H_5 are expected to be the primary products, but this conclusion was not supported by multichannel calculations of reaction rate constants, which are essential to quantify the product branching ratios at various combustion conditions.

Mebel and Lin[30] calculated a variety of the C_6H5O_2 isomers, however the ab-initio methods and moderate basis set employed, do not provide enough accuracy.

Fadden et al.[31] increased the level of theory for calculations and enlarged the number of intermediates and TS calculated, but still, the accuracy expected for barrier heights is not sufficient to generate rate constants. In some cases, also ambiguous transition states were included, with no intrinsic reaction coordinate (IRC) scan to prove their existence.

Sebbar et al. performed multi-channel calculations with the master equation solution for the phenyl peroxy radical and its isomers. They provided rate constants, but the starting PES does not consider all the possible reaction channels that have been identified in other literature works.

As also highlighted by Vourliotakis et al.[32], in literature there are several works that have investigated this reactive system, but uncertainties related to the rate and product distribution of the $C_6H_5 + O_2$ reaction are present.

The purpose of this work was to overcome the limitations present in the previous investigations of the $C_6H_5 + O_2$ reactive system, considering all the reaction channels already highlighted in literature, with an accurate level of theory and completing the study with the evaluation of temperature and pressure dependent kinetic constants through the resolution of the master equation for a multi-channel system.

Chapter 7
Results of Theoretical Calculations

This chapter reports the results of the theoretical calculations computed for the reactive system $C_6H_5+O_2$. In the previous chapter was highlighted the lack of consistent works in the literature about ab-initio calculation of rate constants for this reactive system. In this chapter the calculation methods adopted will be shown and a deepening of the potential energy surface construction will be given. Follows the results discussion.

7.1 Introduction to the Rate Constants Computation

As already anticipated in the previous chapter, the work started with the construction of the potential energy surface for the reactive system C6H5 + O2 and then, the calculation of the temperature and pressure dependent kinetic constants by solving the master equation for a multichannel system with the implementation of the RRKM theory. The determination of the constants was performed in the pressure range of p=0.1-1000 atm and in the temperature range T=300-2500K. The average transferred energy per collision was determined using a single exponential down model with

$$\Delta E_{down} = 260 \cdot \left(\frac{T(K)}{298}\right)^{0.875}$$

The Lennard-Jones parameters were taken from the literature[20].

7.2 Calculation Methods

According to the EStokTP[22] modular environment algorithm, as a first step, the geometries of various reactants, products, and transition states and their vibrational frequencies were optimized using the DFT theory wb97xd/6-311+g(d,p) level. As an input

just the z-matrix of the reactants and products was given. The transition states were determined according to the EStokTP routines, as described in Chapter 5.1. Next, the species energies were refined, computing the total energy as follows:

$$CBSen = en\_cc + en\_mp2\_qz - en\_mp2\_tz + en\_ccsdtcore\_tz - en\_ccsdt\_tz$$

The reliability of the results was checked through the T1 diagnostic, whose maximum value must be equal to 0.04.

The result importance was enhanced by the inclusion of the $C_6H_5+O_2$ entrance channel in the resolution of the ME. The transition state is barrierless and, as all the barrierless TS included in this work, it was determined through VRC-TST by Pratali Maffei et al[26].

7.3 The Potential Energy Surface

The potential energy surface construction started with the identification of the main pathways, starting from the work of Tokmakov et al.[33]. Tokmakov took in exam the widest number of possible reaction channels ever investigated, and the selection of the most important ones was based on the relative energies computed with respect to phenyl and oxygen.

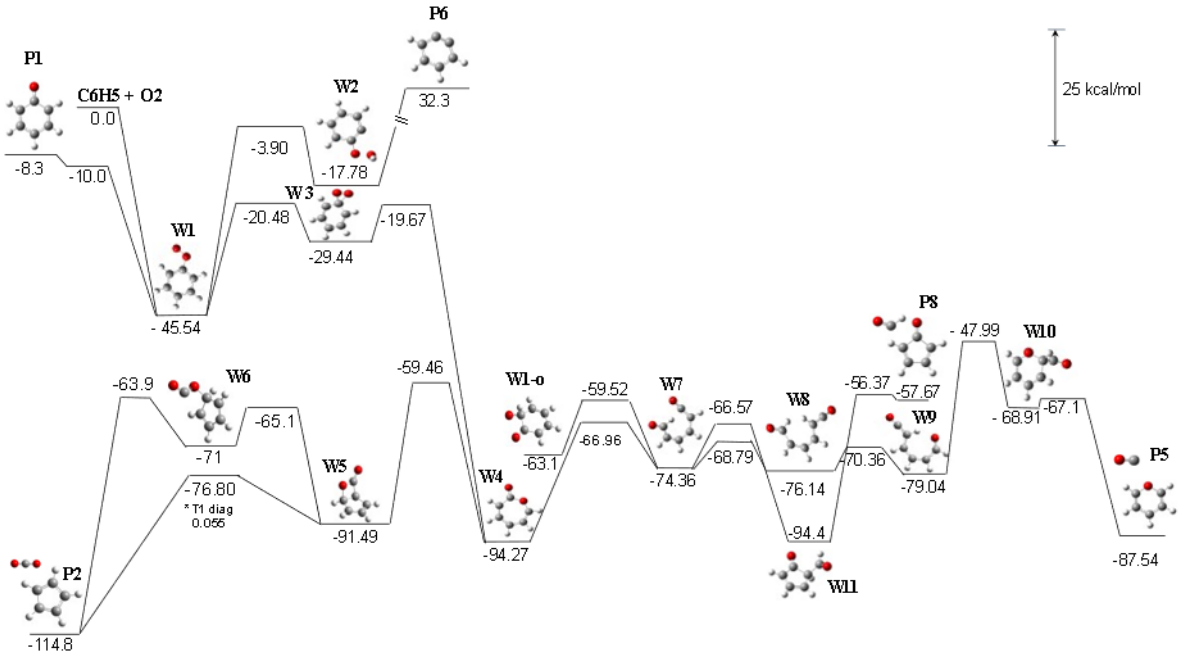

Figure 30 Potential energy diagram for the most important channels of the C_6H_5 + O_2 reaction. Relative energies of the reactants, products, intermediates, and transition states are given in kcal/mol, calculated at the high-level of theory.

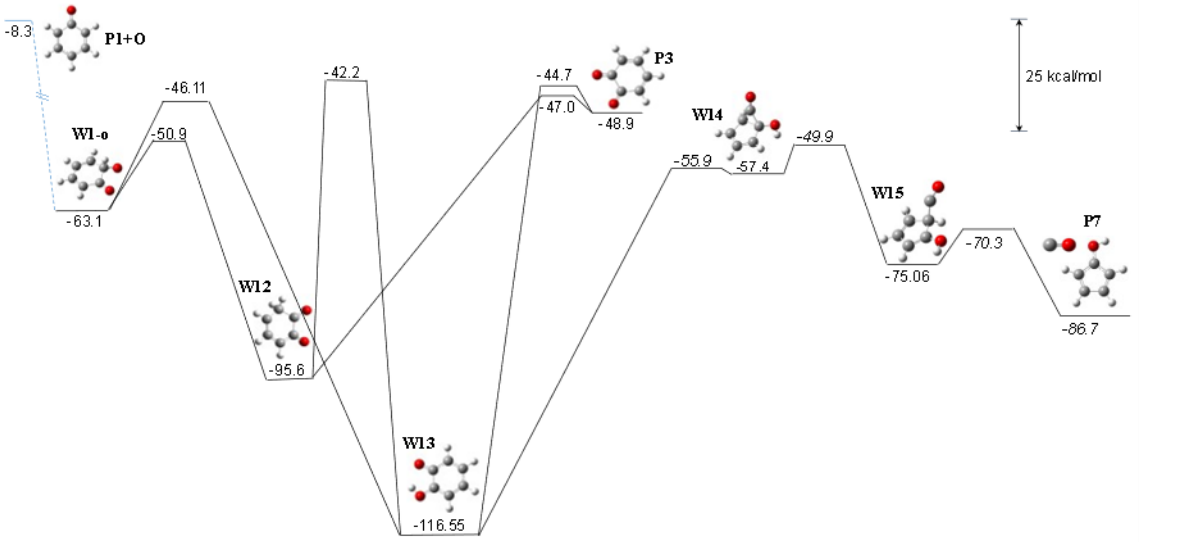

Figure 31 Potential energy diagram for the most important channels of the C_6H_5 + O_2 reaction. Relative energies of the reactants, products, intermediates, and transition states are given in kcal/mol, calculated at the high-level of theory.

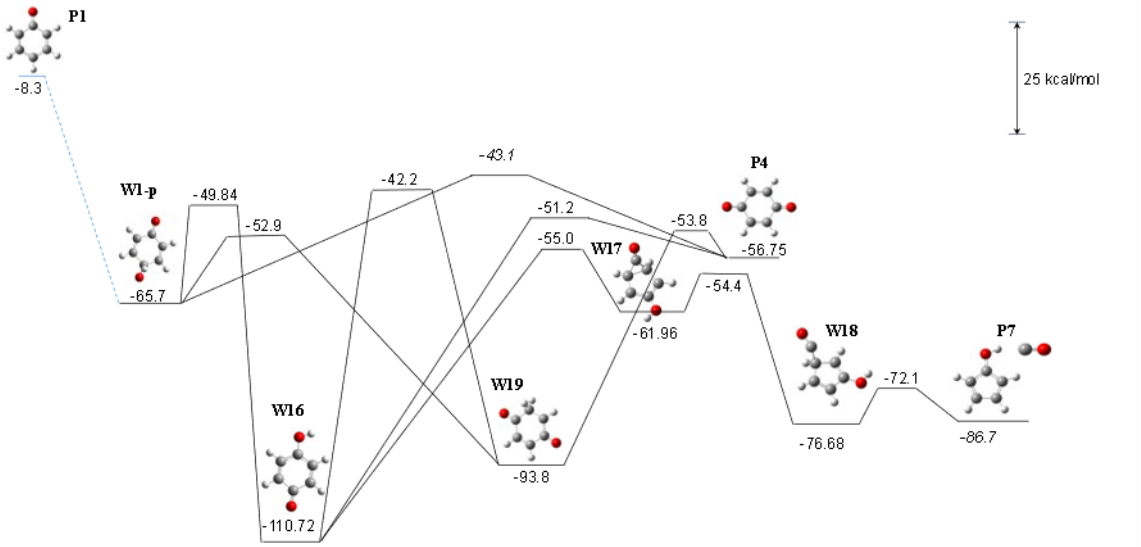

Figure 32 Potential energy diagram for the most important channels to produce p-benzoquinone starting from C6H5O + O(3P). Relative energies of the reactants, products, intermediates, and transition states are given in kcal/mol, calculated at the high-level of theory.

The reaction starts with a barrierless addition of molecular oxygen to phenyl, leading to the formation of the phenylperoxy radical (**W1**) with an exothermicity of 45.54 kcal/mol. The phenylperoxy radical presents a threefold fate: it may turn into the dioxiralyn radical (**W3**), through the formation of a three-member ring among the carbon atom and the two added oxygen atoms; it can lose the terminal oxygen turning into phenoxy radical C6H5O and O(3P) (**P1**) with a barrierless transition state, and, as suggested by Sebbart et al.[26], **W1** may isomerize to ortho-hydroperoxide phenyl radical (**W2**) via H-shift from the aromatic ring to the peroxy group. During the PES construction, it was hypothesized that the OOH group was a good leaving group to form benzyne C6H4 (**P6**), thus, an additional reaction path was introduced. Among this three, the formation of **W3** presents the lowest energy barrier of -20.48 kcal/mol.

When the dioxiralyn radical (**W3**) is formed, one of the oxygen atoms can insert into the ring producing the 2-oxepinyloxy radical (**W4**), which lies in a deep potential well of 94.27 kcal/mol. This rearrangement was not easy to be obtained thus, the optimized z-matrix of this transition state, taken from the work of Tokmakov et al.[20], was given as a first guess to EStokTP[26]. According to their work, **W3** turns into **W4** through the formation of an intermediate structure, that will be called **W3'**, differing from **W3** only by the O-O bond

length. This intermediate can be described as a triradical, since it presents three unpaired electrons. Tokmakov et al.[26]proved that the transition-state **TS W3-W3'** connects the dioxiralyn radical to the 2-oxepinyloxy. In the rearrangement from **W3'** to **W4** no transition state is present.

The energy barrier of the **TS W1-W3** is just 0.81 kcal/mol higher than the one of the **TS W3-W3'**, this comparison plays a fundamental role, since the 2-oxepinyloxy radical (**W3**) may lead to many different products, whereas the reverse reaction step **W3-W1** would lead back to the phenoxy formation.

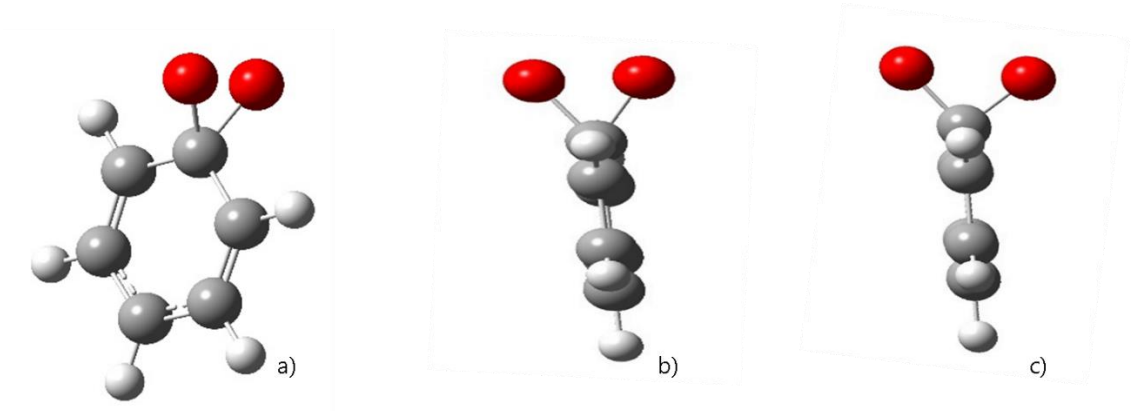

Figure 33 a) W3 molecular structure b) Lateral view of W3 molecular structure c) Lateral view of the TS W3-W3' molecular structure

As just mentioned, the 2-oxepinyloxy radical (**W4**) can lead to different reaction products through ring-opening rearrangements, all the following energy barriers are lower than the one of the reverse reaction thus, it is unlikely that **W4** goes back to **W3**. Overall, the branching ratio between phenoxy and the other products will be controlled by the critical transition states **TS W1-W2, TS W1-W3** and **TS W3-W4**.

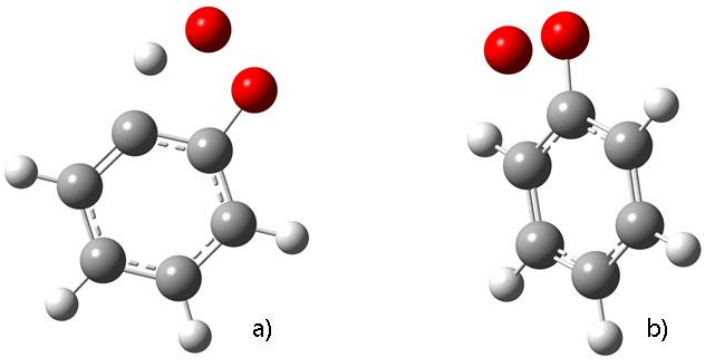

Figure 34 a) TS W1-W2 structure b) TS W1-W3 structure

W4 can undergo ring opening to intermediates **W7, W8** and **W9**, which are obtained through the rotations of the HCCO and HCO groups. The transition states **TS W7-W8** and **TS W8-W9** were difficult to investigate: the only difference from one structure to another was the rotation of the groups. To overcome this obstacle, also in this case, the geometries from Tokmakov et al.[34] were provided as an input to the electronic structure calculations.

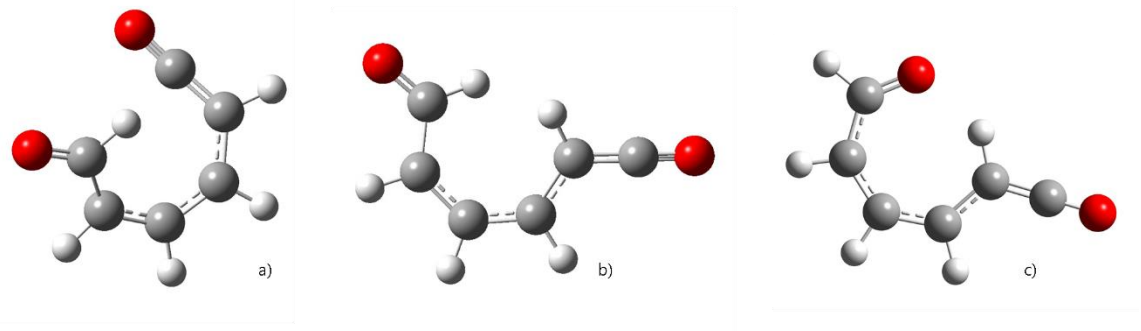

Figure 35 a) W7 molecular structure b) W8 molecular structure c) W9 molecular structure

The chain isomer **W9** can undergo a ring closure (**TS W9-W10)**, leading to the formation of **W10**, responsible of the formation of pyranyl and CO **(P5)** through the out-of-ring C-C bond scission (**TS W10-P5)**. Once that **W10** is formed, the evolution to **P5** is favoured: the energy barrier is just 1.9 kcal/mol, whereas the products **P5** are at 87.54 kcal/mol less than C6H5 and O2.

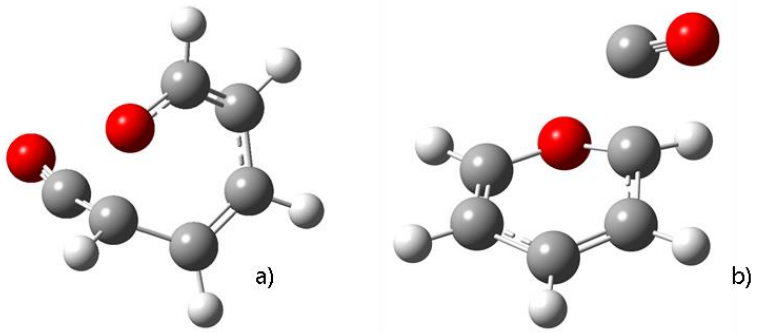

Figure 36 a) TS W9-W10 structure b) TS W10-P5 structure

Another possible faith for **W7** is the ring closure (**TS W7-W11**), forming a five-carbon ring, with groups HCO and O out of it (**W11**). **W11** may undergo C-C bond scission (**TS W11-P8**), producing C5H4O and HCO (**P8**).

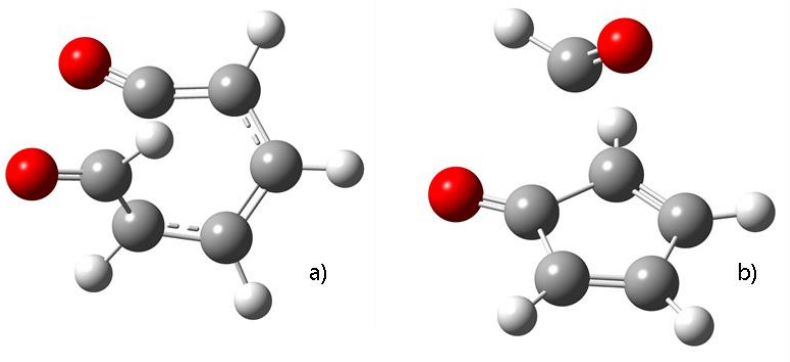

Figure 37 a) TS W7-W11 structure b) TS W11-P8 structure

Alternatively, the intermediate **W7** goes through the C-C bond formation, restoring the aromatic ring with two oxygen atoms out of it in ortho position (**W1-o**). The **W1-o** species is the precursor of ortho-benzoquinone (**P3**): H loss leading to benzoquinone can take place in two different ways. A first possibility is the migration of the H to the adjacent carbon atom (**W12**) to form a CH2 group from which the hydrogen is eliminated. Alternatively, the H atom can be added to the radical oxygen, forming ortho-OC6H4OH (**W13**) that, as **W12**, undergoes H loss, forming the ortho-benzoquinone (**P3**). **W12** and **W13** lie into two very stable wells, whose depth is 95.6 and 116.55 kcal/mol, respectively. Unpublished reaction steps for o-OC6H4OH were introduced in this work: a rearrangement of **W13** is indeed also possible with the formation of a 5C ring sharing two carbons atoms with a 3C ring to which functional groups =O and OH are bonded (**W14**). Then, the breaking of the C-C bond of the three-member ring, produces a 5C ring with two external groups CO and OH. Follows the cleavage of the bond between the ring and the CO group, forming C5H4OH and CO (**P7**). This type of rearrangements and decomposition have already been proposed by Pratali Maffei et al.[25] for phenol decomposition. In this work also the isomerization between **W12** and **W13** was included.

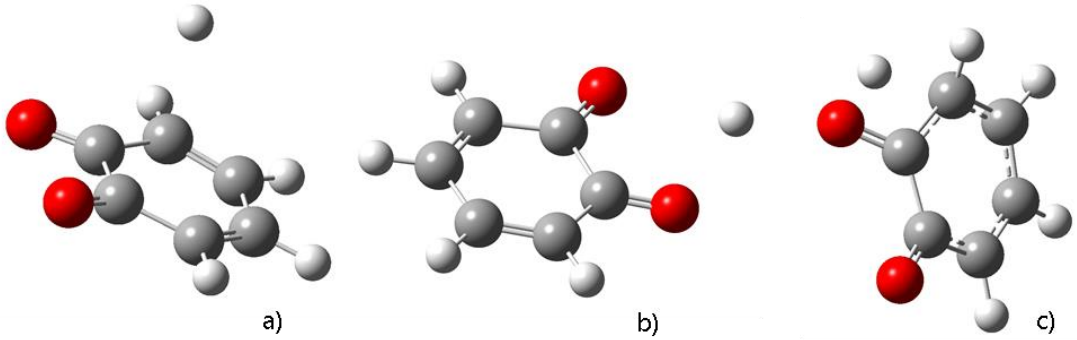

Figure 38 a) TS W12-P3 structure b) TS W13-P3 structure c) TS W12-W13 structure

Going back to **W4**, another possible reaction channel is the formation of **W5**, a bicyclic structure consisting of a five-member C5 and four-member C3O ring with two shared carbon atoms. This new species is responsible of the cyclopentadienyl radical and CO_2 formation (**P2**): with the breaking of the C-C bond there is the opening of the four-member ring, followed by CO_2 and C_5H_5 production lying in a stable well whose energy relative to the reactants is -114.8 kcal/mol, making it the most favourable product. The decomposition to **P2** was computed also without passing through an intermediate structure, but directly through the **TS W4-P2**, however, the T1 diagnostic exceeded the limit value of 0.04.

M.C. Lin et al.[22] investigated a reaction channel that starts from phenoxy and O(3P) and leads to the formation of o-OC6H5O (**W1-o**) through a barrierless transition state by Pratali Maffei et al.[25], giving a double formation path to this species (from **P1** and **W7**).

M.C Lin et al.[35] also supported the formation of the para-isomer of benzoquinone, investigated for the first time in this work. Pratali Maffei et al. calculated the barrierless transition state from the phenoxy and O(3P) to form the para isomer of OC6H5OH (**W1-p)** whose fate is threefold: it can produce the para-benzoquinone (**TS W1p-P4**), which is more thermodynamically stable than its ortho-isomer, it can form p-OC6H4OH (**TS W1p -W16**) or, it can face an H transmigration from the carbon atom bonded to oxygen to an adjacent one (**TS W1p-W19**). If **W16** is formed, it can isomerize to **W19**, or it can take place an H loss producing once again the para-benzoquinone (**P4**), or it can decompose to C5H4OH and CO (**P7**).

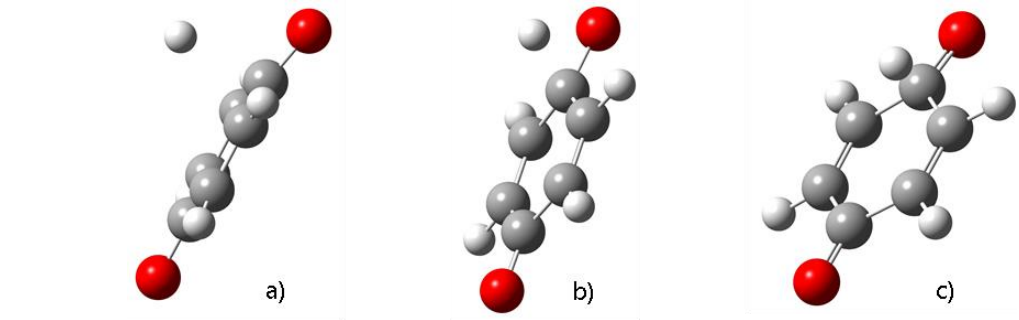

Figure 39 a) TS W1p-P4 structure b) TS W1p-W16 structure c) TS W1p-W19 structure

Clearly, the decomposition would not occur directly, but through rearrangements steps equal to the ones that lead to the production of C5H4OH starting from o-OC6H4OH. The last reaction channel that can lead to the formation of the p-benzoquinone is a possible H loss starting from **W19.**

The PES results showed that the phenyl radical oxidation mainly goes through decomposition to five-member carbon ring, especially to C5H5, which is the most favourable product.

7.4 The Kinetic Rates Parameters

The calculated kinetic parameters are listed in the table below.

		k_0	α	E_a	R2_adj	Temp. Range
C6H5+O2 => C6H5O2		3.43E+55	-14.76	9677.41	1	700 - 1000 K
PLOG	0.01	3.43E+55	-14.76	9677.41	1	700 - 1000 K
PLOG	0.1	3.02E+62	-16.17	14960.09	1	700 - 1100 K
PLOG	1	1.28E+63	-15.76	18747.4	1	700 - 1300 K
PLOG	10	1.59E+56	-13.27	18786.56	1	700 - 1500 K
PLOG	100	1.77E+43	-9.16	14627.85	0.99	700 - 1700 K
C6H5+O2 => C6H5O+O		1.66E+15	-0.8	2216.14	0.95	700 - 2000 K
PLOG	0.01	1.66E+15	-0.8	2216.14	0.95	700 - 2000 K
PLOG	0.1	3.61E+16	-1.17	3292.71	0.96	700 - 2000 K
PLOG	1	1.08E+22	-2.68	7888.49	0.98	700 - 2000 K
PLOG	10	9.19E+29	-4.82	15742.26	1	700 - 2000 K
PLOG	100	2.55E+30	-4.79	20395.62	1	700 - 2000 K
C6H5+O2 => C5H4O+HCO		1.17E+22	-3.23	1601.52	1	700 - 2000 K

PLOG	0.01	1.17E+22	-3.23	1601.52	1	700 - 2000 K
PLOG	0.1	1.02E+24	-3.77	3106.03	1	700 - 2000 K
PLOG	1	3.92E+30	-5.58	8803.8	0.99	700 - 2000 K
PLOG	10	7.66E+36	-7.23	16178.53	0.99	700 - 2000 K
PLOG	100	3.21E+34	-6.38	19780.26	0.99	700 - 2000 K
C6H5O+O => C6H5O2		3.79E+61	-16.23	13246.98	1	700 - 1000 K
PLOG	0.01	3.79E+61	-16.23	13246.98	1	700 - 1000 K
PLOG	0.1	6.18E+63	-16.31	17542.45	1	700 - 1100 K
PLOG	1	2.92E+60	-14.84	19421.01	1	700 - 1300 K
PLOG	10	1.67E+51	-11.75	17729.88	1	700 - 1500 K
PLOG	100	5.14E+37	-7.55	12718.19	0.98	700 - 1700 K
C6H5O+O => C6H5+O2		4.50E+19	-1.93	10989.04		700 - 2000 K
PLOG	0.01	4.50E+19	-1.93	10989.04	1	700 - 2000 K
PLOG	0.1	1.07E+21	-2.31	12087.38	1	700 - 2000 K
PLOG	1	2.78E+26	-3.81	16640.69	1	700 - 2000 K
PLOG	10	2.61E+34	-5.96	24529.19	1	700 - 2000 K
PLOG	100	6.42E+34	-5.92	29140.77	1	700 - 2000 K
C6H5O+O => O-C6H4O2+H		1.50E+00	3.45	1212.8	1	700 - 2000 K
PLOG	0.01	1.50E+00	3.45	1212.8	1	700 - 2000 K
PLOG	0.1	3.80E+02	2.78	3073.41	1	700 - 2000 K
PLOG	1	4.17E+07	1.38	7160.41	1	700 - 2000 K
PLOG	10	1.29E+15	-0.65	14358.5	1	700 - 2000 K
PLOG	100	1.36E+13	0.06	17428.88	1	700 - 2000 K
C6H5O+O => C5H4O+HCO		3.40E+02	2.65	-6624.67	0.91	700 - 2000 K
PLOG	0.01	3.40E+02	2.65	-6624.67	0.91	700 - 2000 K
PLOG	0.1	3.50E+07	1.26	-2567.7	0.48	700 - 2000 K
PLOG	1	1.01E+16	-1.06	4949.14	0.96	700 - 2000 K
PLOG	10	1.01E+21	-2.37	10820.98	1	700 - 2000 K
PLOG	100	2.38E+19	-1.84	11736.93	1	700 - 2000 K
O-C6H4O2+H => O-C6H4O2H		1.51E+76	-18.99	29705.12		700 - 1500 K
PLOG	0.01	1.51E+76	-18.99	29705.12	1	700 - 1500 K
PLOG	0.1	1.51E+66	-15.69	27569.75	0.99	700 - 1600 K
PLOG	1	6.05E+53	-11.8	23397.61	0.96	700 - 1800 K
PLOG	10	5.20E+39	-7.53	17302.29	0.89	700 - 2000 K
PLOG	100	1.68E+23	-2.66	8732.38	0.96	700 - 2000 K
O-C6H4O2+H => O-OC6H4OH		1.25E+81	-20.14	36781.19	1	700 - 1900 K
PLOG	0.01	1.25E+81	-20.14	36781.19	1	700 - 1900 K
PLOG	0.1	7.45E+70	-16.85	34125.17	0.98	700 - 2000 K
PLOG	1	1.91E+54	-11.8	26975.39	0.91	700 - 2000 K
PLOG	10	7.48E+35	-6.33	17811.99	0.93	700 - 2000 K

PLOG	100	3.21E+20	-1.81	9598.36	0.99	700 - 2000 K
O-C6H4O2+H => C5H4OH+CO		1.40E+39	-7	26044.89	1	700 - 2000 K
PLOG	0.01	1.40E+39	-7	26044.89	1	700 - 2000 K
PLOG	0.1	9.51E+44	-8.51	33642.43	1	700 - 2000 K
PLOG	1	3.17E+42	-7.65	36751.7	1	700 - 2000 K
PLOG	10	5.70E+28	-3.62	32675.35	1	700 - 2000 K
PLOG	100	1.54E+08	2.24	23388.84	1	700 - 2000 K
O-C6H4O2+H => C5H4O+HCO		3.48E+30	-4.74	16454.75	0.99	700 - 2000 K
PLOG	0.01	3.48E+30	-4.74	16454.75	0.99	700 - 2000 K
PLOG	0.1	3.22E+38	-6.86	24977.37	1	700 - 2000 K
PLOG	1	1.43E+41	-7.44	31451.82	1	700 - 2000 K
PLOG	10	2.80E+37	-6.21	35120.9	1	700 - 2000 K
PLOG	100	1.22E+27	-3.1	35994.76	1	700 - 2000 K
C5H4OH+CO => O-OC6H4OH		2.84E+68	-17.14	71396.02		700 - 1900 K
PLOG	0.01	2.84E+68	-17.14	71396.02	1	700 - 1900 K
PLOG	0.1	1.77E+56	-13.35	66852.79	1	700 - 2000 K
PLOG	1	5.81E+38	-8.13	58415.26	1	700 - 2000 K
PLOG	10	3.65E+22	-3.36	49891.84	1	700 - 2000 K
PLOG	100	2.41E+12	-0.38	44308.48	1	700 - 2000 K
C5H4OH+CO => C5H4O+HCO		5.34E+34	-6.5	68023.03	1	700 - 2000 K
PLOG	0.01	5.34E+34	-6.5	68023.03	1	700 - 2000 K
PLOG	0.1	4.36E+38	-7.47	74444.58	1	700 - 2000 K
PLOG	1	2.18E+34	-6.11	76221.56	1	700 - 2000 K
PLOG	10	6.53E+10	0.6	64439.65	1	700 - 2000 K
PLOG	100	2.30E-10	6.37	54466.36	1	700 - 2000 K
C5H4OH+HCO => C5H4OCHO		1.70E+73	-19.31	25208.73	1	700 - 1100 K
PLOG	0.01	1.70E+73	-19.31	25208.73	1	700 - 1100 K
PLOG	0.1	1.28E+69	-17.65	26326.88	1	700 - 1200 K
PLOG	1	3.14E+60	-14.71	25159.97	0.99	700 - 1400 K
PLOG	10	2.46E+44	-9.66	19424.08	0.94	700 - 1500 K
PLOG	100	5.28E+29	-5.17	13305.69	0.94	700 - 1800 K
C5H4OH+HCO => C5H5+CO2		7.71E+09	0.13	2625.18	0.98	700 - 2000 K
PLOG	0.01	7.71E+09	0.13	2625.18	0.98	700 - 2000 K
PLOG	0.1	1.80E+17	-1.9	8886.82	0.99	700 - 2000 K
PLOG	1	1.05E+26	-4.28	17214.19	1	700 - 2000 K
PLOG	10	1.85E+32	-5.89	25484.09	1	700 - 2000 K
PLOG	100	6.54E+30	-5.29	30461.35	1	700 - 2000 K
C5H4OH+HCO => C4H5+CO+CO		1.09E+04	2.06	9117.34	1	700 - 2000 K
PLOG	0.01	1.09E+04	2.06	9117.34	1	700 - 2000 K

PLOG	0.1	9.90E+06	1.23	11471.4	1	700 - 2000 K
PLOG	1	1.49E+14	-0.74	17503.84	1	700 - 2000 K
PLOG	10	1.81E+23	-3.2	26462.96	1	700 - 2000 K
PLOG	100	5.87E+25	-3.73	33307.41	1	700 - 2000 K
C5H4OH+HCO => O-C6H4O2+H		2.62E+23	-3.41	25393.06	1	700 - 2000 K
PLOG	0.01	2.62E+23	-3.41	25393.06	1	700 - 2000 K
PLOG	0.1	5.53E+32	-5.92	34870.43	1	700 - 2000 K
PLOG	1	5.39E+34	-6.3	41115.03	1	700 - 2000 K
PLOG	10	6.72E+25	-3.55	41878.05	1	700 - 2000 K
PLOG	100	8.74E+08	1.42	38576	1	700 - 2000 K
C6H5O2 => C5H4OCHO		9.28E+129	-39.33	48841.87	0.54	700 - 1300 K
PLOG	1	9.28E+129	-39.33	48841.87	0.54	700 - 1300 K
PLOG	10	4.13E-34	10.6	-26777.06	0.14	700 - 1500 K
PLOG	100	6.22E+57	-14.07	45912.5	1	700 - 1700 K
C6H5O2 => C6H5+O2		1.11E+66	-15.94	62922.15	1	700 - 1300 K
PLOG	1	1.11E+66	-15.94	62922.15	1	700 - 1300 K
PLOG	10	2.04E+60	-13.81	63379.18	1	700 - 1500 K
PLOG	100	1.87E+49	-10.28	60139.37	1	700 - 1700 K
C6H5O2 => C6H5O+O		2.13E+58	-13.7	54461.41		700 - 1300 K
PLOG	1	2.13E+58	-13.7	54461.41	1	700 - 1300 K
PLOG	10	6.82E+50	-11.14	53532.26	1	700 - 1500 K
PLOG	100	2.59E+39	-7.57	49529.57	1	700 - 1700 K
C6H5O2 => C5H4O+HCO		3.31E+44	-9.98	40525	1	700 - 1300 K
PLOG	1	3.31E+44	-9.98	40525	1	700 - 1300 K
PLOG	10	3.73E+39	-8.29	40341.02	1	700 - 1500 K
PLOG	100	1.12E+38	-7.56	43847.6	1	700 - 1700 K
C5H4OCHO => C5H5+CO2		7.04E+56	-13.69	53912.54	1	700 - 1400 K
PLOG	1	7.04E+56	-13.69	53912.54	1	700 - 1400 K
PLOG	10	3.93E+46	-10.42	50930.14	1	700 - 1500 K
PLOG	100	1.83E+34	-6.64	46014.63	1	700 - 1800 K
C5H4OCHO => C5H4O+HCO		5.27E+64	-15.39	60248.12	1	700 - 1400 K
PLOG	1	5.27E+64	-15.39	60248.12	1	700 - 1400 K
PLOG	10	1.62E+55	-12.27	58069.32	1	700 - 1500 K
PLOG	100	7.74E+42	-8.45	53484.86	1	700 - 1800 K
O-C6H4O2H => C5H4OCHO		9.56E+64	-16.12	66163.32	1	700 - 1400 K
PLOG	1	9.56E+64	-16.12	66163.32	1	700 - 1400 K
PLOG	10	5.50E+53	-12.43	63646.5	1	700 - 1500 K
PLOG	100	4.08E+38	-7.73	58025.16	1	700 - 1800 K

O-C6H4O2H => O-C6H4O2+H		1.28E+53	-11.65	70328.84	1	700 - 1800 K
PLOG	1	1.28E+53	-11.65	70328.84	1	700 - 1800 K
PLOG	10	1.41E+40	-7.71	64802.02	1	700 - 2000 K
PLOG	100	2.13E+25	-3.33	57181	1	700 - 2000 K
O-C6H4O2H => C5H4O+HCO		1.06E+62	-14.33	75166.52	1	700 - 1800 K
PLOG	1	1.06E+62	-14.33	75166.52	1	700 - 1800 K
PLOG	10	1.33E+57	-12.58	77832.26	1	700 - 2000 K
PLOG	100	2.74E+46	-9.23	77692.37	1	700 - 2000 K
O-OC6H4OH => O-C6H4O2+H		9.06E+56	-12.24	96570.23	1	700 - 2000 K
PLOG	1	9.06E+56	-12.24	96570.23	1	700 - 2000 K
PLOG	10	2.08E+39	-6.98	87891.69	1	700 - 2000 K
PLOG	100	1.65E+24	-2.55	79841.65	1	700 - 2000 K
O-OC6H4OH => C5H4OH+CO		2.75E+52	-11.11	88387.35	1	700 - 2000 K
PLOG	1	2.75E+52	-11.11	88387.35	1	700 - 2000 K
PLOG	10	2.91E+37	-6.68	80699.36	1	700 - 2000 K
PLOG	100	9.63E+25	-3.32	74465.07	1	700 - 2000 K
O-OC6H4OH => C5H4O+HCO		1.10E+52	-11.16	90865.84	1	700 - 2000 K
PLOG	1	1.10E+52	-11.16	90865.84	1	700 - 2000 K
PLOG	10	1.24E+36	-6.42	82936	1	700 - 2000 K
PLOG	100	5.69E+22	-2.51	75715.88	1	700 - 2000 K

Table 6 Calculated reaction rate constants for the reaction steps belonging to the C_6H_5+O_2 PES

The kinetic parameters of the reactions belonging to the potential energy surface leading to the formation of p-benzoquinone were computed apart, being the only shared species the phenoxy and O(3P), as shown in Figure 31.

PARA		**k_0**	**α**	**E_a**	**R2_adj**	**Temp. Range**
C6H5O+O => C6H4O2+H		2.55E+12	0.16	-847.48	1	500 - 2000 K
PLOG	0.01	2.55E+12	0.16	-847.48	1	500 - 2000 K
PLOG	0.1	2.81E+12	0.15	-818.48	1	500 - 2000 K
PLOG	1	5.20E+12	0.08	-605.47	1	500 - 2000 K
PLOG	10	2.84E+13	-0.12	160.29	0.89	500 - 2000 K
PLOG	100	4.52E+11	0.41	-530.68	0.89	500 - 2000 K
C6H5O+O => OC6H4OH		1.11E+58	-16.11	12425.55	1	500 - 1700 K
PLOG	0.01	1.11E+58	-16.11	12425.55	1	500 - 1700 K
PLOG	0.1	2.33E+66	-17.81	16088.86	1	500 - 1800 K
PLOG	1	1.72E+64	-16.46	17679.89	1	500 - 2000 K

PLOG	10	1.97E+52	-12.43	14018.97	0.99	500 - 2000 K
PLOG	100	1.09E+39	-8.14	9826.44	0.99	500 - 2000 K
C6H5O+O => C5H4OH+CO		6.99E+13	-0.72	-47.42	1	500 - 2000 K
PLOG	0.01	6.99E+13	-0.72	-47.42	1	500 - 2000 K
PLOG	0.1	4.63E+14	-0.95	540.49	1	500 - 2000 K
PLOG	1	1.13E+19	-2.16	4274.4	0.99	500 - 2000 K
PLOG	10	1.11E+19	-2.05	7180.93	0.98	500 - 2000 K
PLOG	100	2.37E+07	1.4	4106.45	0.98	500 - 2000 K
C6H4O2+H => OC6H4OH		2.77E+68	-16.85	24462.34	0.98	500 - 1700 K
PLOG	0.01	2.77E+68	-16.85	24462.34	0.98	500 - 1700 K
PLOG	0.1	3.38E+61	-14.5	23258.34	0.95	500 - 1800 K
PLOG	1	2.18E+53	-11.82	21203.46	0.88	500 - 2000 K
PLOG	10	4.39E+39	-7.59	15974.98	0.76	500 - 2000 K
PLOG	100	2.93E+21	-2.11	7966.93	0.97	500 - 2000 K
C6H4O2+H => C5H4OH+CO		1.53E+35	-5.91	24779.08	1	500 - 2000 K
PLOG	0.01	1.53E+35	-5.91	24779.08	1	500 - 2000 K
PLOG	0.1	2.44E+34	-5.55	27640.15	1	500 - 2000 K
PLOG	1	8.31E+25	-3	26515.83	1	500 - 2000 K
PLOG	10	5.95E+10	1.43	21496.1	1	500 - 2000 K
PLOG	100	2.00E-06	6.14	15050.61	1	500 - 2000 K
OC6H4OH => C6H4O2+H		6.09E+60	-14.33	79062.07	1	500 - 1700 K
PLOG	0.01	6.09E+60	-14.33	79062.07	1	500 - 1700 K
PLOG	0.1	7.35E+49	-10.85	75597.66	1	500 - 1800 K
PLOG	1	2.33E+40	-7.87	72317.22	1	500 - 2000 K
PLOG	10	3.59E+27	-3.98	66928.76	1	500 - 2000 K
PLOG	100	7.36E+17	-1.06	62614.11	1	500 - 2000 K
OC6H4OH => C5H4OH+CO		4.76E+57	-13.41	74988.02	1	500 - 1700 K
PLOG	0.01	4.76E+57	-13.41	74988.02	1	500 - 1700 K
PLOG	0.1	2.23E+47	-10.15	71504.48	1	500 - 1800 K
PLOG	1	6.82E+38	-7.5	68471.7	1	500 - 2000 K
PLOG	10	3.57E+27	-4.07	63686.85	1	500 - 2000 K
PLOG	100	2.31E+19	-1.61	60042.44	1	500 - 2000 K

Table 7 Calculated reaction rate constants of the reaction steps leading to the formation of para isomer of benzoquinone

The missing constants were not included because the reaction was unlikely to take place and the rate constants computation gave no result at all temperatures and pressures.

7.5 Results Discussion

7.5.1 Rate comparisons

In this paragraph a comparison between some of the computed rate constants and the already existing ones in the CRECK_20_03 model is provided.

The entrance channel of the reactive system $C_6H_5+O_2$ was already investigated in the literature. As a reference, the work of Zhang et al.[36], Kislov et al.[37] and of Da Silva et al.[37] were taken into account. The common ground among the three works is that the triplet nature of O2(3P) results in a barrierless minimum energy path (MEP) for its addition to phenyl radical.

Da Silva et al.[35] computed the reaction rate constant using the VTST. Zhang et al.[36] , on the heels of Kislov et al.[38] , employed the VRC-TST. Their results went beyond, thanks to the higher accuracy of computational methods employed, providing more reliable predictions of both the absolute rate constants and their temperature dependence.

The rate constants were compared also with experimental data collected by Yu et al.[39] and by Schaugg et al.[37].

In the temperature dependence there is discrepancy in theoretical predictions. The calculations of Da Silva et al.[36] predict that the rate coefficient should decrease over the 300–2000 K temperature range. Kislov et al.[39] predict that rate constant should rise over the 418–2500 K range, in qualitative accord with the observation of a positive temperature dependence by Schaugg et al.[40]. Zhang et al.[38]results are in good agreement with the predictions of Da Silva et al. and the experimental measurements of Yu et al.[22]. It is important to keep in mind the higher accuracy of computational methods employed

by Zhang et al. The C_6H_5 + O_2 rate constant implemented in this work was computed by Pratali Maffei et al.[28] employing the VRC-TST.

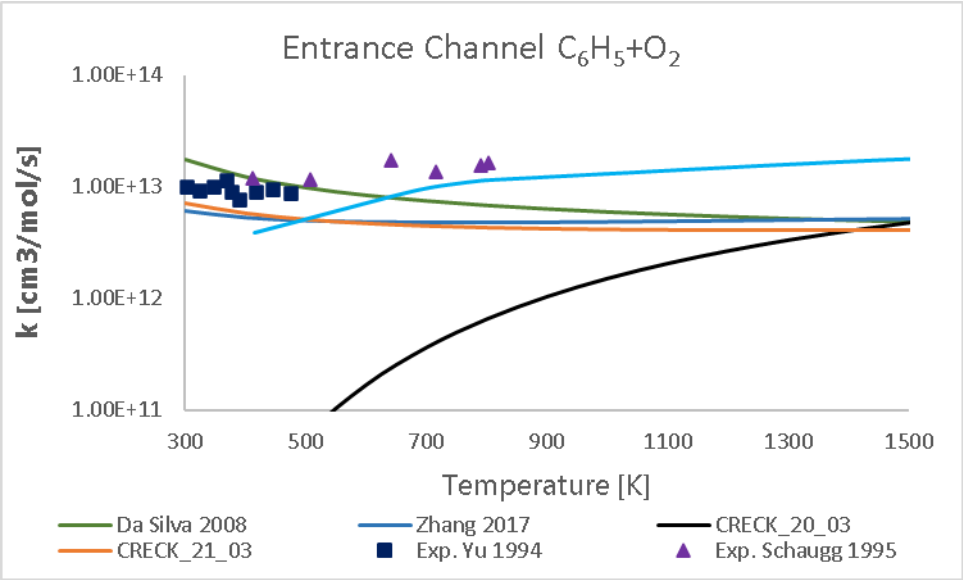

Figure 40 Comparison between calculated rate constants for phenyl + O2 recombination.

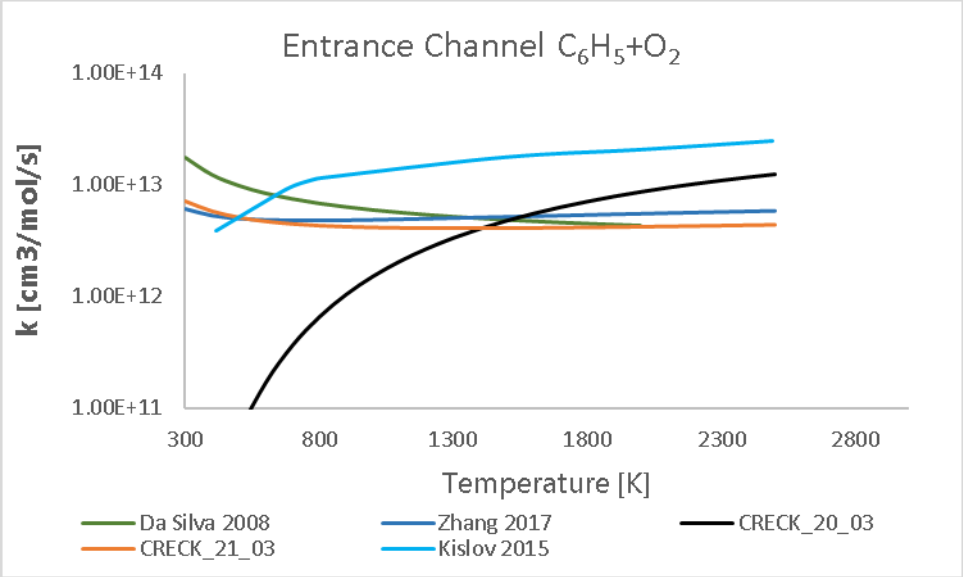

Figure 41 Comparison between calculated and experimental rate constants for phenyl + O2 recombination.

It can be noticed that the rate constant results agree with the work of Da Silva et al. Zhang et al., whose accuracy was higher than Kislov et al. results, whose shape was similar to the old CRECK mechanism kinetic constant.

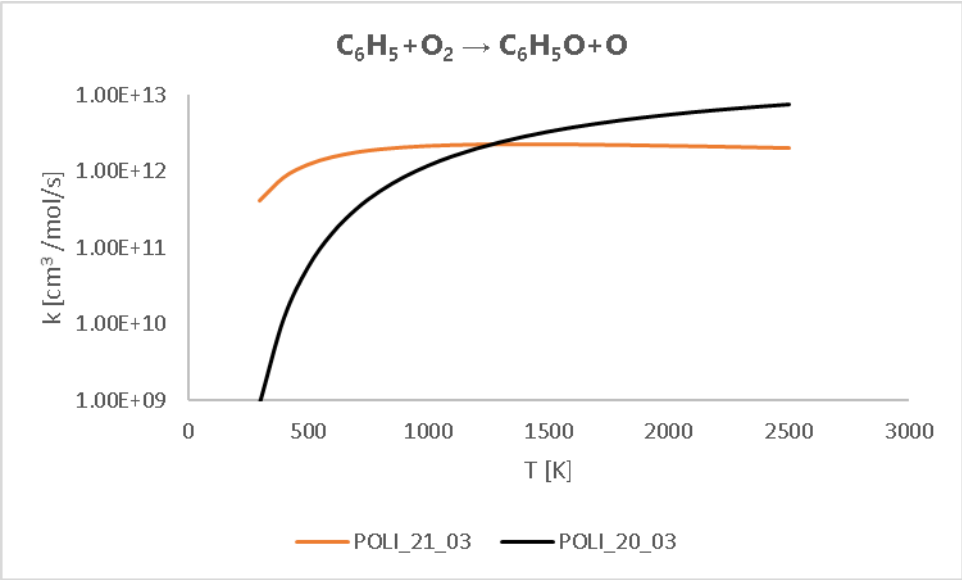

Figure 42 Comparison between the old and the new rate constant for the well-skipping reaction C6H5+O2→C6H5O+O

The second comparison refers to the well-skipping reaction $C_6H_5+O_2 \rightarrow C_6H_5O+O$. From the resolution of a multi-well master equation it was pointed out that the addition of molecular oxygen to phenyl radical can directly lead to the formation of phenoxy radical and O atom. The trend is similar; however, the new reaction rate is flatter being the entrance channel barrierless.

In figure 43, it is possible to notice good agreement between the new implemented rate constant and the old one. The rate constant was not defined with the VRC-TST thus, probably, this determined an easier evaluation of the rate constant also in past decades.

For the reaction $C_6H_5O+O \rightarrow C_6H_4O_2+H$, the two trends are incompatible, the already existing rate constant in the CRECK_20_03 mechanism showed no dependence on temperature, likely defined just to fit the experimental data.

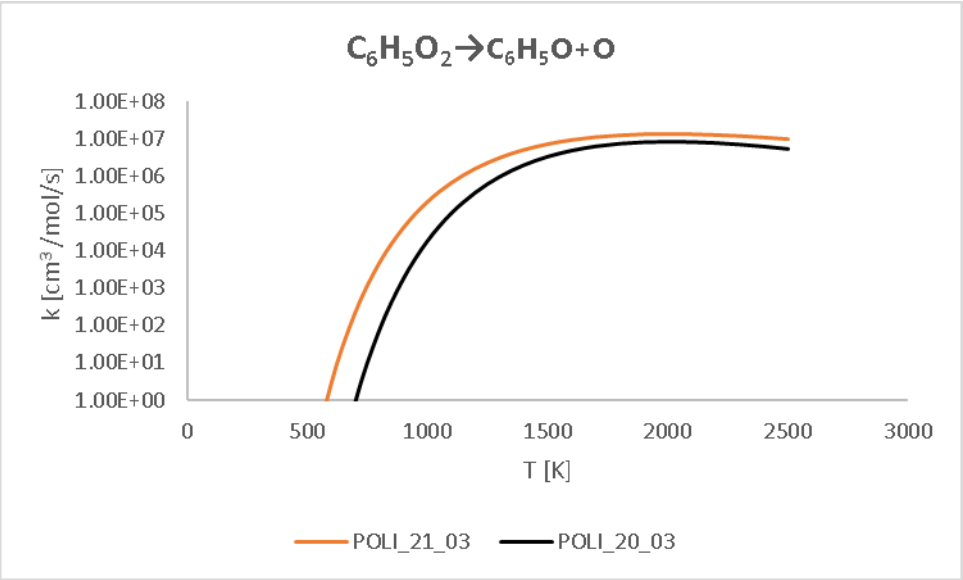

Figure 43 Comparison between the old and the new rate constant for the reaction $C_6H_5O_2 \rightarrow C_6H_5O+O$

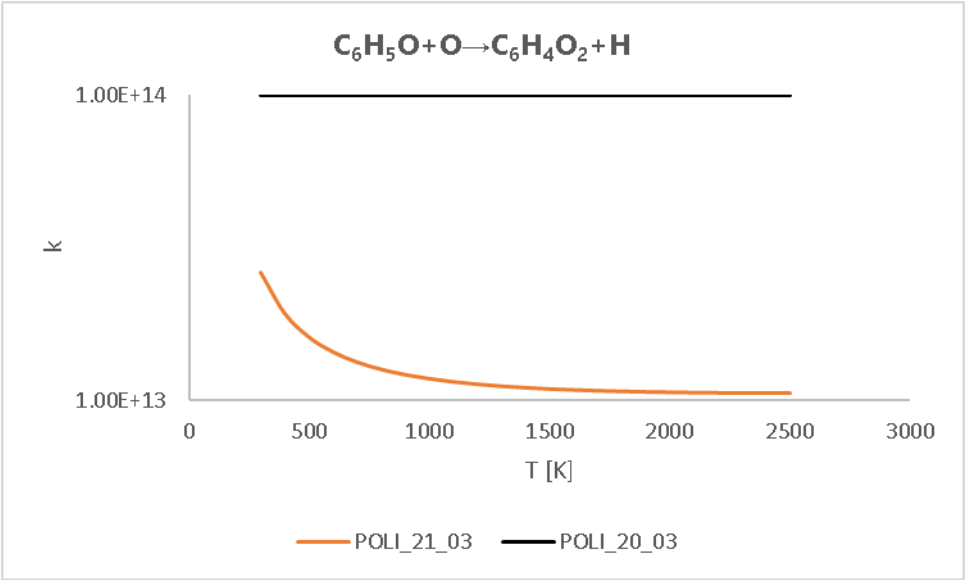

Figure 44 Comparison between the old and the new rate constant for the reaction $C_6H_5O+O \rightarrow C_6H_4O_2+H$

7.5.2 Branching Ratios

The branching ratios for the reactants $C_6H_5+O_2$ were computed. Being the reactions pressure and temperature dependent, two estimates were made: in Figure 45 the branching ratios were computed in the temperature range T=700-1500K at a fixed

pressure of 1 atm. In Figure 46 the branching ratio trends with the change in pressure were calculated, at a fixed temperature of 1000K.

At atmospheric pressure, the production of phenoxy (C_6H_5O+O), without passing through the phenylperoxy radical ($C_6H_5O_2$) formation, dominates the other channels. The only exception is made in the temperature range T=700-850K, where the formation of $C_6H_5O_2$ is faster.

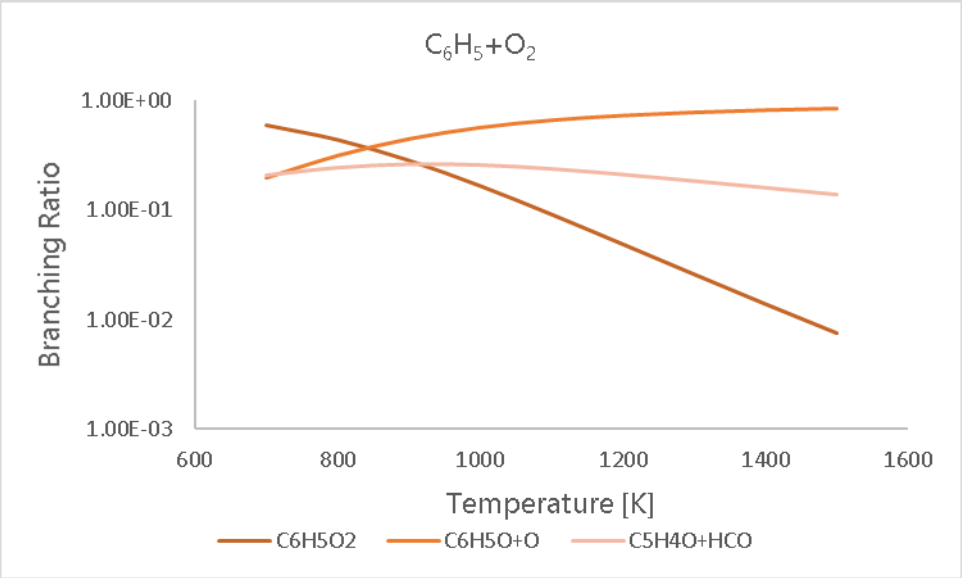

Figure 45 Branching ratios as a function of temperature at a fixed pressure of 1 atm.

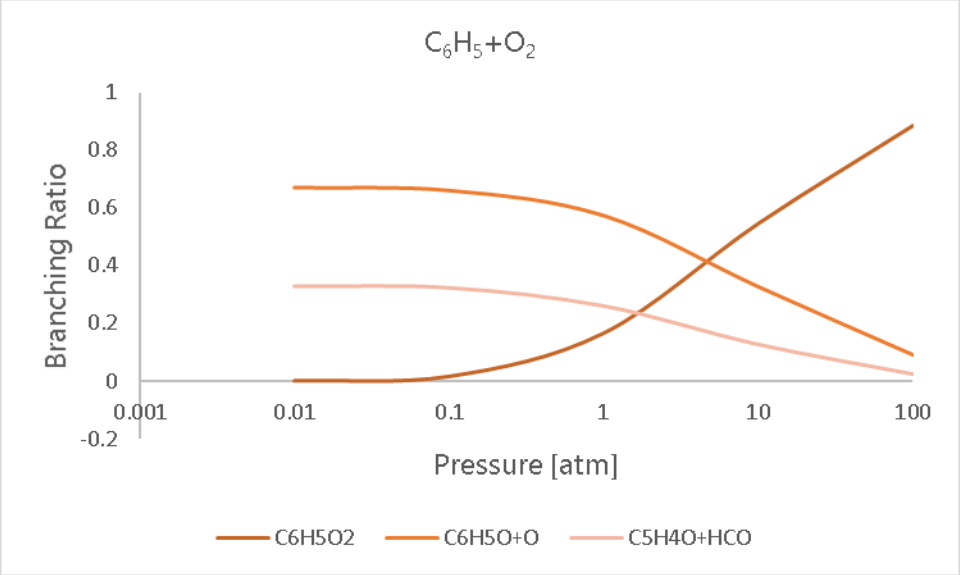

Figure 46 Branching ratios as a function of pressure at a fixed temperature of 1000K.

In the branching ratio-pressure plot, the phenoxy (C_6H_5O+O) formation is still predominant, but at pressures slightly over the atmospheric one, a crossover is observed. The phenylperoxy radical formation is favoured by low temperatures and high pressures.

CHAPTER 8
The Model Validation

The validation stage consists in the simulation of the detailed kinetic mechanism, with the new rates implemented, in different reactors types. By varying the operating conditions, it is possible to figure out to what extent the model well-predicts experimental data. All simulations were performed with the OpenSMOKE++ code, testing the kinetic mechanism POLI_21_03, which is compared to experimental data and to the prediction performances of the starting kinetic mechanism, in this chapter named POLI_20_03. The POLI_20_03 mechanism was already introduced in Chapter 6.

In the following table are listed the simulations whose results are shown in this chapter. Targets missing with respect to tables 2,3,4,5 (Chapter 6.1) can be found in the Appendix.

8.1 Benzene Oxidation in PFRs

8.1.1 Brezinsky et al.[28]

As already presented in Chapter 6.4, the high temperature oxidation of benzene in a plug flow reactor was experimentally investigated by Brezinsky et al.[41] In Figure 48 is reported the comparison of the predictive performances of the two mechanisms at an equivalence ratio of 1. The updated mechanism improves the results, the implemented rates increase benzene reactivity, and an appreciable progress of the predictive performance can be observed for CO production.

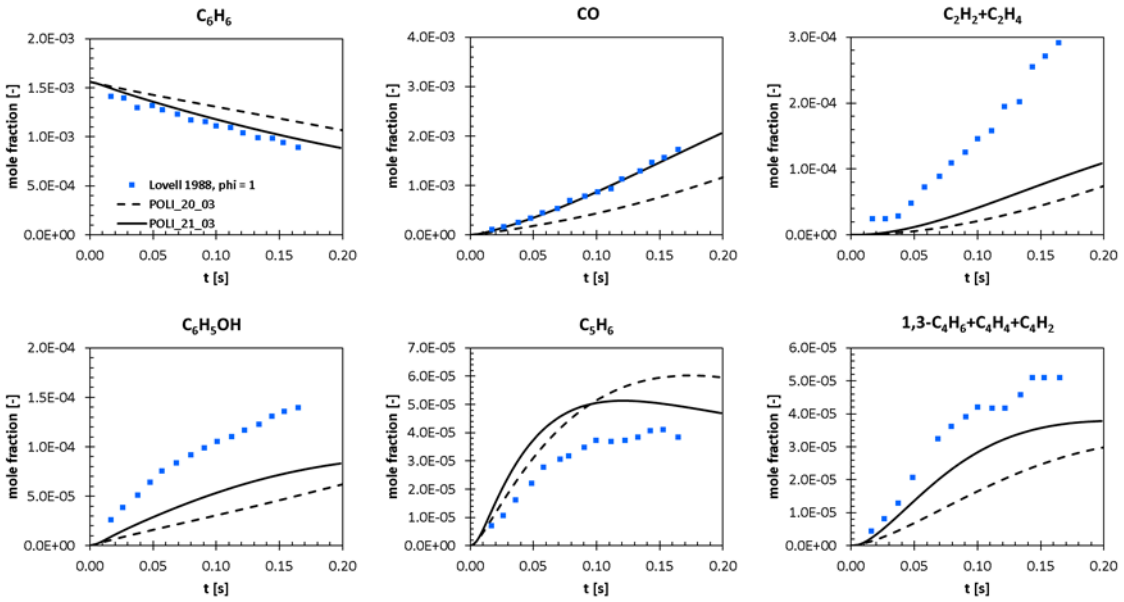

Figure 48 Comparison between the two mechanisms POLI_21_03 and POLI_20_03 for the oxidation of benzene in a PFR at φ=1 and T=1102K.

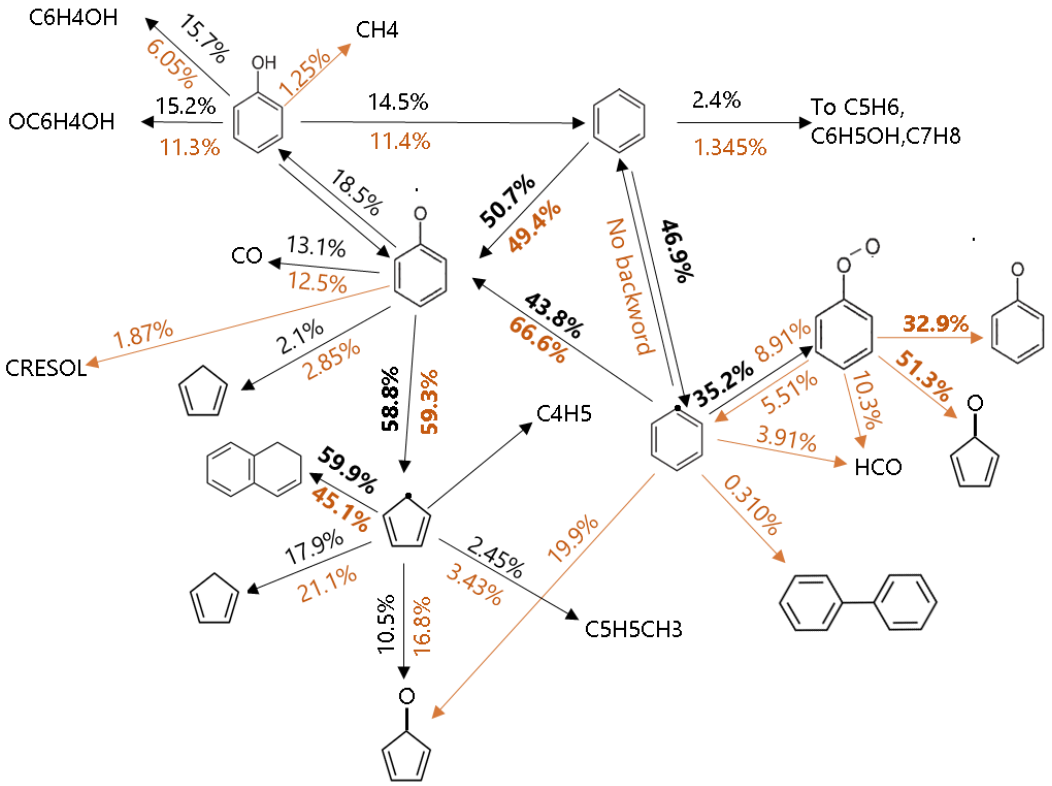

Figure 47 Flow path analysis of POLI_21_03 mechanism for benzene oxidation in a PFR. The percentages in black are referred to past values belonging to the mechanism POLI_20_03. The arrows in blue indicate new reaction paths.

By changing the equivalence ratio value, the results keep coherent. To further investigate the performances, these results are reported in the Appendix.

To better understand what changes in the mechanism, a comparison between the reaction path of POLI_20_03 and POLI_21_03 was made.

The arrows in gold are additional paths not present in POLI_20_03 and the gold percentages are the updated ones.

The main difference is related to phenyl (C_6H_5) reactivity, if before the update more than the 43% of phenyl turned into phenoxy, now this percentage arises to more than 66%. This means that phenoxy reactivity is the main responsible of products formation. Another important difference is the increase in the amount of C_5H_5 that forms dialin ($C_{10}H_{10}$). In this new flow path analysis, it is not present the reaction channel that forms benzoquinone starting from phenyl radical, instead, there is the formation of biphenyl even if at very low amounts.

Overall, the mechanism properly captures products trends.

8.1.2 Venkat et al.[41]

Benzene oxidation was simulated also in another PFR, according to Venkat et al.[28] operating conditions. With respect to Brezinsky et al.[21] ,the residence time is halved, the inlet temperature is slightly higher (1120 K) and the equivalence ratio is lower and amounts to 0.4. Experimental data and modelling predictions are shown in Figure 49 for the mechanisms POLI_20_03 and POLI_21_03. The results are not far from the ones of the POLI_20_03 mechanism: benzene production is still too high at the end of the plug flow reactor, and the trends of C1-C2 species are not well-predicted. From the sensitivity analysis it was figured out that the reactions responsible of the benzene trend were investigated through “ab-initio” methods. Thus, the not accurate model prediction arises from the error-compensation which was perturbed by the implementation of kinetic constants computed a-priori, whose margin of error is far from the experimentally defined ones, being the latter much less accurate.

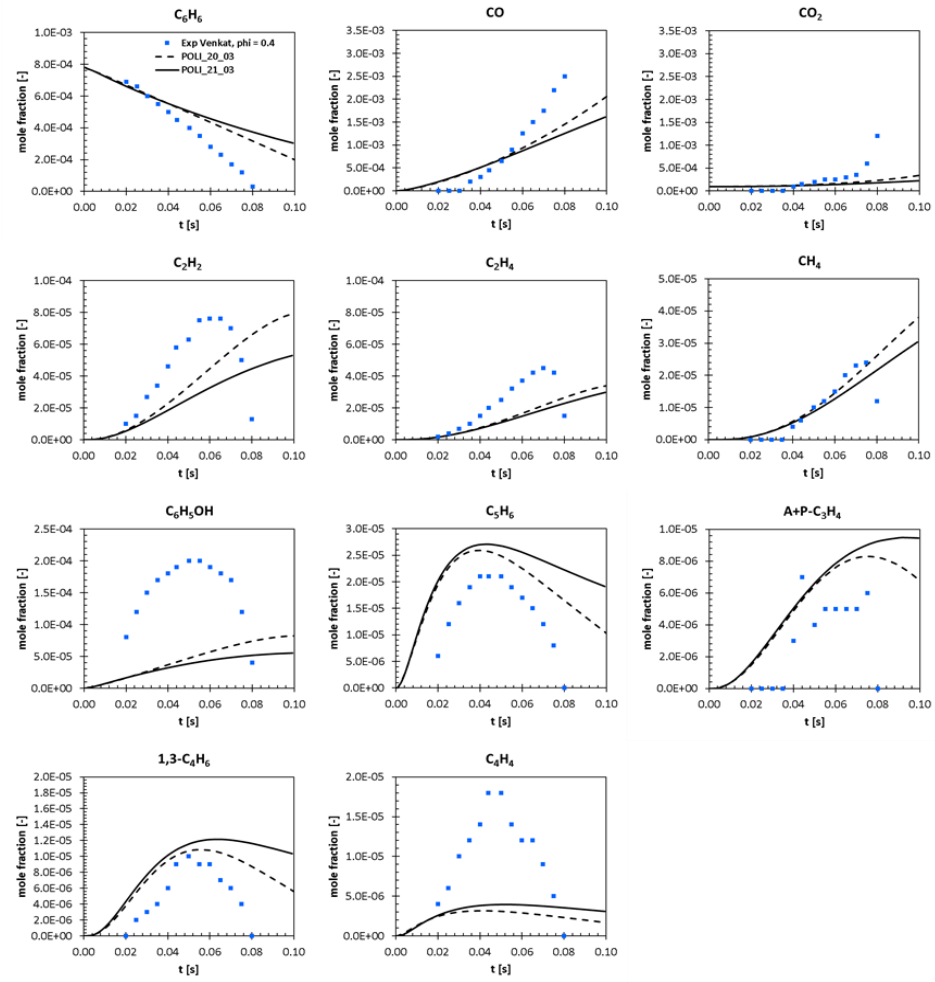

Figure 49 Venkat et al. PFR simulation for mechanisms POLI_21_03 and POLI_20_03

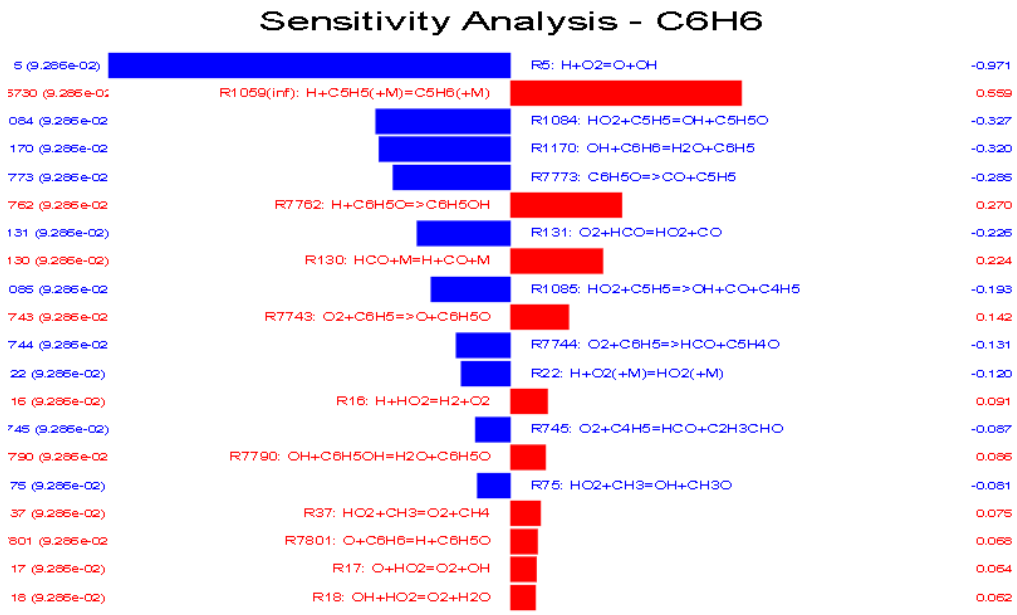

Figure 50 Benzene sensitivity analysis carried out for Venkat et al. PFR

8.2 Benzene Oxidation in JSRs

8.2.1 Ristori et al.[21]

To investigate the prediction performances of the new mechanism in a jet-stirred reactor the simulations outcome according to Ristori et al.[24] database is given. In Chapter 6.5 it was explained that the simulations were carried out at different equivalence ratio but, just the plots computed at ϕ=0.5, 1 and 1. are presented in this paragraph. However, the missing plots can be found in the Appendix.

At lean conditions, the mechanism provides a general agreement with experimental data and, in some cases, better predicts the trends with respect to the starting mechanism. This is the case of CO, CO_2, H_2, CH_4, where the shape is greatly improved. However, the benzene reactivity decreases, distancing the curve from the experimental data. To figure out the reactions that majorly influence this behaviour, a sensitivity analysis was run. For other species is not registered an improvement in the predictions, but these are less relevant since produced in very small quantities.

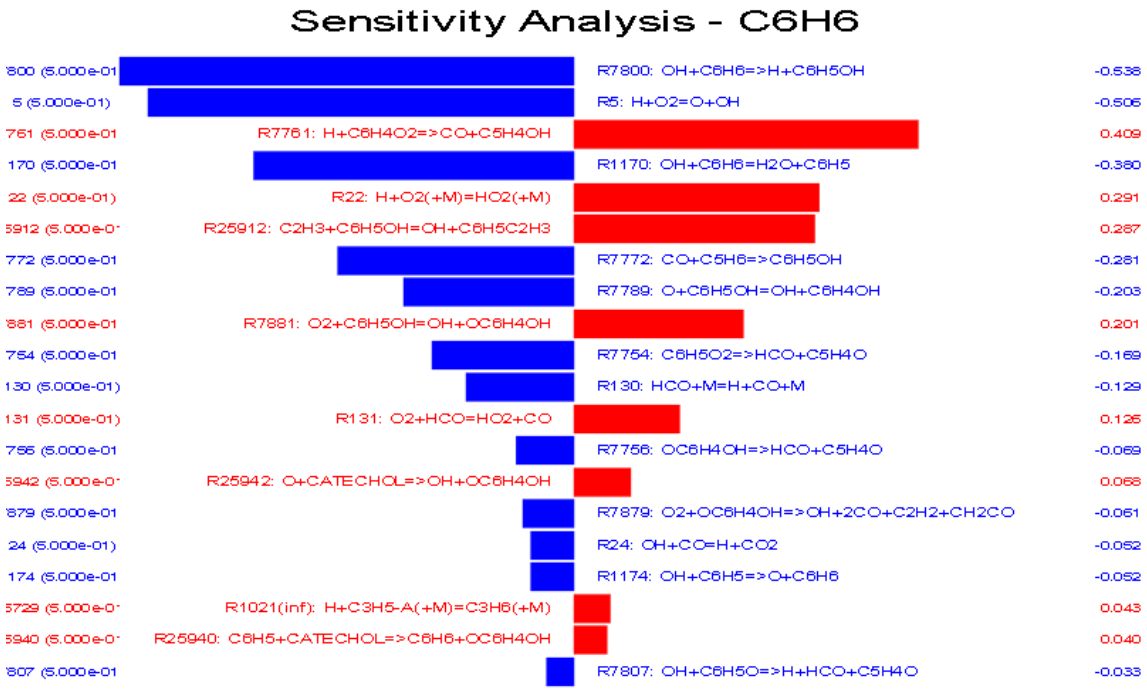

Figure 51 Sensitivity analysis of benzene oxidation at atmospheric pressure in a JSR at φ=0.3. for the mechanism POLI_21_03.

The benzene consumption and production are governed by the H-abstraction reaction with OH as an abstracting agent and by the benzoquinone decomposition into CO and C5H4OH. Both reactions parameters have been defined through ab-initio methods thus, their estimates are much more accurate than kinetic parameters defined experimentally thus, they cannot be substituted. Considering that, reaction parameters obtained experimentally are subjected to an error much higher, it is possible to apply adjustments within a certain limit. Minor reactions parameters (e.g. $C_2H_3+C_6H_5OH=OH+C_6H_5C_2H_3$) have been changed, but their influence is low and there is not a noticeable improvement.

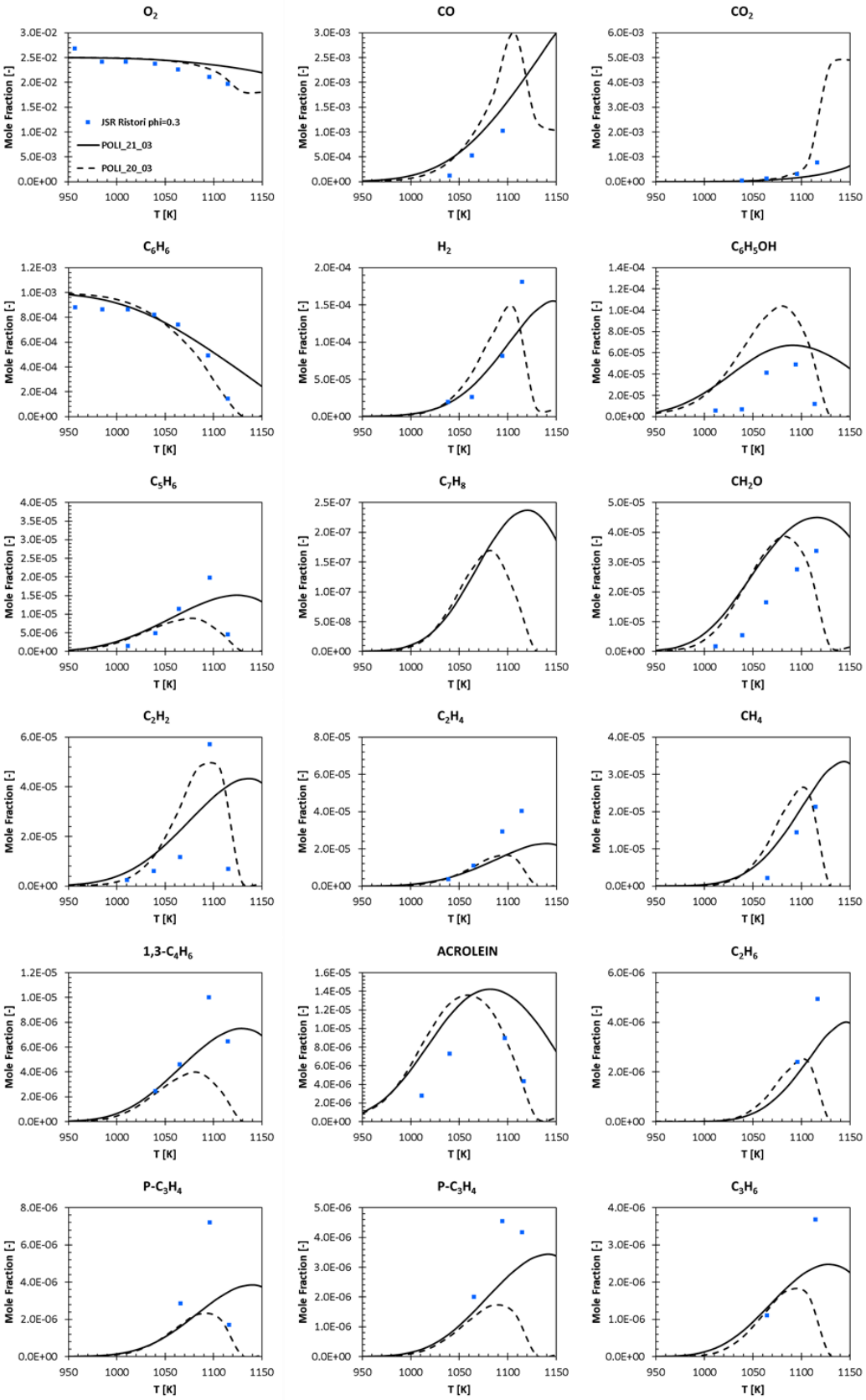

Figure 52 Ristori et al. JSR simulation results at φ=0.3 at a T range=[950,1150]. The two mechanism POLI_21_03 and POLI_20_03 are compared.

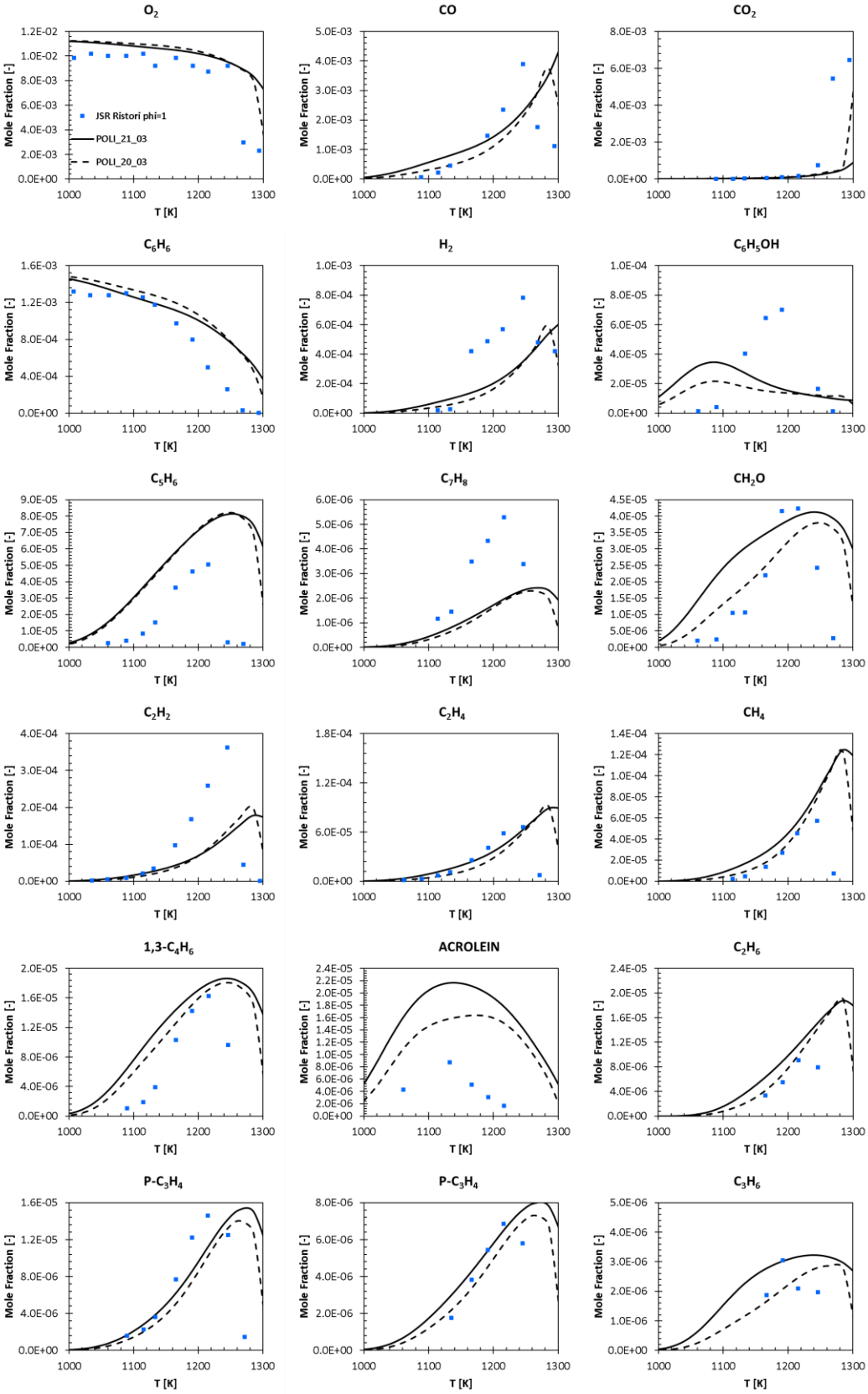

Figure 53 Ristori et al. JSR simulation results at φ=1. at a T range=[950,1150]. The two mechanism POLI_21_03 and POLI_20_03 are compared.

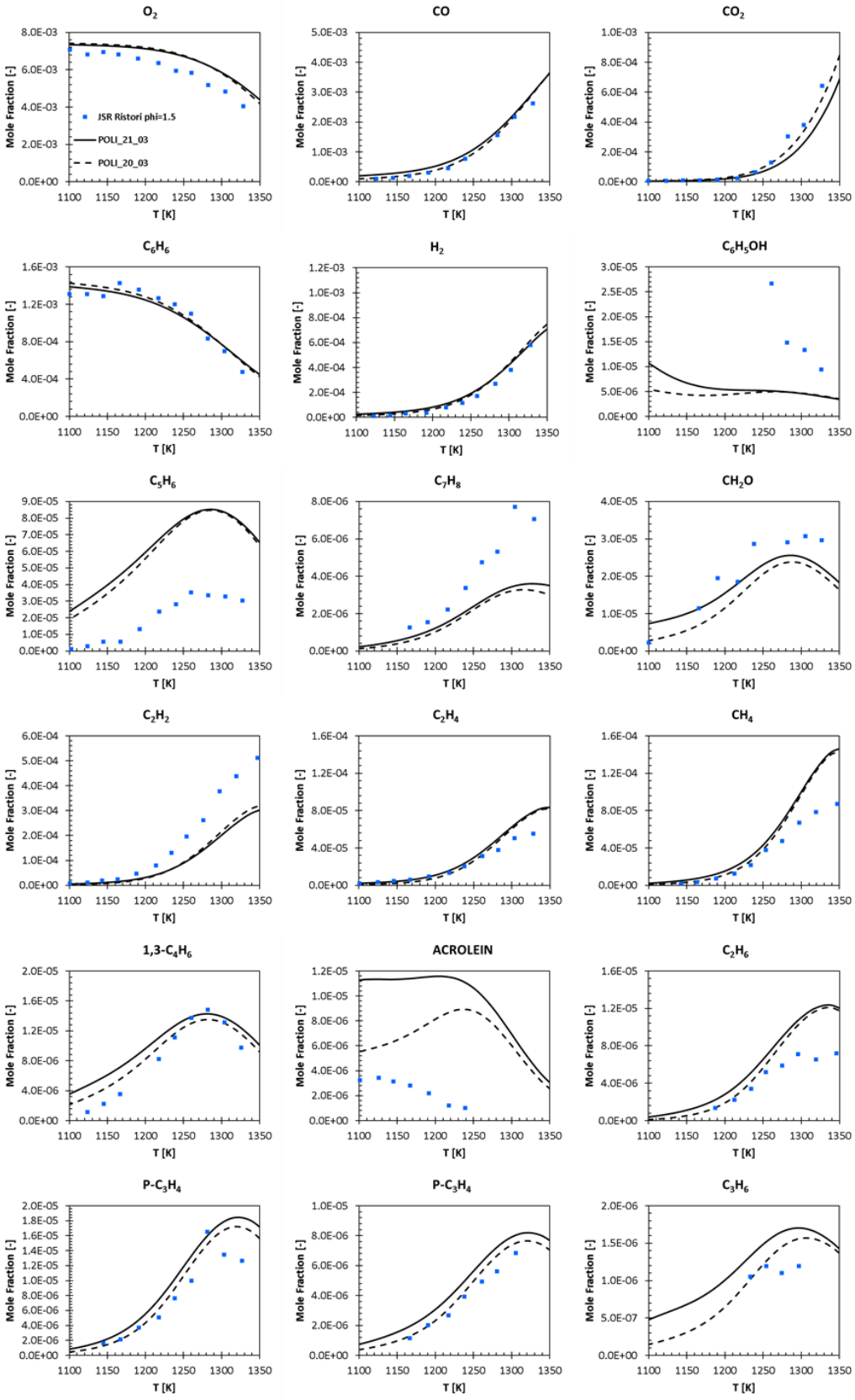

Figure 54 Ristori et al. JSR simulation results at φ=1.5. at a T range=[950,1150]. The two mechanism POLI_21_03 and POLI_20_03 are compared.

At stochiometric and rich conditions, there is always a good agreement and the behaviour of the two mechanism is almost the same.

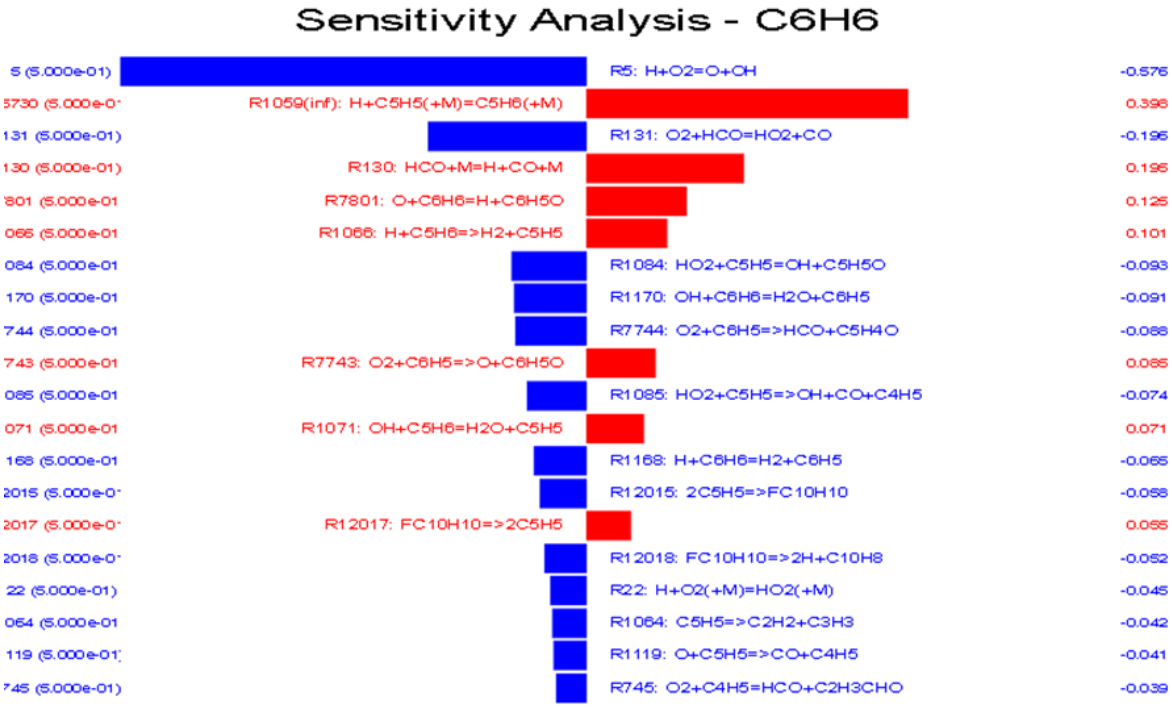

Figure 55 Sensistivity analysis for benzene oxidation in a JSR at atmospheric pressure and φ =0.3 for the kinetic mechanism POLI_21_03

By changing the composition of the inlet mixture, also change the reactions that majorly influence the benzene consumption. In this case an important role is played by the H addition on C_5H_5 to form cyclopentadienyl. The reaction parameters have been defined through ab-initio methods thus, once again there is no room for improvement because the accuracy is high.

In the next page are reported the flow path analysis of benzene oxidation at ϕ=0.3 and ϕ=1. It is provided a comparison between the percentages before updating the mechanism, and the ones obtained with the implementation of the calculated rate constants. Looking at the analysis carried out at ϕ=0.3, the main difference found is about the phenyl radical reactivity, more than the 70% turns into phenoxy radical by oxygen addition. However, it is reduced the percentage of $C_6H_5O_2$ that leads to phenoxy, in fact previously it was 100%. Phenol too changes a lot its reactivity, increasing the amount that goes back to phenoxy radical.

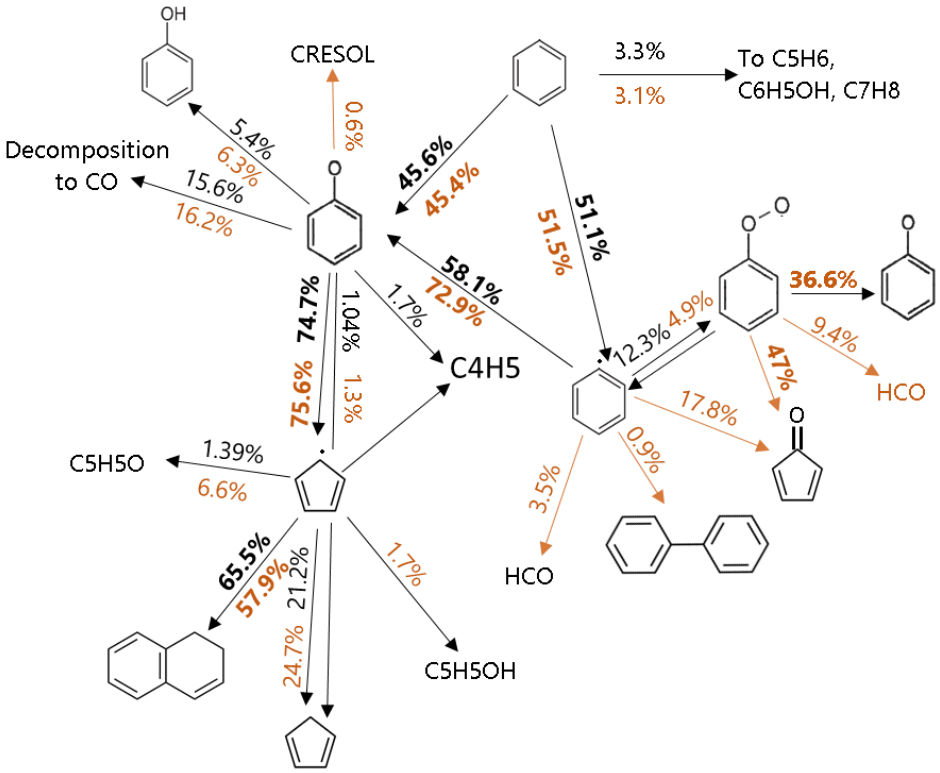

Figure 56 Flow path analysis of benzene oxidation in a JSR at atmospheric pressure and φ=0.3. The percentages in gold are referred to the mechanism POLI_21_03, the ones in black refer to POLI_20_03.

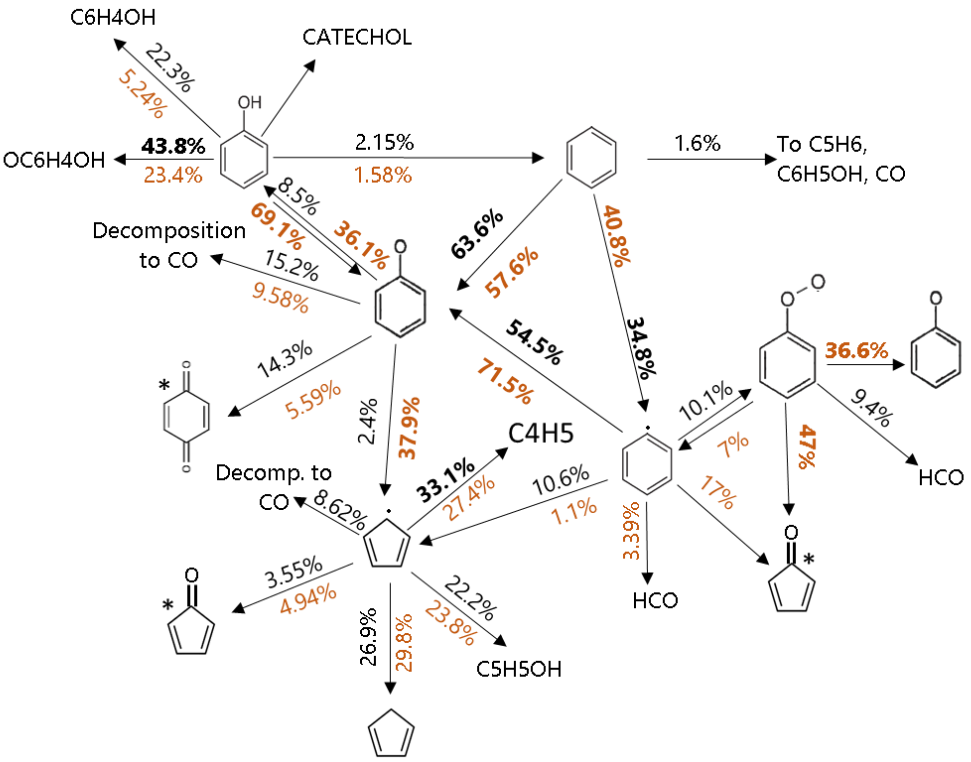

Figure 57 Flow path analysis of benzene oxidation in a JSR at atmospheric pressure and φ=1. The percentages in gold are referred to the mechanism POLI_21_03, the ones in black refer to POLI_20_03.

At ϕ=1, the differences are much smaller, as it was expected looking at the prediction results. The main difference always concerns the phenyl radical, whose largest amount turns into phenoxy radical.

8.2.2 Chai et al.[24]

The wider the range of operating conditions for which the mechanism is validated, the more reliable it is. Thus, POLI_21_03 was also tested for the experimental data obtained by Chai and Pfefferle[21] ,already introduced in Chapter 6.2.2. While in Ristori et al.[42]the oxidation was carried out at atmospheric pressure, in this case the model is validated at a pressure of 0.46 atm, in a micro-JSR. The model well predicts the experimental data, even though the benzene (C_6H_6) reactivity, phenol (C_6H_5OH) and CPD (C_5H_6) production are still overestimated. An evident improvement can be spotted for benzoquinone ($C_6H_4O_2$), one of the products of the investigated PES.

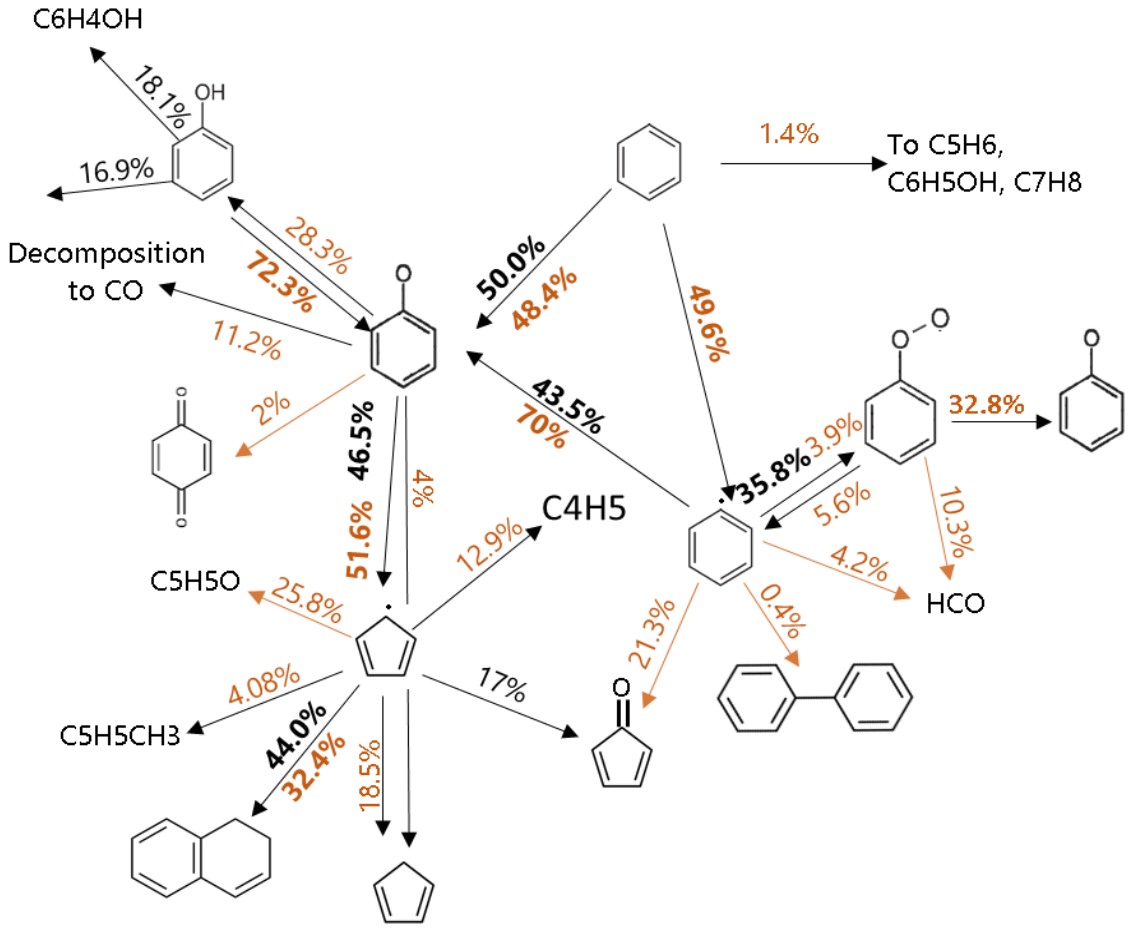

Figure 58 Flow path analysis for benzene oxidation in Chai et al. JSR at φ=1.02

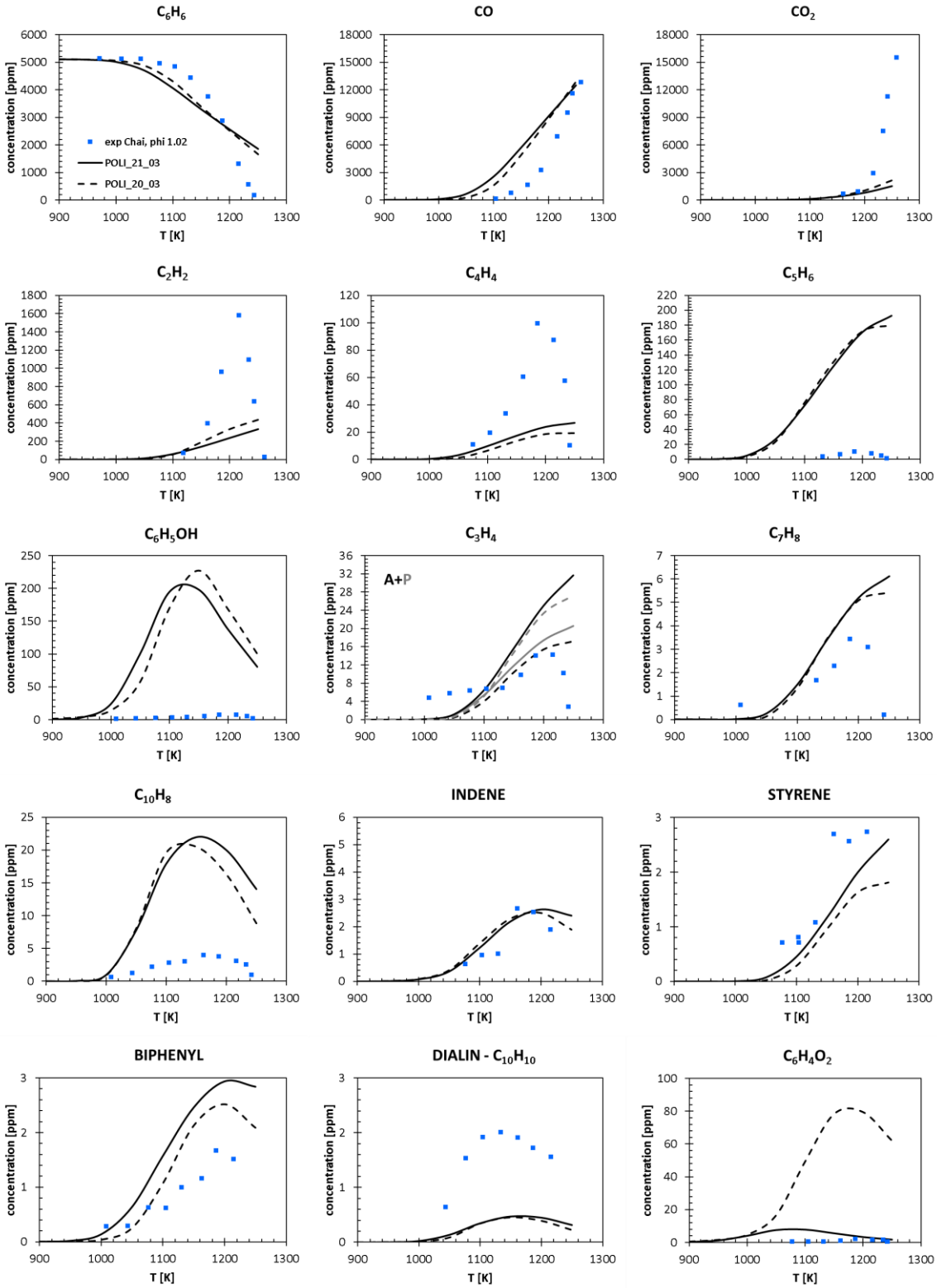

Figure 59 Model prediction for Chai et al. experimental database in a micro-JSR at 0.46 atm and φ=1.02.

In figure 55, the reaction flow path is shown. As already explained, the gold arrows refer to new reaction paths, that were not present in the reaction flow of the mechanism POLI_20_03. The gold percentage refer to the new ones, the black ones come from POLI_20_03 , to highlight the main differences between the two mechanisms. As for Ristori, the rate of production shows that the implementation of the new rates increases the percentage of phenyl radical that undergoes oxygen addition to form the phenoxy radical. Moreover, benzoquinone from phenyl is no more produced. Another recurrent difference in JSR with respect to the flow path of POLI_20_03 (Chapter 6) is that more phenol is produced from phenoxy radical, but a large part of it undergoes the backword reaction. These results are coherent with the previous ones, that were computed at higher pressures. The simulation was also carried out at lower ϕ=0.19, the result can be found in the Appendix.

8.2.3 Marchal et al.[42]

To validate the kinetic mechanism at different pressure, it was tested against the high-pressure data of Marchal et al.[43]. These data refer to 10 atm, residence time of 0.7 s, over a wide range of temperatures (900–1200 K) and equivalence ratios (0.5–1.5). In this paragraph only results related to the simulation carried out at ϕ=1.5 are shown, the other are reported in the Appendix.

From Figure 60, there is generally satisfactory agreement between the model prediction and the experimental data, thus confirming the model ability to properly account for the pressure effects. The mechanism performance is improved if compared to POLI_20_03.

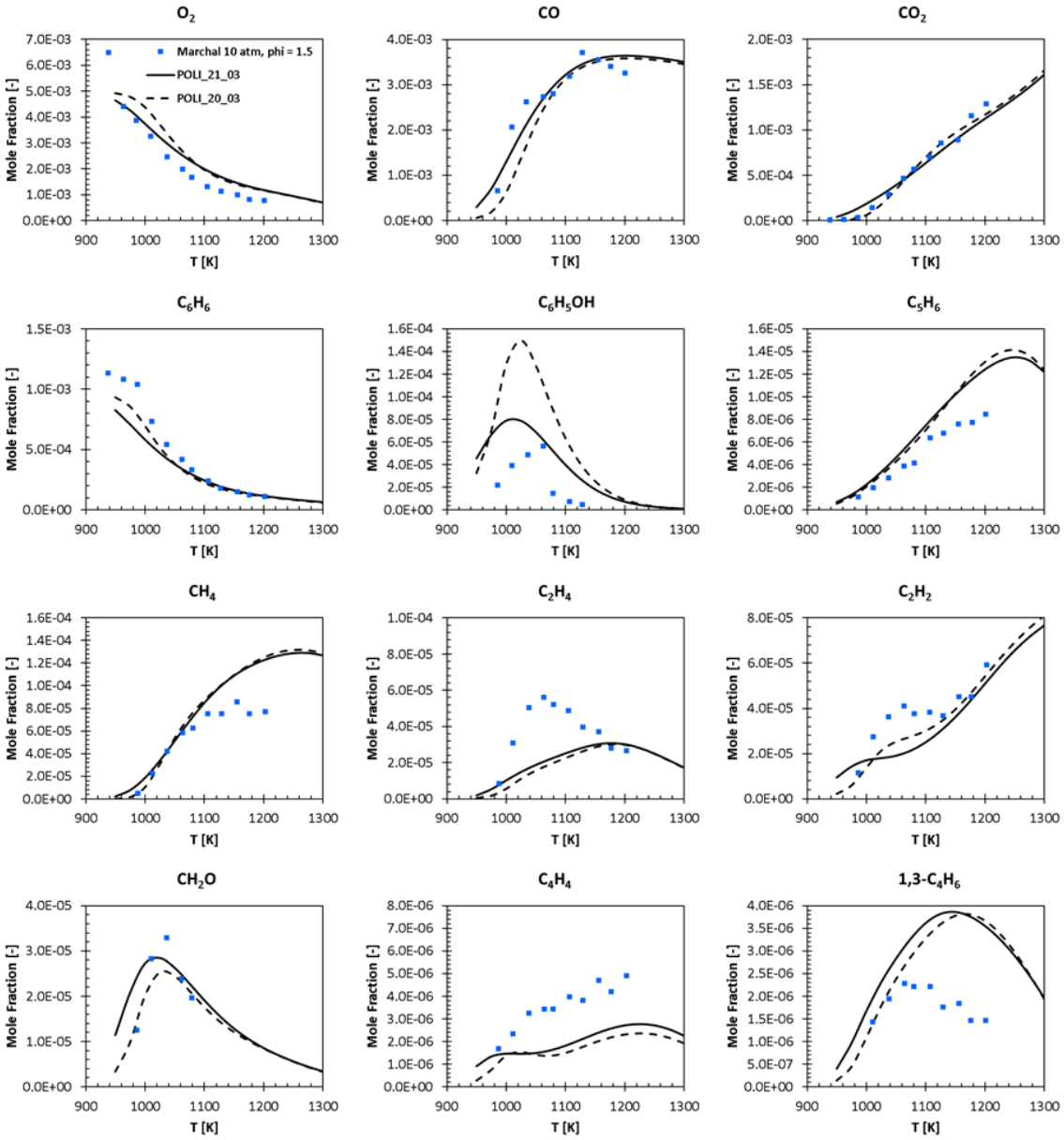

Figure 60 POLI_21_03 mechanism prediction for benzene oxidation in a JSR at 10 atm compared to the Marchal et al. experimental database and POLI_20_03 model predictions.

8.3 IDT in Shock Tubes (ST)

8.3.1 Burcat et al. [43]

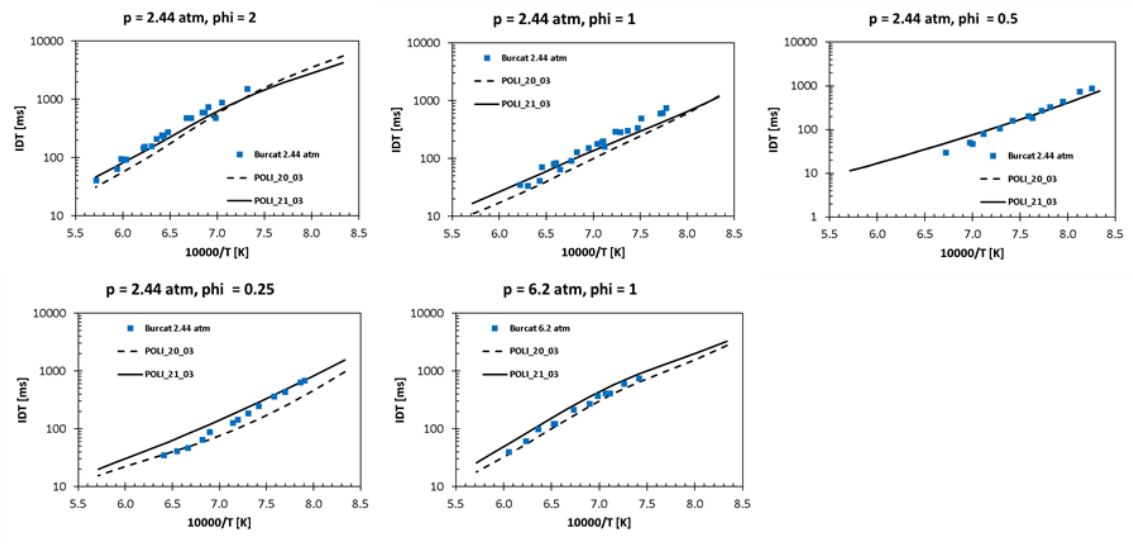

Figure 61 Ignition delay time for benzene oxidation compared to Burcat et al. experimental database and prediction performance of POLI_20_03 mechanism.

The ignition delay time is a feature that directly impacts the anti-knocking propensity of fuels. The higher is the ignition delay time, the higher is the fuel resistance to auto-ignition thus, it is suitable for internal combustion engines with spark ignition.

The measurements were carried out in a shock tube, for an inlet mixture of benzene and oxygen diluted in Argon, at 1200K. The tested temperature range is 1200-1750 K, with a fuel equivalence ratio range ϕ=0.25-2 and shock pressures from 2.44 to 6.2 atm. The experimental database was reviewed by Burcat et al.[44]

The mechanism is able to closely reproduce the experimental auto-ignition behaviour, despite pressure and inlet mixture composition effects, and better than the mechanism POLI_20_03. At lower equivalence ratio (0.25) the ignition delay time is overpredicted, but at lower temperatures the curve fits the experimental points.

8.4 Catechol oxidation in PFR

8.4.1 Thomas et al. [44]

The model validation proceeded with the catechol oxidation simulations. The examined database was reviewed by Thomas et al.[45]

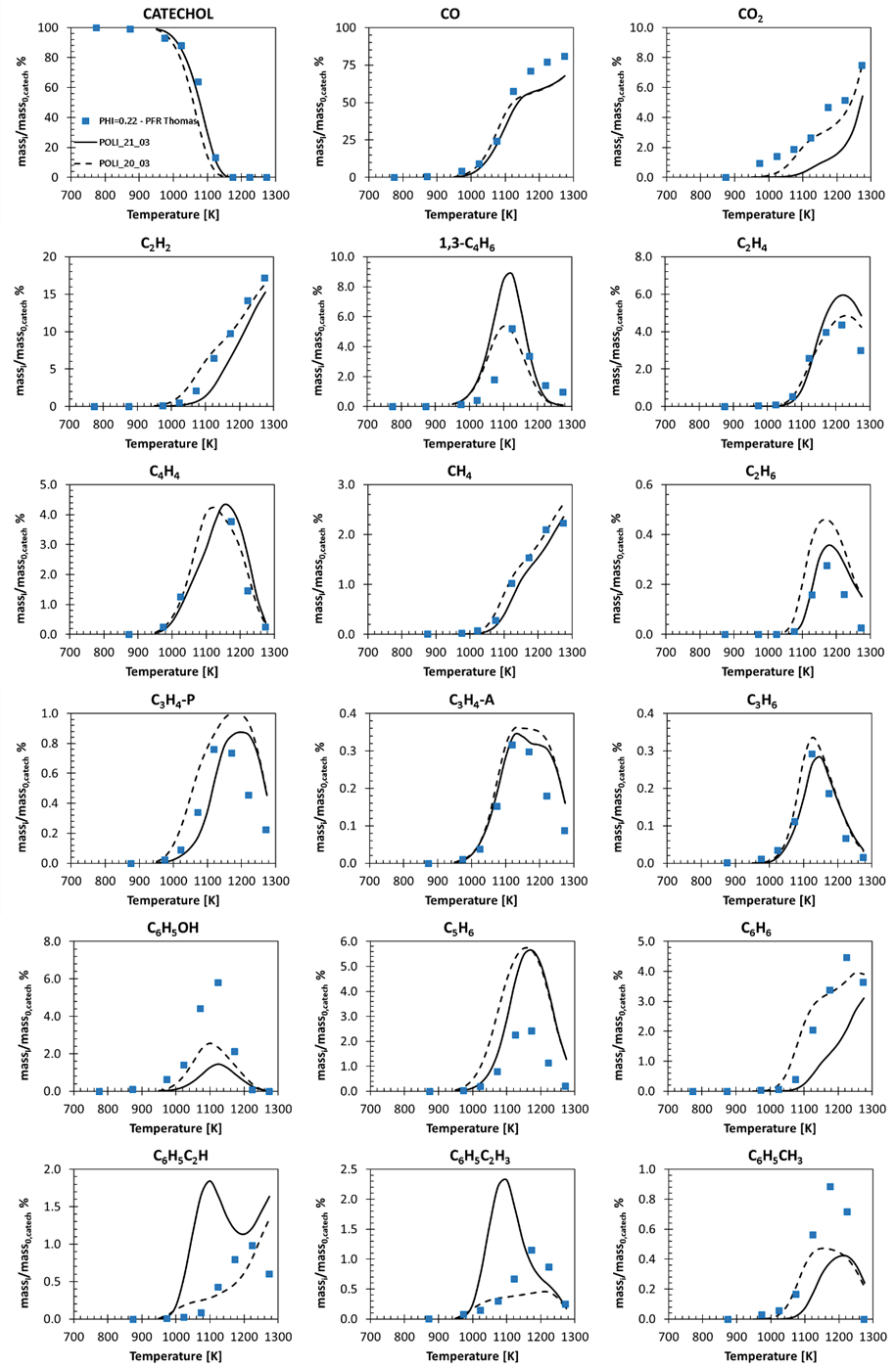

Figure 62 Catechol oxidation in a PFR at 1100K and atmospheric pressure. The experimental data belong to the work of Thomas et al.[44]

The inlet mixture composition had an equivalence ratio equal to 0.22 but, the model was tested also at other ϕ, simulations results are available in the Appendix, together with the pyrolysis case; they are not shown in this paragraph since the trends are similar. The residence time in the isothermal PFR was set at 0.3s and the inlet temperature of the mixture was 1100K.

Overall, the mechanism shows good agreement with experimental data, even though for some species the predictions are not very accurate. Looking at the production of styrene and phenylacetylene, they are clearly overestimated. To find out the reason behind this lack of precision, a sensitivity analysis was carried out.

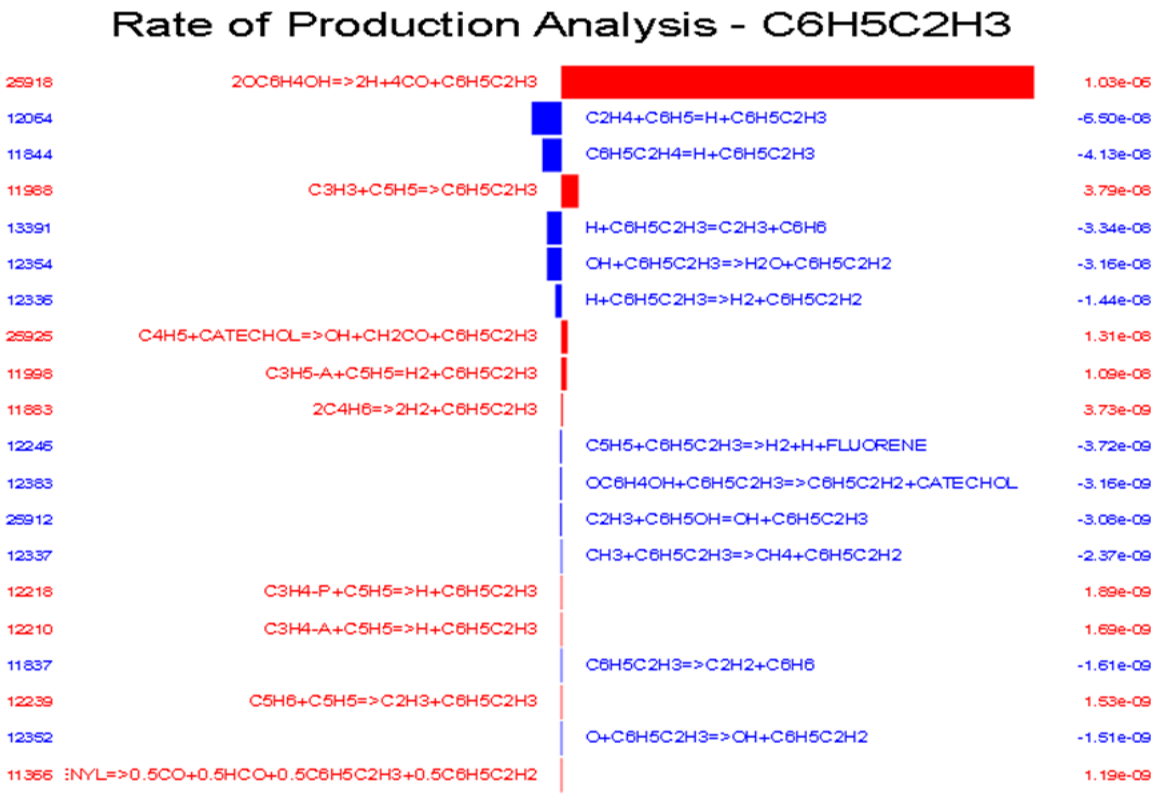

Figure 63 Sensitivity analysis of styrene production in Thomas et al.[46] PFR for catechol oxidation.

The first reaction to appear (25916) presents kinetic parameters defined experimentally, for this reason, taking into account the unavoidable error of experimental measurements, it has been changed within the limits to better predict styrene production. However, styrene is still overestimated.

The same applies for phenylacetylene, whose sensitivity analysis is reported.

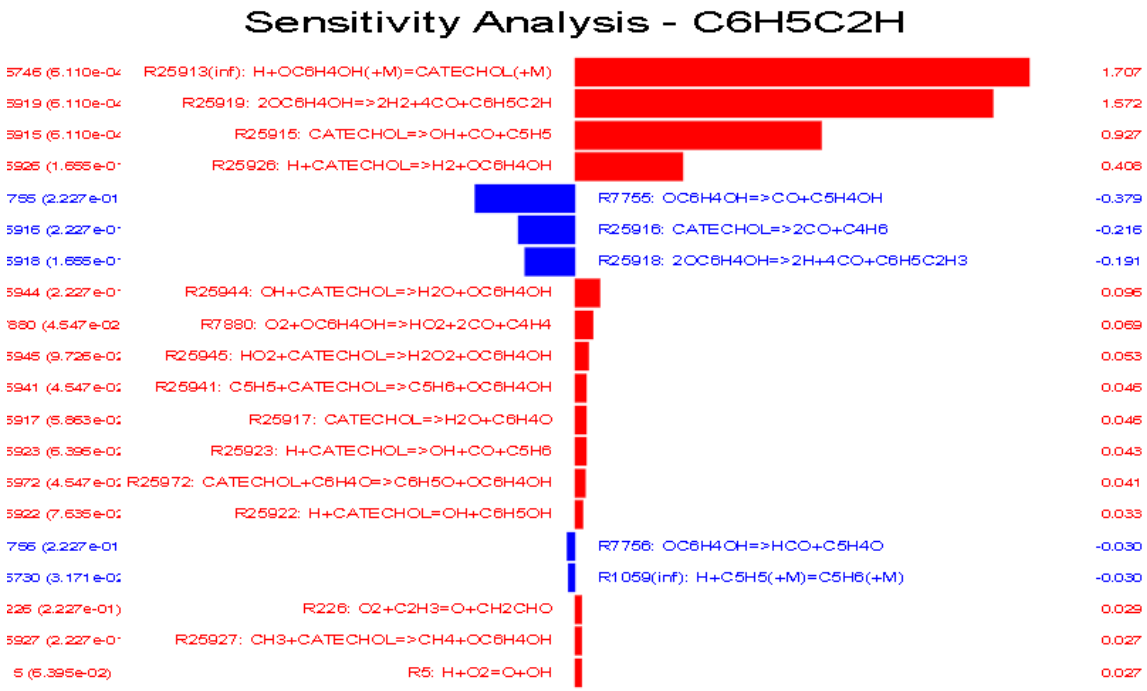

Figure 64Sensitivity analysis of phenylacetylene production in Thomas et al.14 PFR for catechol oxidation.

The first reaction must be updated with in progress ab-initio calculations for kinetic parameters. The second one, as for styrene, as been changed according to the experimental error range, to balance the perturbation on error-compensation provided by the new implemented reactions. Working on the kinetic parameter of the third reaction would mean to reduce catechol reactivity, losing the well-predicted trend on this species. The H-abstraction on catechol was investigated theoretically.

Catechol pyrolysis was carried out also in another PFR, to simulate the experimental database of Poddar, Thomas and Wornat[46]. They performed pyrolysis experiments in an isothermal plug flow reactor at temperatures, 950-1275 K and residence time of 0.3 s, with propyne and catechol together (in a catechol-to-propyne molar ratio of 0.938) and with pure catechol. The results are shown in the Appendix since the implemented reaction rates have no great influence on the model prediction.

8.5 Guaiacol oxidation in a JSR

Finally, the last species whose oxidation was investigated in an ideal reactor is guaiacol. The simulation was run according to the operating conditions of the experimental set reviewed by Nowakowska et al.[47] The simulated oxidation was carried out in an isothermal-constant-pressure JSR, tested in a temperature range of 650-950 K, at a pressure of 1.06 atm. The inlet mixture made of oxygen and guaiacol was diluted in He. In Figure 65 the results are reported. Despite the error-compensation perturbation, the mechanism still reproduces the main trends, with little improvement for some species with respect to the mechanism POLI_20_03.

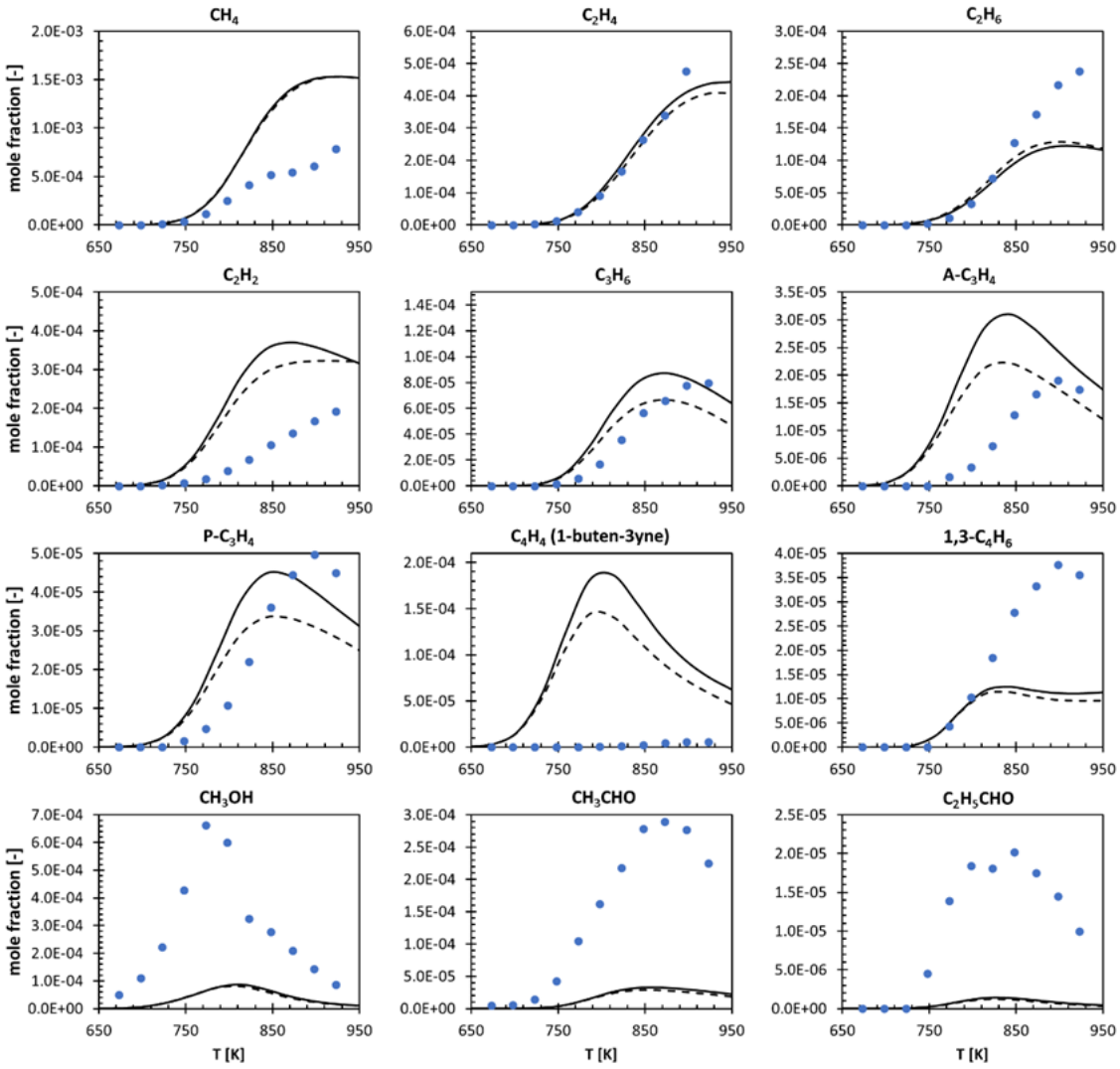

Figure 65 Guaiacol oxidation in a JSR simulated in a temperature range T=650-950K at 1.06 atmosphere according to Nowakowska et al.[46] experimental database.

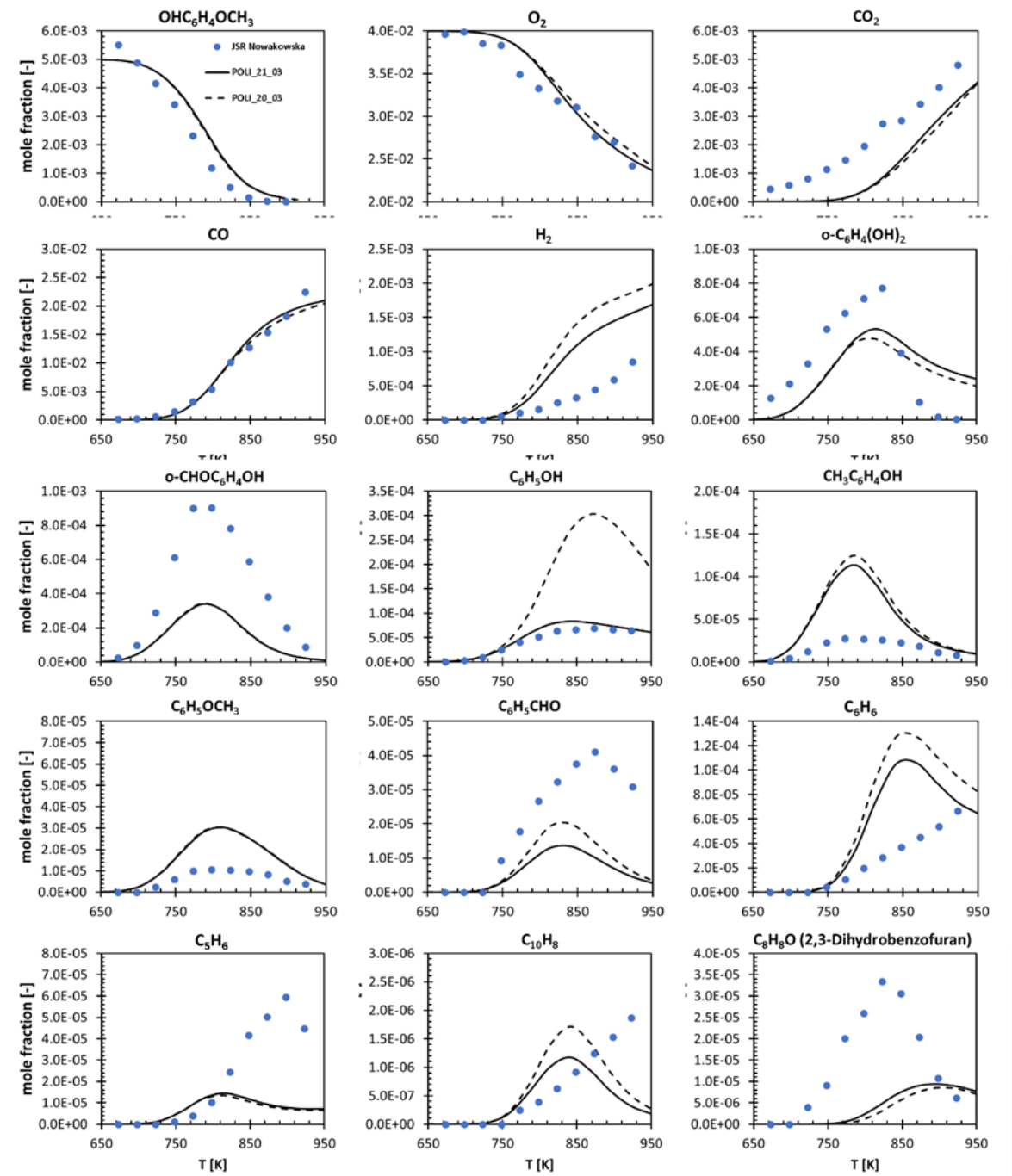

Figure 66 Guaiacol oxidation in a JSR simulated in a temperature range T=650-950K at 1.06 atmosphere according to Nowakowska et al.[47] experimental database.

8.6 Premixed Flames

In the end, the mechanism was tested in premixed laminar flames for high temperature ranges. The simulations were carried out according to the operating conditions described in the work of Bakali et al.[29] , Bittner et al.[48] , Tregrossi et al[47].

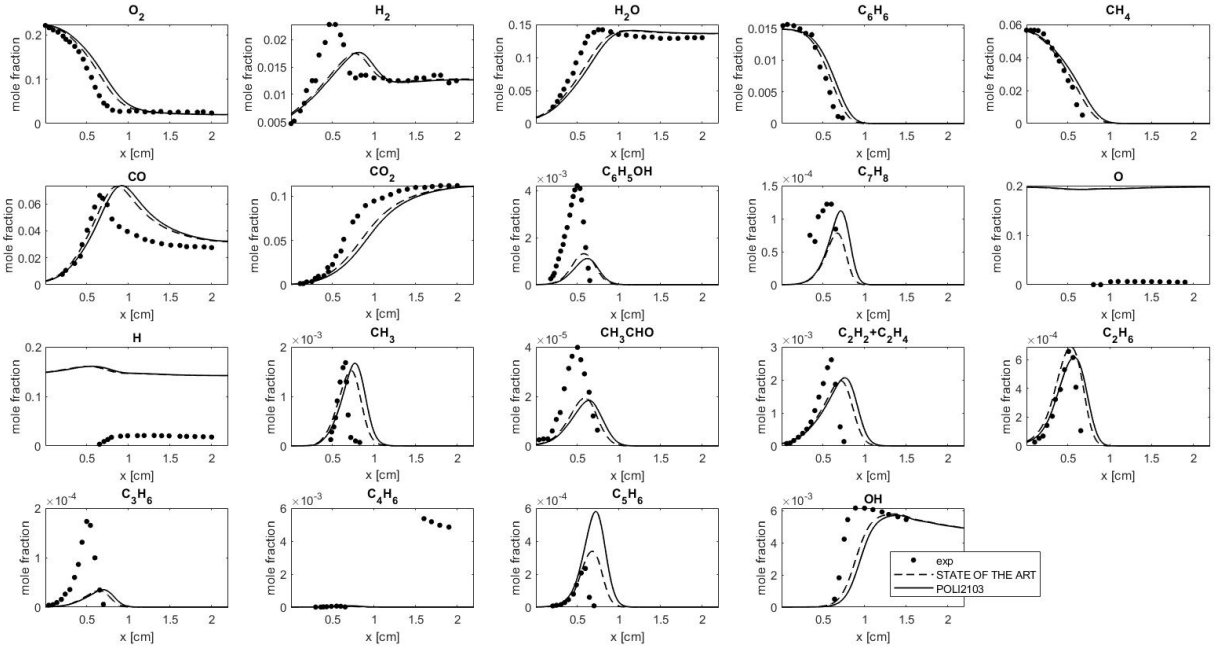

Figure 67 Premixed laminar flames simulated according to Bakali et al.[29]

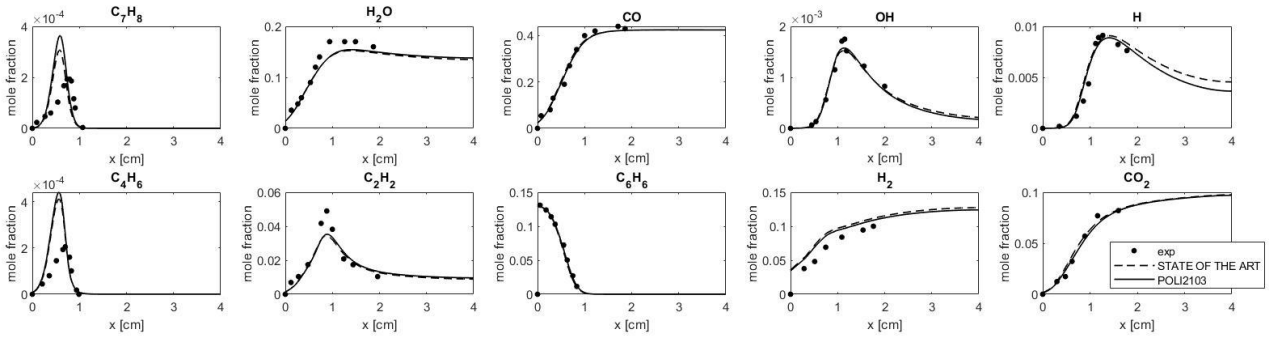

Figure 67 Premixed laminar flames simulated according to the work of Bittner et al.[48]

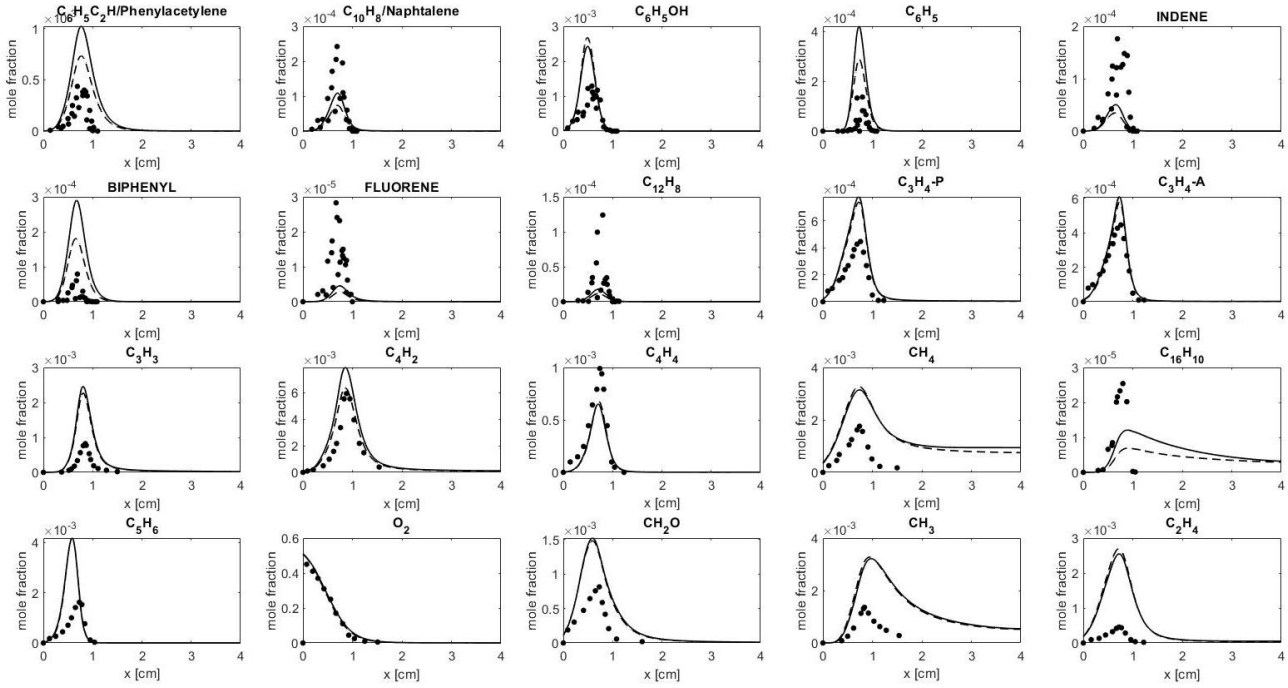

Figure 68 Premixed laminar flames simulated according to the work of Bittner et al.[29]

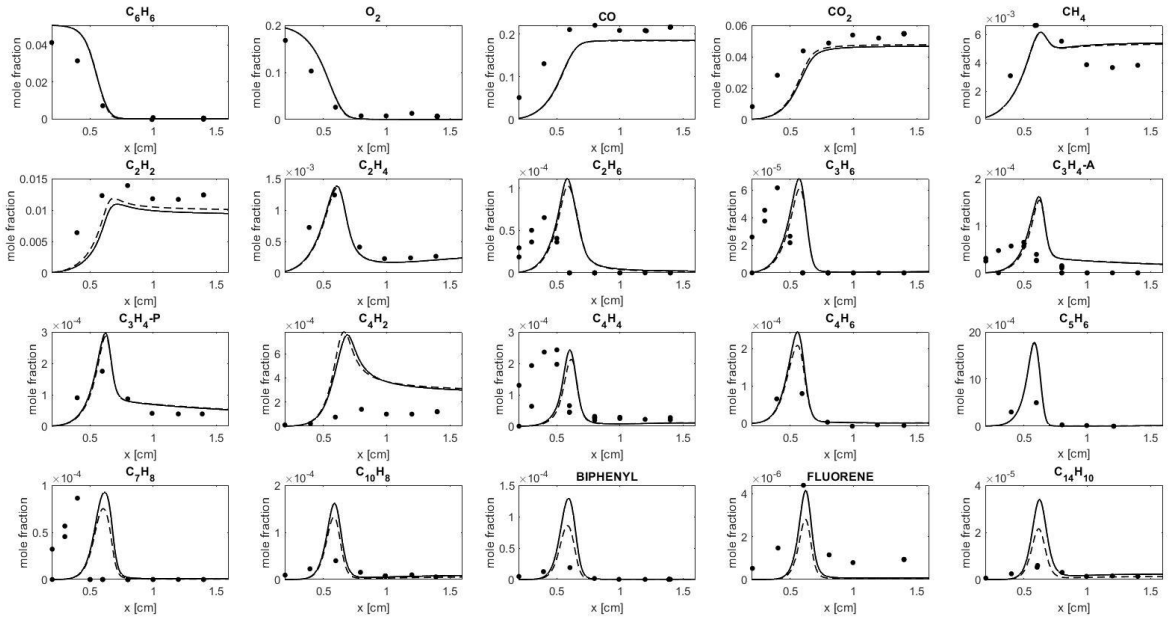

Figure 69 Premixed laminar flames simulated according to the work of Tregrossi et al.[48]

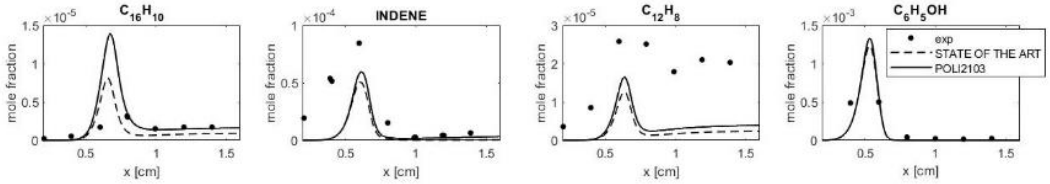

Figure 70 Premixed laminar flames simulated according to the work of Tregrossi et al.[21]

The simulation results are in good agreement with the experimental data.

In Bakali et al.[48] results, it can be grasped an underestimation of oxygen reactivity, that was already present in the POLI_20_03 mechanism.

In Bittner, the phenylacetylene is still in excess, as in Thomas PFR, together with the phenyl radical, whose reactivity is reduced with the implementation of the new rate constants. The biphenyl production is increased.

For what concerns Tregrossi et al.[28] simulation, looking at benzene, even though the simulation input is well-set, its molar fraction at the entrance is not equal to the one of experimental data, this is due to back-mixing phenomenon that cannot be avoided. There is also an overestimation of PAH.

CHAPTER 9
Conclusions

Formulation of new fuels suitable for existing engine technologies strongly relies on an accurate description of combustion chemistry over a broad range of operating conditions and regimes. Due to the complexity of real fuels in terms of the number of components, it is standard practice to refer to surrogate mixtures of a limited number of compounds representative of the families of species found in commercial gasoline, diesel and jet fuels. The development of accurate kinetic mechanisms to describe the reactivity of single components present in surrogate mixtures requires a progressive revision of existing reaction steps. A part of the revision consists in the theoretical computation of kinetic parameters to obtain more accurate estimates.

This thesis has investigated the reaction mechanism of the system $C_5H_6+O_2$.

As a first step, the potential energy surface was built and examined, computing the energy contents and the vibrational frequencies of all transition states, reactants and products by means of ab-initio methods. Then, the kinetic parameters of the identified reaction channels were evaluated with Ab-initio Transition State Theory based Master Equation methods (AI-TST-ME). Coupled cluster calculations were performed at level CCSD(T)/aug-cc-pVTZ to determine the energy contents. The latter were then corrected using MP2/aug-cc-pVTZ and MP2/aug-cc-pVQZ to converge to the basis set limit, also including core corrections using cc-PVTZ basis set. For the master equation resolution, it was assumed that the reaction takes place in the pressure range p=0.1-1000 atm and in a temperature range T= 300 - 2500K.

Thereafter, the new rates constants were implemented in the CRECK combustion kinetic mechanism and their impact on model predictions was evaluated with a model validation step. The validation was carried out on a wide range of experimental data present in the literature.

Overall, the kinetic model results are satisfactory: the trends are pretty in accordance with experimental data collected at different temperature and pressure ranges. Despite the

integration of kinetic rate constants determined theoretically, that could have mined the model intrinsic error-compensation, a remarkable worsening of prediction performances was not registered. Moreover, a significant improvement for the predictions of some species production, such as benzoquinone, was shown.

The accuracy provided for the estimation of model parameters allows to extend their values through analogy to the kinetic modelling of oxygenated aromatics, such as catechol, guaiacol and anisole, representative of biofuels components.

Appendix

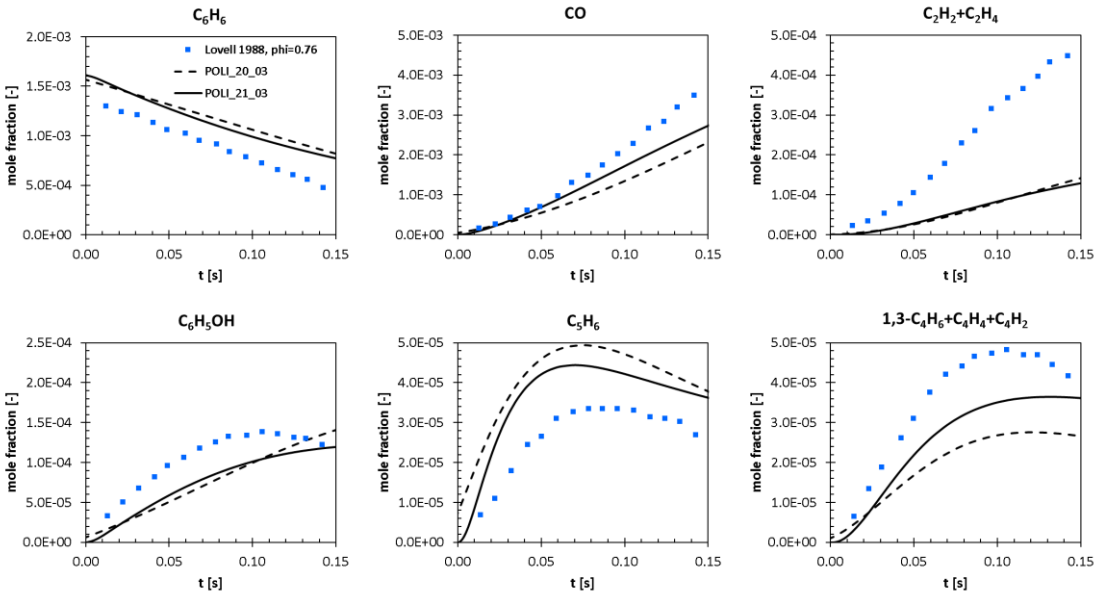

Figure 71 Comparison between the two mechanisms POLI_21_03 and POLI_20_03 for the oxidation of benzene in a PFR at φ=0.76 and T=1102K reviewed by Brezinsky et al.[28].

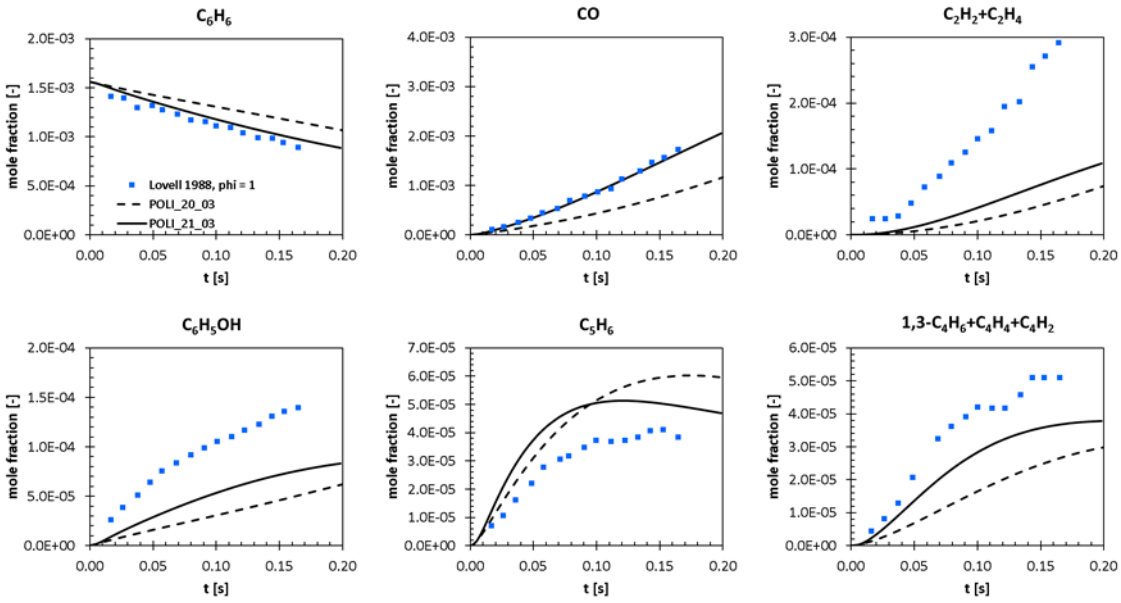

Figure 72Comparison between the two mechanisms POLI_21_03 and POLI_20_03 for the oxidation of benzene in a PFR at φ=1.36 and T=1102K reviewed by Brezinsky et al.[24].

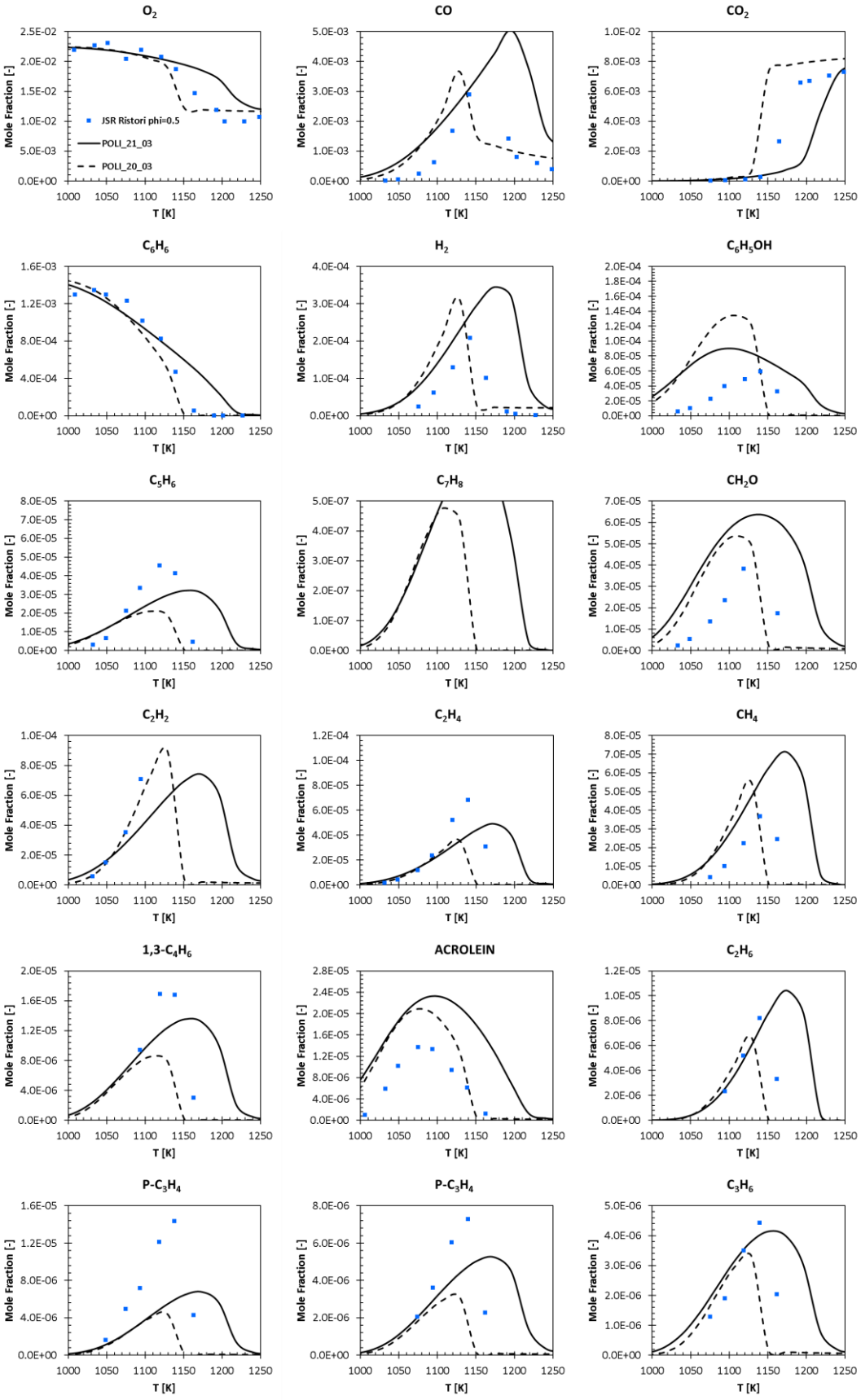

Figure 73 JSR Ristori et al.[50] simulation at phi=0.5 with compared the mechanisms POLI_21_03 and POLI_20_03

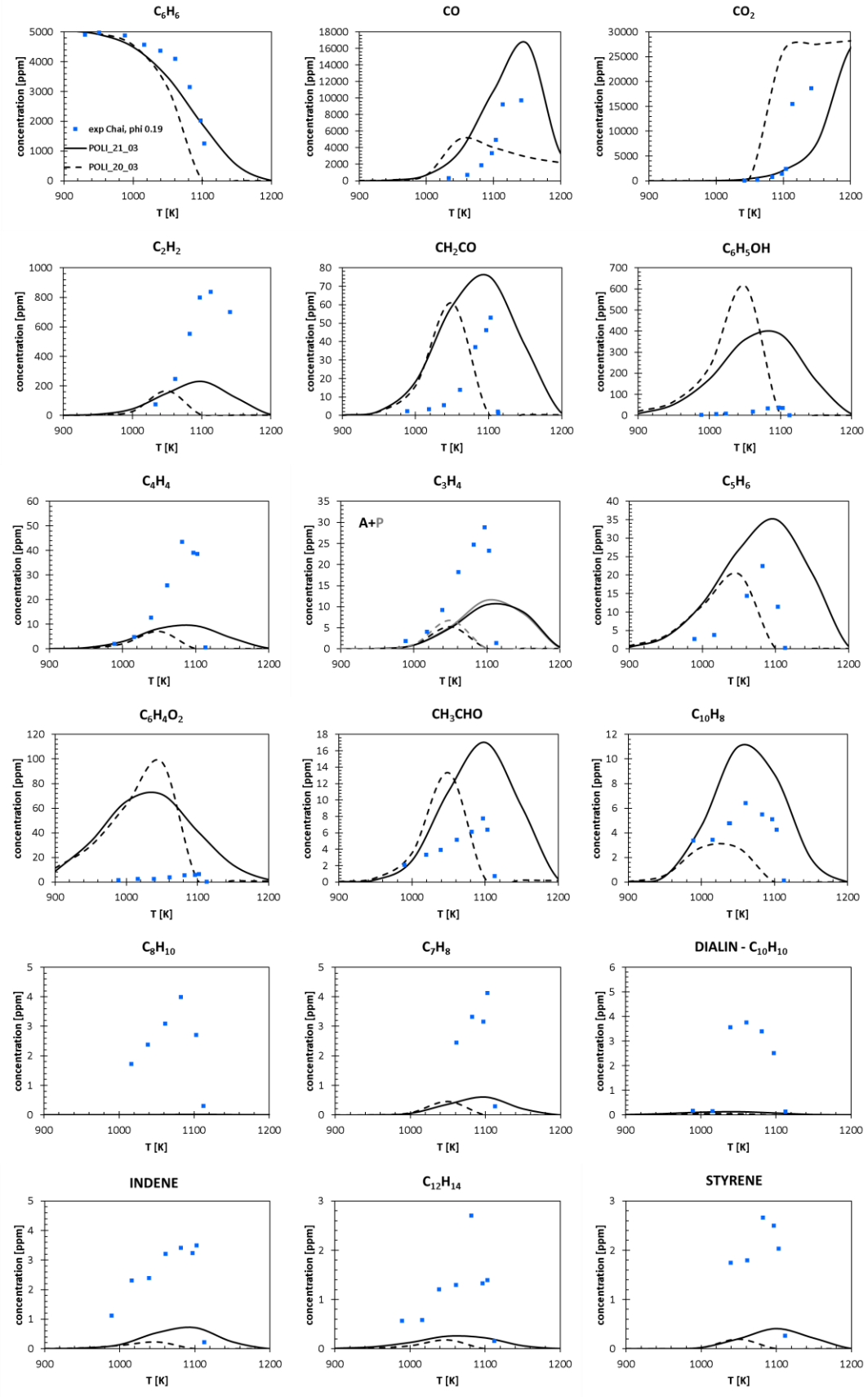

Figure 74 Model prediction for Chai et al.[42] experimental database in a micro-JSR at 0.46 atm and φ=0.19.

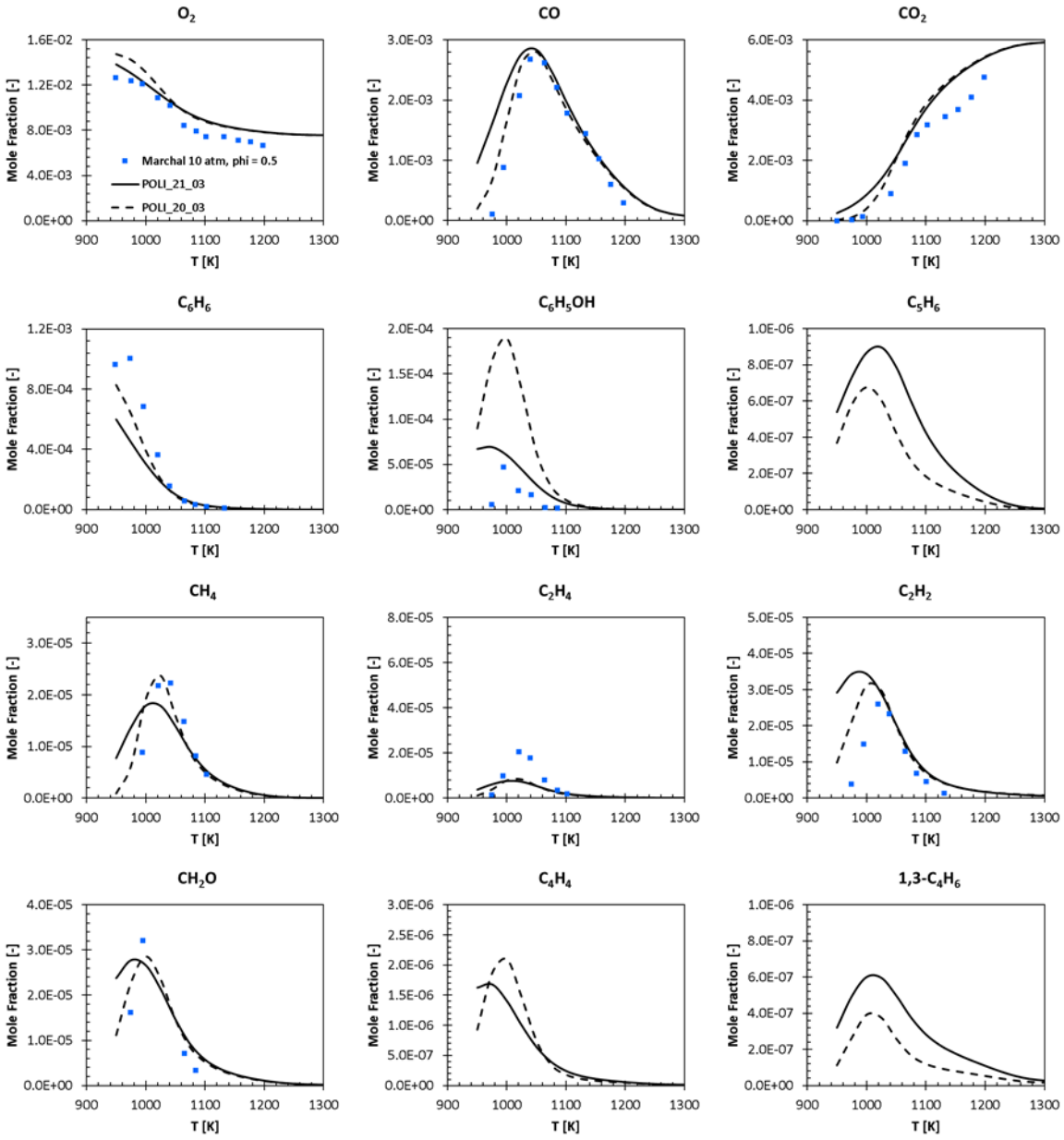

Figure 75 JSR simulation at 10 atm according to Marchal et al.[49] experimental database.

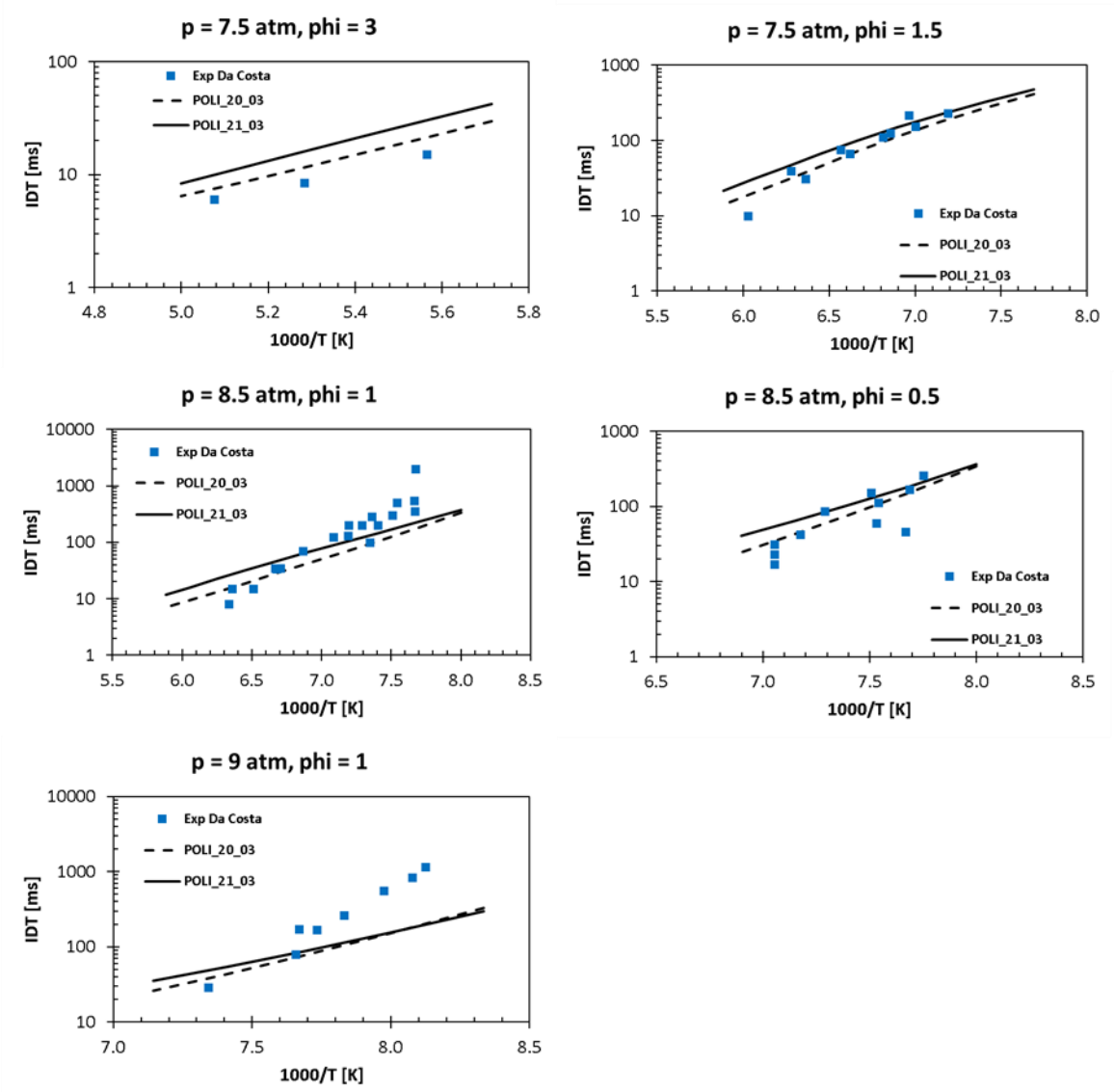

Figure 76 Ignition delay time in a shock tube compared to the experimental database reviewed by Da Costa.[44]

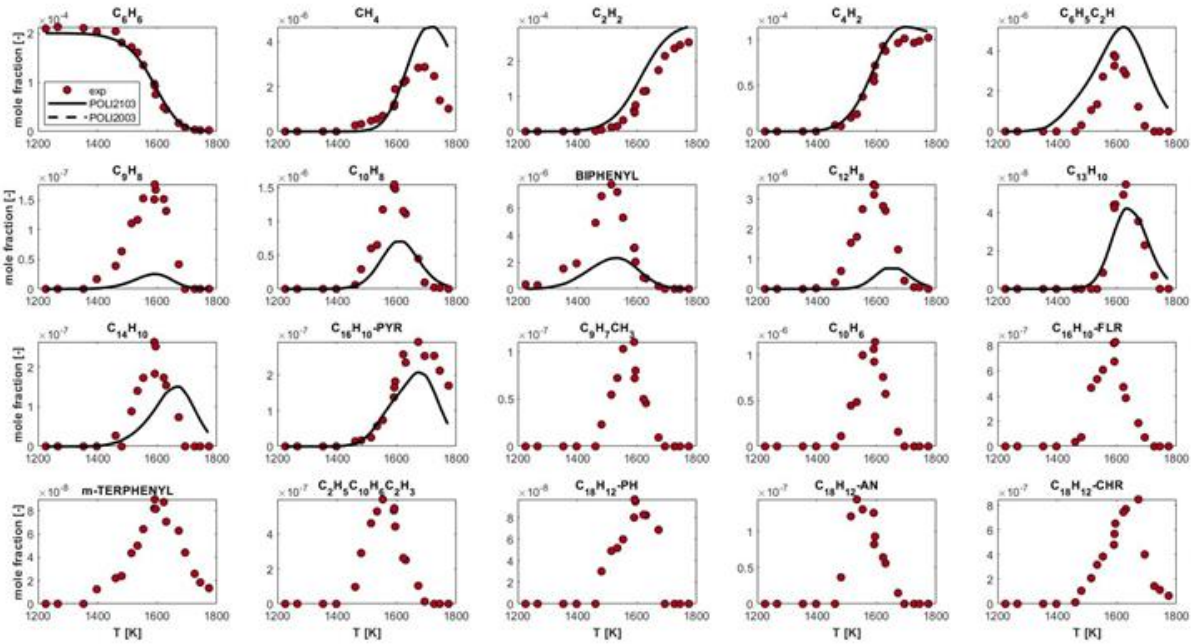

Figure 77 Benzene pyrolysis in a shock tube to predict the experimental database of Sun W et al.[50]

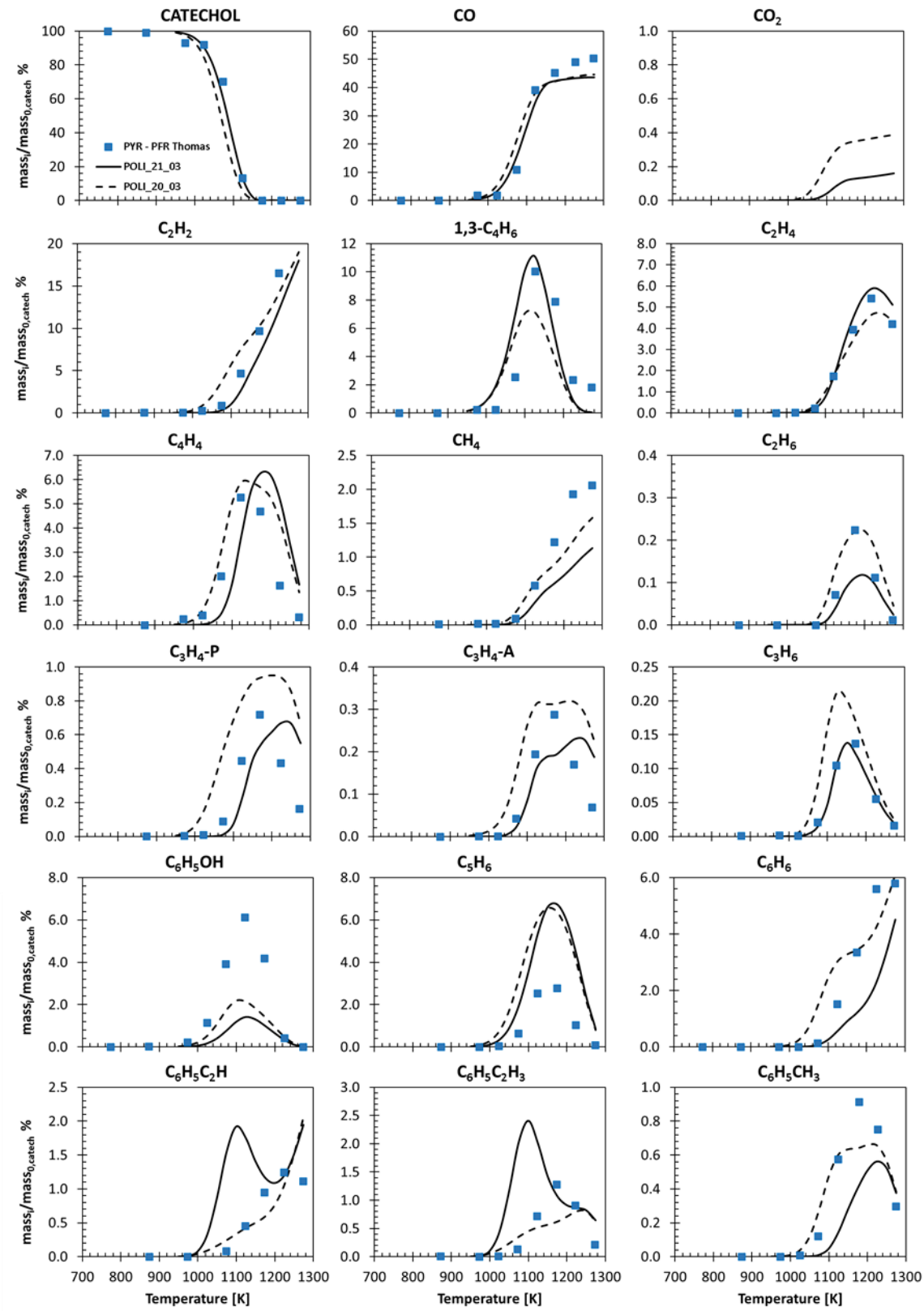

Figure 78 Catechol pyrolysis in a PFR at atmospheric pressure with an inlet temperature of 1100K. Experimental data are provided by Thomas et al.[44]

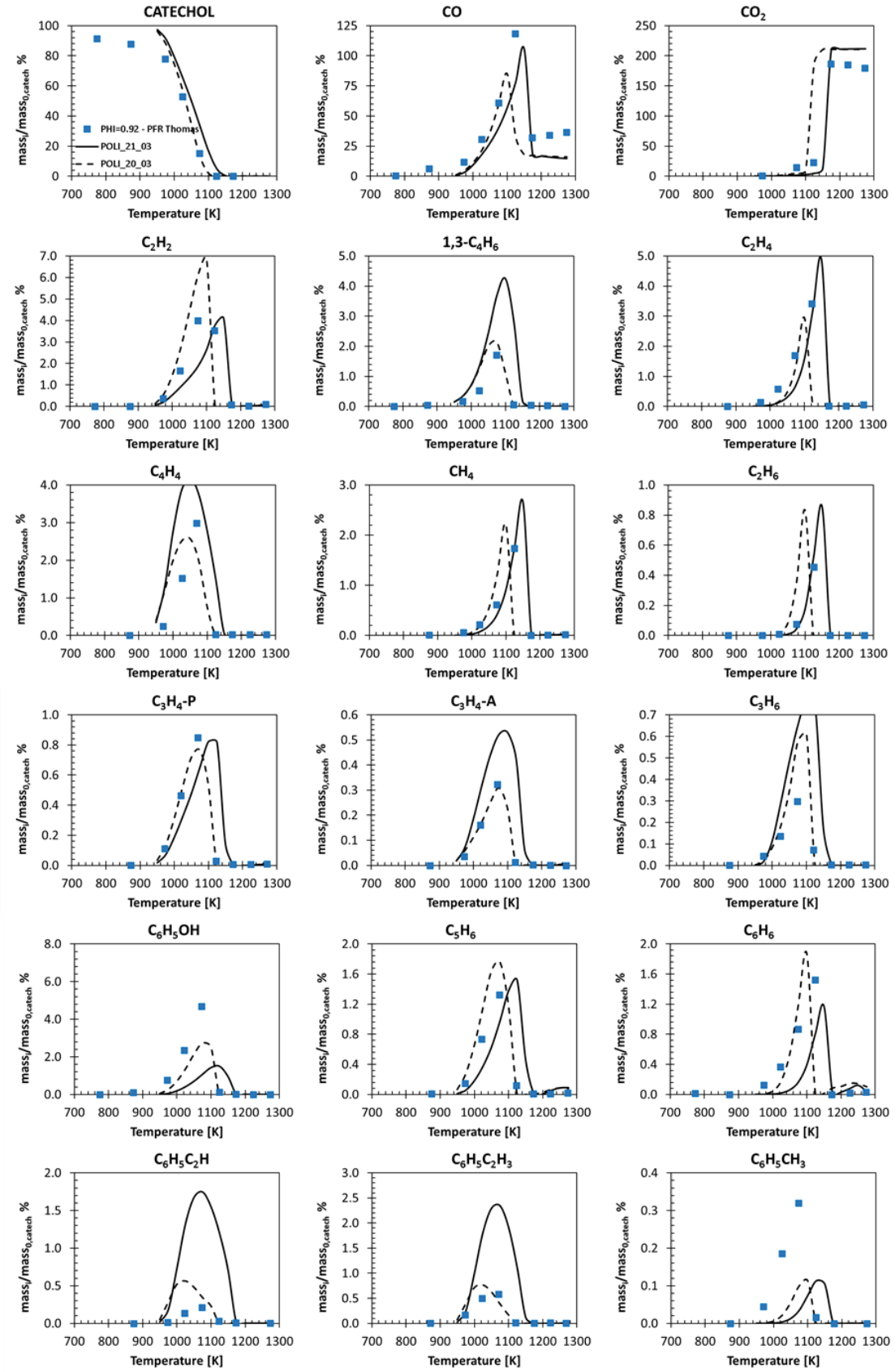

Figure 79 Catechol oxidation in a PFR at atmospheric pressure, φ=0.92, with an inlet temperature of 1100K. Experimental data are provided by Thomas et al.[44]

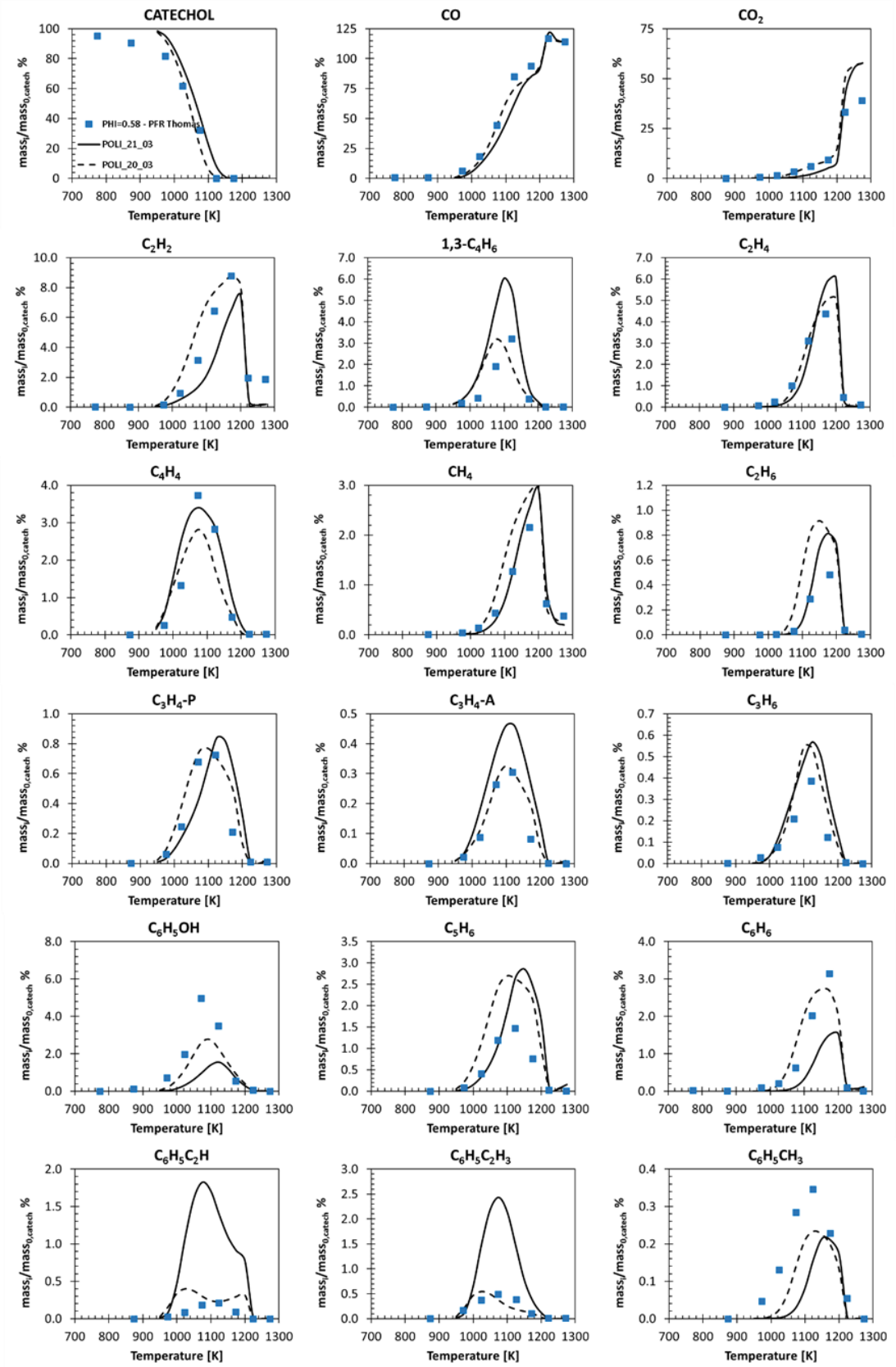

Figure 80 Catechol oxidation in a PFR at atmospheric pressure, φ=0.58, with an inlet temperature of 1100K. Experimental data are provided by Thomas et al.[45]

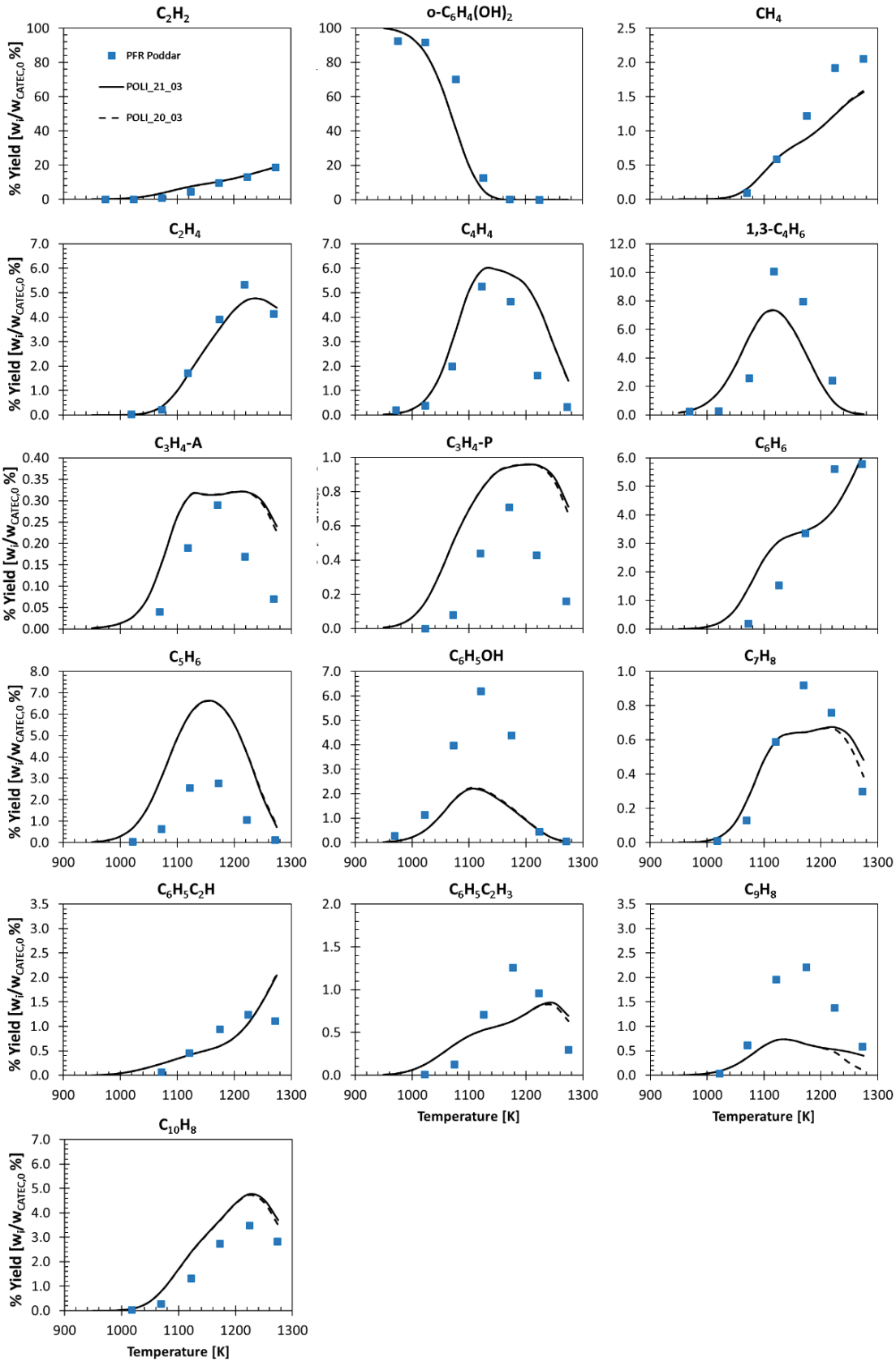

Figure 81 Cathecol pyrolysis experiments in an isothermal laminar-flow reactor, at temperatures 700-1000 °C[45].

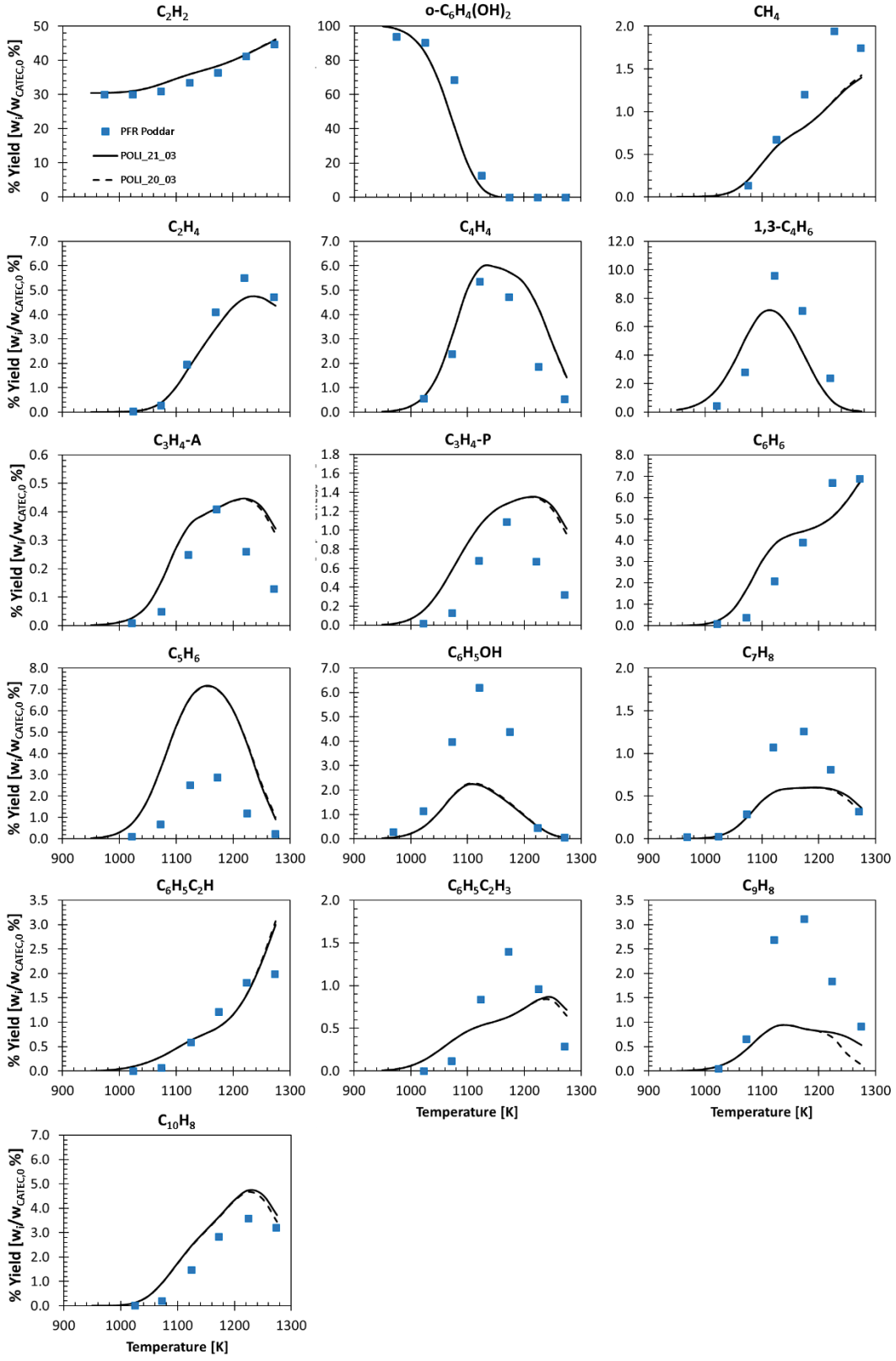

Figure 82 Cathecol and C2H2 mixture pyrolysis experiments in an isothermal laminar-flow reactor, at temperatures 700-1000 °C in a catechol-to-propyne molar ratio of 0.938[44]

Bibliography

1. K. S. Lackner. “Can fossil carbon fuel the 21st century?” . 2002;44:1122-1133.
2. Sadeghinezhad E, Kazi SN, Sadeghinejad F, et al. A comprehensive literature review of bio-fuel performance in internal combustion engine and relevant costs involvement. *Renewable and Sustainable Energy Reviews*. 2014;30:29-44. doi:10.1016/j.rser.2013.09.022
3. Kalghatgi GT. The outlook for fuels for internal combustion engines. *International Journal of Engine Research*. 2014;15(4):383-398. doi:10.1177/1468087414526189
4. Mittal G, Sung CJ. Autoignition of toluene and benzene at elevated pressures in a rapid compression machine. *Combustion and Flame*. 2007;150(4):355-368. doi:10.1016/j.combustflame.2007.04.014
5. Ranzi E, Dente M, Goldaniga A, Bozzano G, Faravelli T. Lumping procedures in detailed kinetic modeling of gasification, pyrolysis, partial oxidation and combustion of hydrocarbon mixtures. *Progress in Energy and Combustion Science*. 2001;27(1):99-139. doi:10.1016/S0360-1285(00)00013-7
6. Cuoci A, Frassoldati A, Faravelli T, Ranzi E. OpenSMOKE++: An object-oriented framework for the numerical modeling of reactive systems with detailed kinetic mechanisms. *Computer Physics Communications*. 2015;192:237-264. doi:10.1016/j.cpc.2015.02.014
7. Stagni A, Cuoci A, Frassoldati A, Faravelli T, Ranzi E. Lumping and reduction of detailed kinetic schemes: An effective coupling. *Industrial and Engineering Chemistry Research*. 2014;53(22):9004-9016. doi:10.1021/ie403272f
8. RANZI E, FRASSOLDATI A, STAGNI A, PELUCCHI M, CUOCI A, FARAVELLI T. Reduced Kinetic Schemes of Complex Reaction Systems: Fossil and Biomass-Derived Transportation Fuels. *International Journal of Chemical Kinetics*. 2014;46(9):512-542. doi:10.1002/kin.20867

9. van't Hoff MJH. Etudes de dynamique chimique. *Recueil des Travaux Chimiques des Pays-Bas*. 1884;3(10):333-336. doi:10.1002/recl.18840031003

10. Lindemann FA, Arrhenius S, Langmuir I, Dhar NR, Perrin J, Lewis WCMcC. Discussion on "the radiation theory of chemical action." *Transactions of the Faraday Society*. 1922;17(0):598-606. doi:10.1039/TF9221700598

11. Gordon S and BJM. "Computer program for calculation of complex equilibrium compositions, rocket performance, incident and reflected shocks, and Chapman-Jouguet detonations." NASA SP-273 168 (1971). Accessed April 4, 2021. https://scholar.google.com/scholar?hl=it&as_sdt=0%2C5&q=S.+Gordon%3B+B.+McBride%2C+Computer+program+for+calculation+of+complex+equilibrium+composition%2C+rocket+performance%2C+incident+and+reflected+shocks+and+Chapman-Jouguet+detonations%2C+NASA+SP-273+168+%281971&btnG=#d=gs_cit&u=%2Fscholar%3Fq%3Dinfo%3AsecEy0PL6TMJ%3Ascholar.google.com%2F%26output%3Dcite%26scirp%3D0%26hl%3Dit

12. Hirschfelder JO, Curtiss CF, Bird RB. Molecular Theory of Gases and Liquids . *Physics Today*. 1955;8(3):17-17. doi:10.1063/1.3061949

13. Zhao Y, Truhlar DG. The M06 suite of density functionals for main group thermochemistry, thermochemical kinetics, noncovalent interactions, excited states, and transition elements: Two new functionals and systematic testing of four M06-class functionals and 12 other functionals. *Theoretical Chemistry Accounts*. 2008;120(1-3):215-241. doi:10.1007/s00214-007-0310-x

14. Grimme S, Antony J, Ehrlich S, Krieg H. A consistent and accurate ab initio parametrization of density functional dispersion correction (DFT-D) for the 94 elements H-Pu. *Journal of Chemical Physics*. 2010;132(15):24103. doi:10.1063/1.3382344

15. Grimme S. Semiempirical hybrid density functional with perturbative second-order correlation. *Journal of Chemical Physics*. 2006;124(3):034108. doi:10.1063/1.2148954

16. Grimme S, Steinmetz M. Effects of London dispersion correction in density functional theory on the structures of organic molecules in the gas phase. *Physical Chemistry Chemical Physics*. 2013;15(38):16031-16042. doi:10.1039/c3cp52293h

17. M. Frisch; G. Trucks; H. B. Schlegel; G. Scuseria; M. Robb; J. Cheeseman; G. Scalmani; V. Barone; B. Mennucci; G. Petersson. Gaussian 09. 2009;Revision A. 02.

18. Werner HJ, Knowles PJ, Knizia G, Manby FR, Schütz M. Molpro: A general-purpose quantum chemistry program package. *Wiley Interdisciplinary Reviews: Computational Molecular Science*. 2012;2(2):242-253. doi:10.1002/wcms.82

19. Georgievskii Y, Miller JA, Burke MP, Klippenstein SJ. Reformulation and solution of the master equation for multiple-well chemical reactions. *Journal of Physical Chemistry A*. 2013;117(46):12146-12154. doi:10.1021/jp4060704

20. Cavallotti C, Pelucchi M, Georgievskii Y, Klippenstein SJ. EStokTP: Electronic Structure to Temperature- and Pressure-Dependent Rate Constants-A Code for Automatically Predicting the Thermal Kinetics of Reactions. *Journal of Chemical Theory and Computation*. 2019;15(2):1122-1145. doi:10.1021/acs.jctc.8b00701

21. Ristori A, Dagaut P, el Bakali A, Pengloan G, Cathonnet M. Benzene oxidation: Experimental results in a JDR and comprehensive kinetic modeling in JSR, shock-tube and flame. *Combustion Science and Technology*. 2001;167(1):223-256. doi:10.1080/00102200108952183

22. L. Pratali Maffei. Personal Communication. Published online 2021.

23. Luna Pratali Maffei MPRDBKAHTFCC. Rate constants for the H-abstraction reactions from mono-aromatic hydrocarbons by Ḣ, ĊH3, ȮH and 3O2: a systematic theoretical investigation. *in preparation*.

24. Chai Y, Pfefferle LD. An experimental study of benzene oxidation at fuel-lean and stoichiometric equivalence ratio conditions. *Fuel*. 1998;77(4):313-320. doi:10.1016/S0016-2361(97)00192-0

25. Lin MC, Mebel AM. Ab initio molecular orbital study of the O + C6H5O reaction. *Journal of Physical Organic Chemistry*. 1995;8(6):407-420. doi:10.1002/poc.610080605

26. Tokmakov I v., Kim GS, Kislov V v., Mebel AM, Lin MC. The reaction of phenyl radical with molecular oxygen: A G2M study of the potential energy surface. *Journal of Physical Chemistry A*. 2005;109(27):6114-6127. doi:10.1021/jp051712k

27. A. Laskin AL. Proc. Combust. Inst. 26. Published online 1996:669-677.

28. Brezinsky K. The high-temperature oxidation of aromatic hydrocarbons. *Progress in Energy and Combustion Science*. 1986;12(1):1-24. doi:10.1016/0360-1285(86)90011-0

29. J.D. Bittner JBH. Proc. Combust. Inst. 28 . Published online 1981:1105-1116.

30. Fadden MJ, Hadad CM. Unimolecular decomposition of the 2-oxepinoxy radical: A key seven-membered ring intermediate in the thermal oxidation of benzene. *Journal of Physical Chemistry A*. 2000;104(34):8121-8130. doi:10.1021/jp0017238

31. Vourliotakis G, Skevis G, Founti MA. A detailed kinetic modeling study of benzene oxidation and combustion in premixed flames and ideal reactors. *Energy and Fuels*. 2011;25(5):1950-1963. doi:10.1021/ef101712p

32. Tanaka K, Ando M, Sakamoto Y, Tonokura K. Pressure dependence of phenylperoxy radical formation in the reaction of phenyl radical with molecular oxygen. *International Journal of Chemical Kinetics*. 2012;44(1):41-50. doi:10.1002/kin.20615

33. (PDF) The phenyl+ O2 reaction: Thermodynamics and kinetics. Accessed April 5, 2021. https://www.researchgate.net/publication/228493691_The_phenyl_O2_reaction_Thermodynamics_and_kinetics

34. Pratali Maffei L, Pelucchi M, Faravelli T, Cavallotti C. Theoretical study of sensitive reactions in phenol decomposition. *Reaction Chemistry and Engineering*. 2020;5(3):452-472. doi:10.1039/c9re00418a

35. Zhang F, Nicolle A, Xing L, Klippenstein SJ. Recombination of aromatic radicals with molecular oxygen. *Proceedings of the Combustion Institute*. 2017;36(1):169-177. doi:10.1016/j.proci.2016.06.021

36. Kislov V v., Singh RI, Edwards DE, Mebel AM, Frenklach M. Rate coefficients and product branching ratios for the oxidation of phenyl and naphthyl radicals: A theoretical RRKM-ME study. *Proceedings of the Combustion Institute*. 2015;35(2):1861-1869. doi:10.1016/j.proci.2014.06.135

37. da Silva G, Bozzelli JW. Variational analysis of the phenyl + O2 and phenoxy + O reactions. *Journal of Physical Chemistry A*. 2008;112(16):3566-3575. doi:10.1021/jp7118845

38. Yu T, Lin MC. *Kinetics of the CeHs + O2 Reaction at Low Temperatures*. Vol 116.; 1994. Accessed April 6, 2021. https://pubs.acs.org/sharingguidelines

39. J. Schaugg RSTH-HG. Eighth International Symposium on Transport Phenomena in Combustion. 1996;Ed., Taylor & Francis:130-141.

40. Zhang F, Nicolle A, Xing L, Klippenstein SJ. Recombination of aromatic radicals with molecular oxygen. *Proceedings of the Combustion Institute*. 2017;36(1):169-177. doi:10.1016/j.proci.2016.06.021

41. Venkat C, Brezinsky K, Glassman I. High temperature oxidation of aromatic hydrocarbons. *Symposium (International) on Combustion*. 1982;19(1):143-152. doi:10.1016/S0082-0784(82)80186-0

42. A. Marchal MCPDMRMAGBJ-FB. Proceedings of the Joint Meeting of the French and German Sections ofthe Combustion Institute. *Proceedings of the Joint Meeting of the French and German Sections of the Combustion Institute, Mulhouse*. Published online October 1995:11-13.

43. Burcat A, Snyder C, Brabbs T. *Ignition Delay Times of Benzene # r and Toluene With Oxygen. in Argon Mixtures NF) SL)ICK?* Vol 873.; 1986.

44. Thomas S, Wornat MJ. The effects of oxygen on the yields of polycyclic aromatic hydrocarbons formed during the pyrolysis and fuel-rich oxidation of catechol. *Fuel*. 2008;87(6):768-781. doi:10.1016/j.fuel.2007.07.016

45. Poddar NB, Thomas S, Wornat MJ. Polycyclic aromatic hydrocarbons from the co-pyrolysis of catechol and propyne. *Proceedings of the Combustion Institute*. 2011;33(1):541-548. doi:10.1016/j.proci.2010.06.072

46. Nowakowska M, Herbinet O, Dufour A, Glaude P-A. Pyrolysis and Oxidation of Guaiacol. *Journal of Physical Chemistry A*. 2018;122(39):7894-7909. doi:10.1021/acs.jpca.8b06301ï

47. Bakali A el, Ribaucour M, Saylam A, et al. *Benzene Addition to a Fuel-Stoichiometric Methane/O 2 /N 2 Flat Flame and to n-Heptane/Air Mixtures under Rapid Compression Machine • ARTICLE Pages 881-895 NO Prediction in Natural Gas Flames Using GDF-Kin ® 3.0 Mechanism NCN and HCN Contribution to Prompt-NO Formation Development and Validation of a Theoretical Model for Diesel Spray Penetration •*. Vol 85.; 2006. Accessed April 5, 2021. http://www.sciencedirect.com/science?_ob=IssueURL&_toc...sion=0&_userid=10&md5=384d2c9e76b7f9061a64c19bdceb4811

48. Tregrossi A, Ciajolo A, Barbella R. The combustion of benzene in rich premixed flames at atmospheric pressure. *Combustion and Flame*. 1999;117(3):553-561. doi:10.1016/S0010-2180(98)00157-6

49. Costa I da, Fournet R, Billaud F, Battin-Leclerc F. Experimental and modeling study of the oxidation of benzene. *International Journal of Chemical Kinetics*. 2003;35(10):503-524. doi:10.1002/kin.10148

50. Sun W, Hamadi A, Abid S, Chaumeix N, Comandini A. Probing PAH formation chemical kinetics from benzene and toluene pyrolysis in a single-pulse shock tube. *Proceedings of the Combustion Institute*. Published online July 31, 2020. doi:10.1016/j.proci.2020.06.077